



UNIVERSITÀ  
DEGLI STUDI  
DI PADOVA



Leibniz  
Universität  
Hannover

Università degli Studi di Padova

Leibniz Universität Hannover

Dipartimento di Ingegneria Industriale  
Corso di Laurea in Ingegneria Elettrica

# Numerical Analysis of Inhomogeneous Inductive Heating of Forging Parts

*Thesis by:*  
Francesco Rui

*Supervisors:*  
Prof. Dr.-Ing Egbert Baake  
Dipl.-Ing. Thomas Steinberg  
Prof. Michele Forzan

2014/2015



## **Abstract**

In this research work has been investigated the topic of the inhomogeneous induction heating. The idea is to realize an heating process which allows to heat a billet of steel in different zones at different temperatures. There is not much literature about this technology which has been not deeply investigated yet. The motivations which stay under this project are the energy saving and the experimentation of a new kind of forging process. The most important task is to verify the theoretical possibility to generate an inhomogeneous controlled temperature distribution along the length and the radius of a cylindrical work-piece. To study this phenomena a numerical model has been created and several FEM simulations have been done . The results are very interesting since the main problem has been solved and the advantages which come from this new technology are significant. Comparing the traditional induction heating method and the inhomogeneous induction heating it comes that the second one allows to save 5.6% of the energy. This field of material processing is still at the beginning, improving the research in this topic it will be possible to increase the efficiency and the advantages of this new method for billets heating.



## Acknowledgment

First I would like to thank Prof. E. Bake and Dipl.-Ing. T. Steinberg, always present and available to guide me and to solve my doubts during the preparation of this work. A sincerely thank also to the staff of Institut für Elektroprozessstechnik (ETP) who were always kind and friendly making my permanence in this institute comfortable. A particular thank also to prof. M. Forzan who helped me to organize this exchange program. I wish also to thank the international office of the Leibnitz University and Padua University for the cultural exchange offered to me, for the important support and collaboration demonstrated. At the end, I would thank my family Andrea, Chiara, Alessandro and Bruna for their support during my study career. A particular thank to Silvia who helped me in the difficult moments. To finish, a great thank to all my friends who were always present.



# Contents

<b>1</b>	<b>Introduction</b>	<b>13</b>
<b>2</b>	<b>Background and Theory</b>	<b>15</b>
2.1	Induction heating system . . . . .	16
2.1.1	Physics and theory of induction heating . . . . .	19
2.2	Forging Process . . . . .	34
<b>3</b>	<b>Description of the problem</b>	<b>41</b>
3.1	The goal of the investigation . . . . .	41
3.2	The work-piece . . . . .	43
3.2.1	42CrMo4 material properties for FEM analysis . . . . .	44
3.3	Finite elements method and ANSYS software . . . . .	50
3.3.1	Fem Method (hints) . . . . .	50
3.3.2	Ansys Mechanical Apdl . . . . .	50
<b>4</b>	<b>First analysis</b>	<b>57</b>
4.1	Initial parameters . . . . .	57
4.1.1	Geometry of the work-piece . . . . .	58
4.1.2	Hot and Cold Zone Dimension . . . . .	58
4.1.3	Frequency . . . . .	59
4.1.4	Inductor - Work-piece Air Gap . . . . .	59
4.1.5	Inductors . . . . .	60
4.2	First fem model analysis . . . . .	61
4.2.1	Preprocessing . . . . .	61
4.2.2	Postprocessing . . . . .	62
4.3	Second model . . . . .	65
4.3.1	Preprocessing . . . . .	65
4.3.2	Postprocessing . . . . .	65
<b>5</b>	<b>Third model analysis</b>	<b>69</b>
5.1	Magnetic flux controllers and active em-field shielding . . . . .	69
5.1.1	Magnetic Flux Controllers . . . . .	69
5.1.2	Active em-shielding . . . . .	70
5.2	Third model . . . . .	73
5.2.1	Second model updates . . . . .	73
5.2.2	Preprocessing . . . . .	74
5.2.3	Postprocessing . . . . .	77

5.2.4	Inductor thermal analysis and cooling system . . . . .	85
<b>6</b>	<b>Further analysis</b>	<b>91</b>
6.1	Different length tests . . . . .	91
6.1.1	Three Turns Inductor 25cm Work Piece . . . . .	91
6.1.2	Seven Turns Inductor 37cm Work Piece . . . . .	93
6.2	Different diameter tests . . . . .	95
6.2.1	Diameter: 4cm . . . . .	96
6.2.2	Diameter: 5cm . . . . .	97
6.2.3	Diameter: 6cm . . . . .	99
6.3	Comparison between traditional process and inhomogeneous process . . .	100
6.3.1	Geometry . . . . .	101
6.3.2	Input quantities . . . . .	101
6.3.3	Process comparison . . . . .	102
6.3.4	Power, energy, efficiency . . . . .	103
	<b>Conclusions</b>	<b>105</b>
	<b>Bibliography</b>	<b>109</b>



# List of Figures

2.1	induction system scheme . . . . .	16
2.2	power and frequencies required for different treatments . . . . .	17
2.3	inductor and workpiece . . . . .	19
2.4	relative radial distributions of magnetic field intensity . . . . .	21
2.5	P and Q trends as a function of "m", trend of active and reactive power as function of m (A,B) . . . . .	22
2.6	relative radial current density distribution . . . . .	23
2.7	current distribution at different frequencies example . . . . .	23
2.8	relative volume power distribution along the radius . . . . .	24
2.9	$A_i$ trend as function of m . . . . .	25
2.10	electrical efficiency: A - steel heated to 800°C, B - steel heated from 800°C to 1200°C, C - steel from 0°C to 1200°C, D - aluminum heated to 500°C, E - brass heated to 800°C . . . . .	26
2.11	radial thermal distribution . . . . .	29
2.12	$F(m), F'(m), F''(m)$ trends . . . . .	30
2.13	$F^*(m)$ trends as a function of m . . . . .	32
2.14	trends of the specific power $P_0$ as a function of temperature. $P_{0c}, P_{0\theta}$ are the maximum power and the power at $\theta$ temperature. $H_0$ is the intensity of the surface magnetic field . . . . .	33
2.15	example of open die forging . . . . .	34
2.16	cogging forming step example . . . . .	35
2.17	example of impression die forming . . . . .	35
2.18	example of flashless forging . . . . .	36
2.19	face and axis temperature trend during a static heating process . . . . .	37
2.20	surface and axis temperature trend during a step heating process . . . . .	37
2.21	electric scheme for hot metal forming: 1 grid supply, 2 transformer, 4 rectifier, 5 leveling inductance, 6 inverter, 7 capacitors for power factor correction, 8 inductor and load . . . . .	38
2.22	range of optimal efficiency for magnetic steel 20°C-1200°C, c = best option, a,b are the border for reasonable choice . . . . .	39
2.23	1 electrical, 2 thermal, 3 global efficiency trends . . . . .	40
2.24	1 electrical, 2 thermal, 3 global efficiency trends . . . . .	40
3.1	example of hot and cold zones division in a work-piece . . . . .	42
3.2	different inductors example . . . . .	42
3.3	thermal fluxes direction . . . . .	42
3.4	ideal thermal profile example . . . . .	43

3.5	42CrMo4 datasheet . . . . .	46
3.6	42CrMo4 thermal conductivity variation with the temperature . . . . .	47
3.7	specific heat capacity variation with the temperature . . . . .	47
3.8	42CrMo4 thermal conductivity variation with the temperature . . . . .	48
3.9	42CrMo4 B-H-T surface . . . . .	48
3.10	42CrMo4 $\mu_r$ -H-T surface . . . . .	49
3.11	42CrMo4 magnetic relative permeability variation with the temperature .	49
3.12	ANSYS Mechanical interface. . . . .	52
4.1	work-piece geometry and 3D rendering . . . . .	58
4.2	optimal frequencies range . . . . .	59
4.3	penetration depth as a function of temperature . . . . .	60
4.4	penetration depth as a function of temperature . . . . .	61
4.5	ANSYS model geometry and model 3D rendering . . . . .	62
4.6	work piece mesh mapping . . . . .	62
4.7	Temperature distribution on the work-piece . . . . .	63
4.8	first: profile on the work-piece, second: temperature difference between the surface and the core . . . . .	64
4.9	second model 3D rendering . . . . .	65
4.10	second model temperature distribution . . . . .	66
4.11	temperature profile and difference between surface and core . . . . .	67
5.1	example of magnetic flux concentrator [FLUXTROLinc] . . . . .	70
5.2	Fluxtrol products . . . . .	70
5.3	FluxtrolA datasheet . . . . .	71
5.4	magnetic field distribution for a short coil with equal currents . . . . .	72
5.5	example of passive shielding . . . . .	72
5.6	example of active shielding . . . . .	73
5.7	induction field profiles . . . . .	73
5.8	shielding effect . . . . .	74
5.9	third model geometry . . . . .	75
5.10	third model 3D rendering . . . . .	75
5.11	process scheme . . . . .	76
5.12	magnetic field distribution in the first step . . . . .	77
5.13	magnetic field distribution in the second step . . . . .	78
5.14	eddy current distribution in the first step . . . . .	78
5.15	eddy current distribution in the second step . . . . .	79
5.16	power distribution in the first step . . . . .	79
5.17	power distribution in the second step . . . . .	80
5.18	third model - temperature distribution along the work-piece . . . . .	80
5.19	third model - thermal profile . . . . .	81
5.20	temperature over time in an hot-zone . . . . .	81
5.21	temperature over time in a cold-zone . . . . .	82
5.22	thermal profile evolution up: along the length, down along the radius (hot zone) . . . . .	83
5.23	cooling profile . . . . .	83
5.24	efficiency . . . . .	84

5.25	power induced in the work-piece . . . . .	84
5.26	speed profile inside a tube . . . . .	85
5.27	water Cp . . . . .	86
5.28	water viscosity . . . . .	87
5.29	water density . . . . .	87
5.30	water thermal conductivity . . . . .	88
5.31	Moody's diagram . . . . .	88
5.32	Dean's vortex example . . . . .	89
5.33	temperature distribution in the hot (up) and cold (down) zone inductor .	90
5.34	current distribution . . . . .	90
6.1	three turns, 25cm work-piece temperature profile . . . . .	92
6.2	zone temperature profile for different currents in the A2 turn . . . . .	93
6.3	37cm workpiece, 7 turns thermal profile . . . . .	94
6.4	hot zone temperature profile for different currents in the A4 turn . . . . .	95
6.5	4 cm diameter temperature profile . . . . .	97
6.6	4 cm diameter temperature profile . . . . .	97
6.7	5 cm diameter thermal profile and temperature distribution . . . . .	99
6.8	6 cm diameter thermal profile and temperature distribution . . . . .	100
6.9	model A and model B 3D rendering . . . . .	101
6.10	temperature distribution model A and B . . . . .	102
6.11	temperature profile, model A and model B . . . . .	103
6.12	power comparison . . . . .	104
6.13	efficiency comparison . . . . .	105



## Sommario

In questo lavoro di tesi è stato affrontato il tema del riscaldamento ad induzione non omogeneo. Questo tipo di processo si basa sull'idea di riscaldare il pezzo di lavoro in diverse zone a diverse temperature. Il processo di forgiatura richiede una fase di preriscaldamento dell'acciaio in modo tale da favorirne la lavorazione. Generalmente tutto il pezzo viene scaldato fino alla temperatura di forgiatura (tipicamente  $1200^{\circ}\text{C}$ ) e successivamente viene formato dagli appositi macchinari. L'idea è dunque quella di indagare sulla possibilità di realizzare un processo di riscaldamento che interessi solamente le zone della billetta che devono essere lavorate in modo da ottenere un risparmio energetico rispetto al processo tradizionale. Il profilo termico richiesto risulta avere un andamento a gradini lungo la lunghezza assiale della billetta prevedendo un alternarsi di zone fredde ( $900^{\circ}\text{C}$ ) e calde ( $1200^{\circ}\text{C}$ ) la cui temperatura deve risultare più uniforme possibile. Inoltre è richiesta anche una distribuzione della temperatura il più uniforme possibile lungo il raggio del cilindro. Poiché la tecnologia dei processi ad induzione prevede un riscaldamento inizialmente di tipo superficiale e, solo successivamente, uniforme lungo il raggio, è difficile riuscire a mantenere un confine netto fra zone calde e fredde in quanto, più è lungo il tempo di processo, più diventa evidente l'effetto di diffusione termica fra una zona e l'altra. L'approccio al problema è stato prevalentemente di tipo numerico in quanto la complessità dei modelli sotto esame era di difficile descrizione analitica. Dopo uno studio preliminare riguardante i parametri caratteristici del materiale (42CrMo4), è stato studiato un sistema molto semplice ovvero composto solamente da due induttori (zone calde) e il pezzo di lavoro (cilindro di acciaio 42CrMo4). Il profilo termico ottenuto, tramite la simulazione agli elementi finiti, non è stato ritenuto accettabile in quanto caratterizzato da un andamento non a gradini e altamente non uniforme all'interno delle singole zone. Per raggiungere il risultato sono stati quindi inseriti dei controllori di flusso, degli induttori per il controllo della temperatura delle zone fredde ed è inoltre stata implementata l'idea della schermatura attiva. Quest'ultima prevede di utilizzare la spira centrale degli induttori in maniera tale da dividere il campo magnetico al loro interno andando quindi a modificare la distribuzione di potenza indotta all'interno delle singole zone. Grazie all'utilizzo di questo metodo è quindi possibile riuscire a teorizzare un processo di riscaldamento diviso in due intervalli. Nel primo intervallo le zone calde vengono scaldate in maniera tradizionale e successivamente, nel secondo intervallo, entra in gioco la schermatura. Per questo motivo le sorgenti di calore si spostano dal centro della zona calda per collocarsi ai bordi della stessa innalzandone la temperatura. Contemporaneamente la temperatura del centro della zona si abbassa e il risultato che ne esce risulta essere un profilo altamente uniforme all'interno della zona stessa. Ottenuto questo risultato è stata poi estesa l'analisi a configurazioni diverse ovvero modificando la lunghezza e il diametro del pezzo di lavoro. Si nota che il processo non è di facile ripetibilità su scale diverse in quanto i parametri (potenza, tempo, frequenza), se modificati anche di poco, comportano grandi differenze nei risultati. Infine è presentato un confronto fra il processo di riscaldamento non omogeneo e tradizionale. Dall'analisi dei risultati è emerso che il processo tradizionale presenta un'unica zona calda alla temperatura di  $1200^{\circ}\text{C}$  e un rendimento medio superiore a quello del processo non omogeneo. Questo perché nel secondo, alcune spire non vengono più utilizzate per riscaldare direttamente la billetta, ma per separare il campo magnetico all'interno delle bobine. Sta di fatto che in ogni caso il processo non

omogeneo richiede un dispendio energetico minore in quanto non tutto il pezzo necessita di essere riscaldato. Tale risparmio è di circa 5.6% rispetto al processo tradizionale. Va comunque aggiunto che la realizzazione pratica del processo di riscaldamento non omogeneo non è stata ancora analizzata ed è difficile effettuare un confronto in termini di costo delle apparecchiature necessarie. Il lavoro di ricerca in questa direzione è destinato a continuare e, molto probabilmente, verranno studiate delle soluzioni per ridurre la complessità dei modelli in gioco, migliorare l'efficienza di processo e semplificare la realizzabilità dello stesso. In ogni caso si può concludere sostenendo che la ricerca sul tema risulta essere molto promettente e di interesse per lo sviluppo in una possibile realtà industriale.

# Chapter 1

## Introduction

In this work has been investigated an innovative idea of inhomogeneous induction heating for forging process. This chapter is a summary of the work, providing a general overview of the contents and an easy identification of the chapters. The aim of this work is to find a way in order to heat a steel billet in different zones at different temperatures. These zones should be hot and cold alternately. The reason which stays under this idea is that heating to the hot forging temperature only the parts which need to be formed instead of heating the whole work-piece should allows to save energy. There is almost no literature about this kind of process so the results which come from these analyses are very new and they need to be verified with many experimental tests. To get the required temperature distribution along the work-piece, the study started with a simple model and then, getting the information from the FEM simulations, it has been updated in order to improve the process. The structure of this thesis consists in six chapters:

Chapter 1: Introduction and summary

Chapter 2: Theoretical Background about the induction heating processes and the forging process. It gives an overview about the analytical equations which stays under these phenomena and a short description about how a forging process is carried on.

Chapter 3: In this chapter is described the idea of the inhomogeneous induction heating process. Also the chosen work-piece is described and its material properties are reported. In the last part there is a description about the used software and how the solution algorithm has been implemented.

Chapter 4: First test and results. Here it is shown how the parameter for the FEM analysis have been decided. There is also the explanation of how the first and the second models are build and the results are reported

Chapter 5: In this chapter are explained the ideas of using the magnetic flux controllers and the active electro-magnetic shielding. After it is possible to find the description of the third model and a deep analysis of its results.

Chapter 6: This is the last chapter. In the first part there is an extension of the analysis in order to have a little amount of information about what happens if the work-piece changes. In particular some test are made changing the length and the diameter of the work-piece. In the last part of the chapter there is a comparison between the inhomogeneous heating process and the traditional induction heating process.





# Chapter 2

## Background and Theory

The induction heating is one of the most used process for heating metals or other electrically-conductive materials. The main advantages that make this kind of technology so diffused and successful are:

- the development of the heating sources is inside the work-piece
- the possibility to localize the heating sources in order to realize custom processes
- the amount of time required for the processes is very low due to the high specific power generated
- high efficiency
- high automatization of the production plants
- very low environment pollution

The heating phenomenon of conductive materials is generated by the action of alternating magnetic fields from alternating currents which circulate into the induction coil. These magnetic fields, that have the same frequency of the current inside the coil, concatenating with the work-piece, induce another type of currents, eddy currents, inside the material which start to be heated due to joule effect. This kind of technology finds many applications in industry world and can be divided in traditional or innovative. The traditional processes consist in:

- hardening ( total hardening or localized)
- forging
- welding and brazing
- melting

There are also, as written above, other applications that do not involve necessarily metallic material like food heating process, paper treatments or chemistry processes.

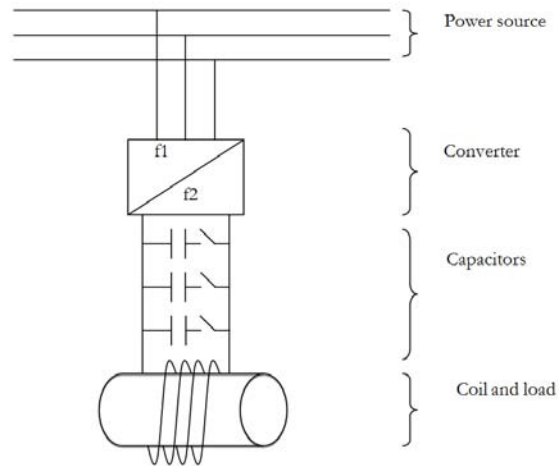


Figure 2.1: induction system scheme

## 2.1 Induction heating system

An induction heating system is made mainly by:

- power source
- frequency converter
- capacitors group
- inductor and load
- cooling system
- control and command system

The power source has the aim to guarantee enough energy to sustain the whole process. The frequency converter is one of the key elements. The choice of the frequency is very important in order to decide the current distribution inside the work piece and then the result of the treatment. The range of used frequencies goes from 50Hz ( industrial frequency) to tens of MHz. For this reason many researcher are working in order to optimize this kind of conversion unit; nowadays with the evolution of power electronics it is possible to find many solution to achieve the best frequency and current required by the process. In fig.2.1it is shown how the conversion technique and heating application are connected with the frequency.

The capacitors group is required in order to set the power factor  $\cos(\varphi)$  as close as possible to 1. Regarding the inductors, there are many shapes and configurations for a lot of different applications. That gives the possibility to realize many kind of localized or special heating also for complex work pieces. Coil design is very important for the efficiency of an induction heating process. The right way is to design the coil by first understanding where the heat needs to be generated in the work piece and then design the coil to reach the heating effect. Induction coils are water-cooled copper conductors made of copper tubing that is readily formed into the shape of the coil for the induction

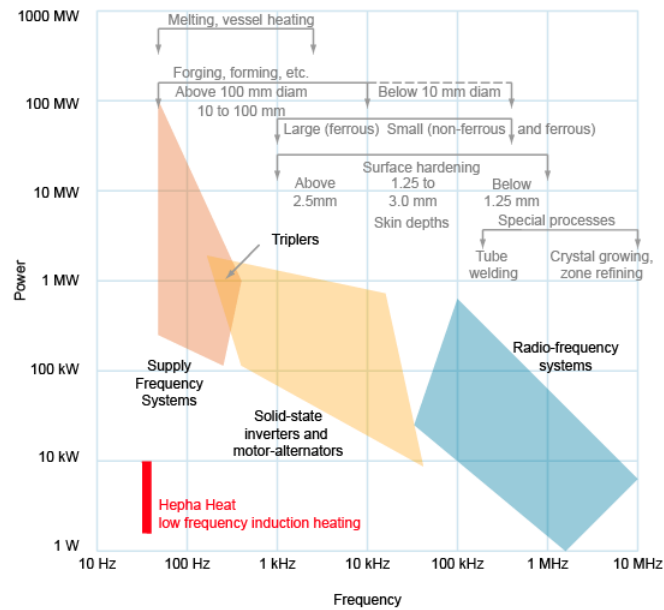


Figure 2.2: power and frequencies required for different treatments

heating process. Induction heating coils are cold and do not themselves get hot when water is flowing through them. Matching the coil to the induction power supply is also essential to the efficiency of the process. Inductors can be designed with different section shape too (square or circular mostly) according to the cost effective goal of the process. Water cooled inductors allows very high density power usage in order to work with small and cheap coils for fast and efficient treatment. A good estimation of the cooling system parameters during the design phase of the project is essential to increase the inductor life time and the process safety. The following table shows the most used inductors types and, as it is possible to see, every different process requires a particular inductor, so with this technology is possible to realize very customizable heating operations.




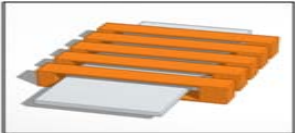
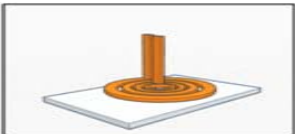
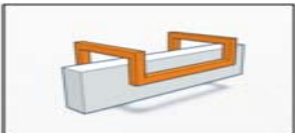
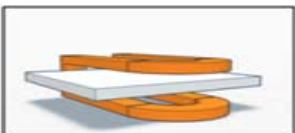
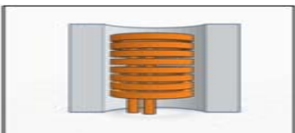
Inductor type	Description	Application
	Long inductor (turns diameter $\gg$ work piece length)	Continuous heating of billets. Round or square section of the tube Homogeneous load of temperature.
	Short inductor ( inductor length $<$ inductor diameter)	Used for high power density, with localized heating: heat treatment, brazing round or square section of the tube.
	Single turn	Continuous hardening of shafts. Required precautions regarding the length of connections.
	Flat inductor	Used for strip heating. Magnetic field more intense at the edges so it is hard do reach an uniform temperature.
	Flat coil inductor	Used for surfaces heating.
	Harpin inductor	Used for bars hardening.
	Transversal flux inductor	High efficiency heating system for continues strip heating.
	Internal inductor	Treating of holes and bores. Not homogeneous heating, smaller diameter on the ends can be used to overcome it.

Table 2.1: Inductor types

### 2.1.1 Physics and theory of induction heating

Let's consider a metal cylinder with constant magnetic permeability and resistivity which is inside an induction coil like in the following figure.

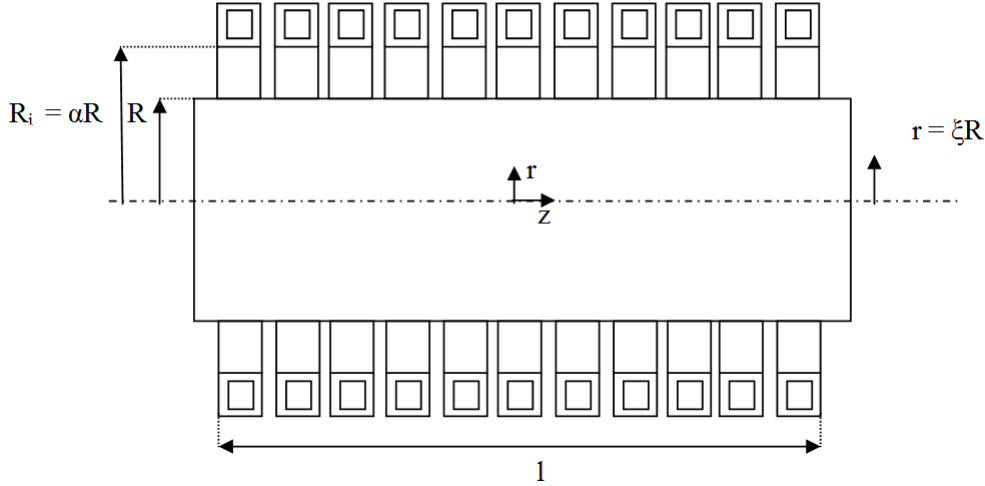


Figure 2.3: inductor and workpiece

Using a cylindrical coordinates system  $(r, \varphi, z)$  it is possible to define all the parameters needed to build the mathematical model of the configuration shown in fig.2.3.

Parameter symbol	Meaning
$R, R_i$	External cylinder radius and internal inductor radius
$\xi = r/R, \alpha = R/R_i$	Ratio between $r$ ( radial coordinate) and the two parameter explained above
$l$	Inductor length
$N$	Number of turns
$I$	RMS current value
$\omega = 2\pi f$	Angular frequency
$f$	Frequency
$\rho, \mu$	Resistivity and permeability
$\mu_0$	Empty space magnetic permeability

Defining  $l$  as a little portion of an infinite cylindrical configuration, the magnetic field in the space between the inductor and the cylinder is directed along the  $z$  axis with the same magnitude as the one generated by a coil without the work piece inside. It is possible to describe this field with the formula:

$$\overline{H}_0 = N \frac{\overline{I}}{l} \quad (2.1)$$

As far as the current is sinusoidal and the frequency is low enough to keep both electric and magnetic field separated, it is possible to write the Maxwell's equations in the following formulation:

$$\begin{cases} \nabla \cdot \bar{H} = \frac{\bar{E}}{\rho} \\ \nabla \cdot \bar{E} = -j\omega\mu\mu_0\bar{H} \end{cases} \quad (2.2)$$

with  $\bar{H}, \bar{E}$  intensity of magnetic and electric fields and  $j = \sqrt{-1}$

In this particular geometry, the only non-zero components are  $\bar{H}_0$  and  $\bar{E}_\varphi$ , so 2.2 can be written as:

$$\begin{cases} [\nabla \cdot \bar{H}]_\varphi = -\frac{\partial \bar{H}_z}{\partial r} = \frac{\bar{E}}{\rho} \\ [\nabla \cdot \bar{E}]_z = -\frac{\partial \bar{E}_\varphi}{\partial r} + \frac{\bar{E}_\varphi}{r} = -j\omega\mu\mu_0\bar{H}_z \end{cases} \quad (2.3)$$

So, removing the indexes  $\varphi$  and  $z$  comes out that:

$$\begin{aligned} \bar{E} &= -\rho \frac{d\bar{H}}{dr} = -\frac{\rho}{R} \frac{d\bar{H}}{d\xi} \\ \rho \frac{d^2\bar{H}}{dr^2} + \frac{1}{\xi} \frac{d\bar{H}}{d\xi} + \beta^2 &= 0 \end{aligned} \quad (2.4)$$

where:

$$\begin{cases} \beta^2 = \frac{-j\omega\mu\mu_0}{\rho} R^2 = -jm^2 = \frac{\sqrt{2}R}{\delta} \\ \delta = \sqrt{\frac{2\rho}{\omega\mu\mu_0}} \cong 503 \sqrt{\frac{\rho}{\mu f}} \rightarrow \text{penetration depth} \end{cases} \quad (2.5)$$

The solution of the second formula from 2.4 is:

$$\bar{H} = C_1 J_0(\beta\xi) + C_2 Y_0(\beta\xi) \quad (2.6)$$

with  $J_0$  and  $Y_0$  order zero Bessel's function from the first kind.  $C_1$  and  $C_2$  are constants which are determined by the following boundary conditions:

$$\begin{cases} \bar{H} \neq \infty \text{ for } \xi = 0 \\ \bar{H} = \bar{H}_0 \text{ for } \xi = 1 \end{cases} \quad (2.7)$$

From the first of 2.7 results that, being  $Y_0(0) = -\infty$ ,  $C_2 = 0$  and from the second it comes that  $C_1 = \bar{H}_0 / (J_0(\beta))$ .

So, eq.2.6 becomes:

$$\bar{H} = \bar{H}_0 \frac{J_0(\beta\xi)}{J_0\sqrt{-jm}} = \bar{H}_0 \frac{J_0(\sqrt{-jm}\xi)}{J_0(\sqrt{-jm})} \quad (2.8)$$

Due to make the computation easier is better to separate the real part and the imaginary part of Bessel's function  $J_0(\sqrt{-jm})$ :

$$J_0(\sqrt{-jm}) = ber(m) + jbei(m)$$

and with this simplification the eq.2.8 becomes:

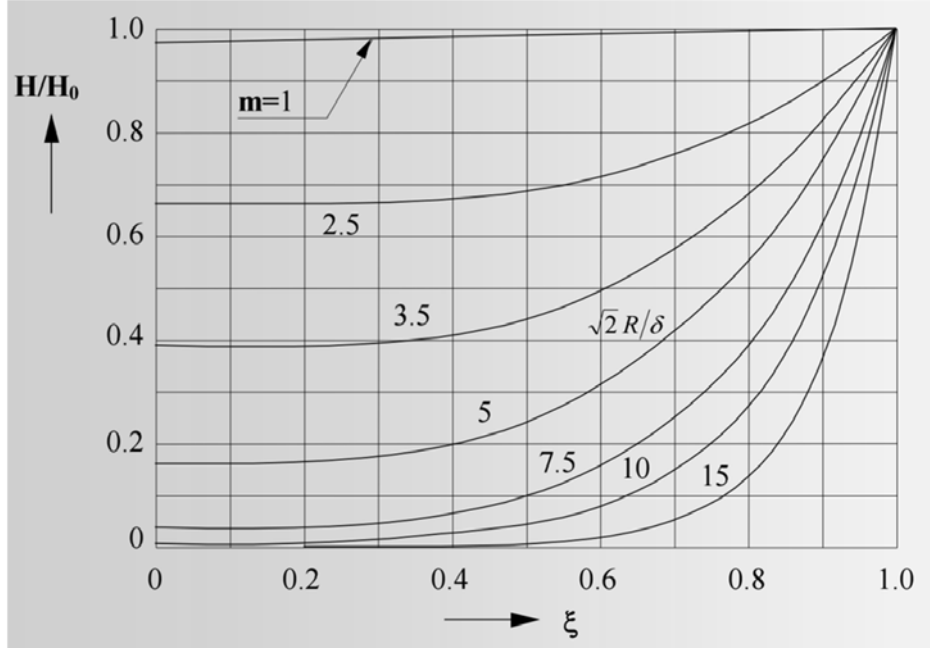


Figure 2.4: relative radial distributions of magnetic field intensity

$$\begin{cases} \bar{H} = \bar{H}_0 \frac{\text{ber}(m\xi) + j\text{bei}(m\xi)}{\text{ber}(m) + j\text{bei}(m)} \\ \left| \frac{\bar{H}}{\bar{H}_0} \right| = \sqrt{\frac{\text{ber}(m\xi)^2 + \text{bei}(m\xi)^2}{\text{ber}(m)^2 + \text{bei}(m)^2}} \end{cases} \quad (2.9)$$

The eq.2.9 shows that moving from the surface of the cylinder it is possible to see that the magnitude and the phase of the magnetic field change. That means that the currents induced into the work piece push the flux lines of the magnetic fields to the surface. This phenomena is stronger when "m" is bigger.

To find the current distribution inside the cylinder it is possible to start from eqs. 2.4 and 2.8. From them, remembering the relation:

$$J_0'(x) = -J_1(x)$$

is possible to write that:

$$\bar{E} = \frac{\sqrt{-j} \bar{H}_0 \rho}{\delta} \sqrt{2} \frac{J_1(\sqrt{-j} m \xi)}{J_0(\sqrt{-j} m)} \quad (2.10)$$

and

$$\bar{G} = \frac{\bar{E}}{\rho} = \sqrt{-j} \frac{\sqrt{2}}{\delta} \bar{H}_0 \frac{J_1(\sqrt{-j} m \xi)}{J_0(\sqrt{-j} m)} \quad (2.11)$$

now it is possible to split the Bessel's functions again in their real and imaginary part, obtaining:

$$\bar{G} = \frac{\bar{E}}{\rho} = -\frac{\bar{H}_0}{R} m \frac{\text{ber}'(m\xi) + j\text{bei}'(m\xi)}{\text{ber}(m) + j\text{bei}(m)}$$

And making the ratio with the values at the surface of the cylinder:

$$\begin{cases} \frac{\bar{E}}{\bar{E}_0} = \frac{\bar{G}}{\bar{G}_0} = \frac{ber'(m\xi) + jbei'(m\xi)}{ber'(m) + jbei'(m)} \\ \left| \frac{\bar{E}}{\bar{E}_0} \right| = \left| \frac{\bar{G}}{\bar{G}_0} \right| = \sqrt{\frac{ber'^2(m\xi) + bei'^2(m\xi)}{ber'^2(m) + bei'^2(m)}} \end{cases} \quad (2.12)$$

In particular from eq.2.11 we get:

$$\begin{cases} \bar{G}_0 = \frac{\bar{E}_0}{\rho} = \sqrt{-j} \bar{H}_0 \frac{\sqrt{2}}{\delta} \frac{J_1(\sqrt{-j}m)}{J_0(\sqrt{-j}m)} = -\frac{\bar{H}_0}{R} m(P + jQ) \\ G_0 = \frac{E_0}{\rho} = \frac{\bar{H}_0}{R} m \sqrt{P^2 + Q^2} \end{cases} \quad (2.13)$$

with:

$$\begin{aligned} P + jQ &= -\sqrt{-j} \frac{J_1(\sqrt{-j}m)}{J_0(\sqrt{-j}m)} \\ &= \frac{ber'm + jbei'm}{ber(m) + jbei(m)} \\ &= \frac{ber(m) ber'm + bei(m) ber'm}{ber^2m + bei^2m} + j \frac{ber(m) bei'm - bei(m) ber'm}{ber^2m + bei^2m} \end{aligned} \quad (2.14)$$

The coefficients P and Q can be found from the next figure as function of m.

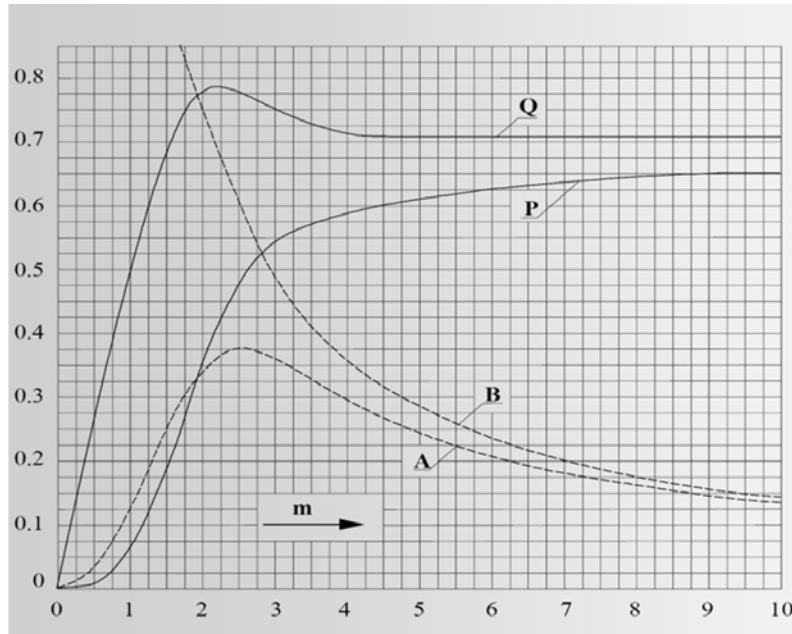


Figure 2.5: P and Q trends as a function of "m", trend of active and reactive power as function of m (A,B)

Then the distribution of the currents inside the work piece looks like fig.2.6  
So from these results has been found that

- moving from the surface to the axis, the currents value decrease and the phase changes



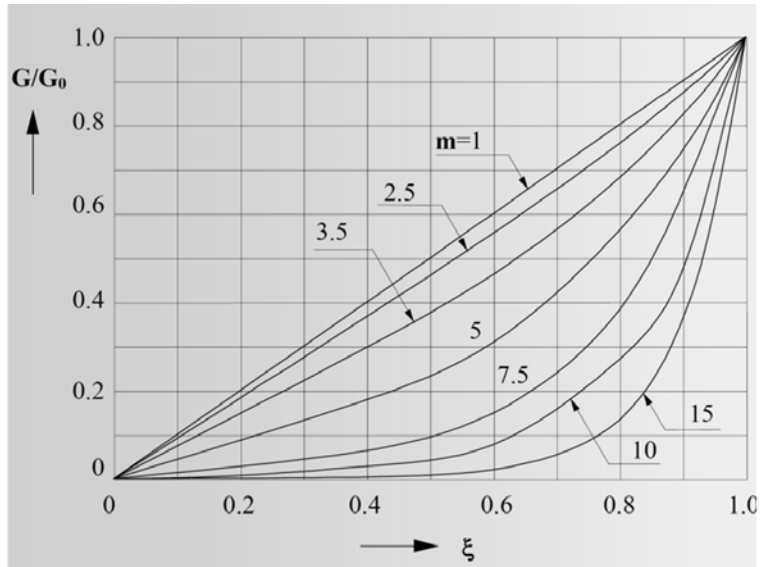


Figure 2.6: relative radial current density distribution

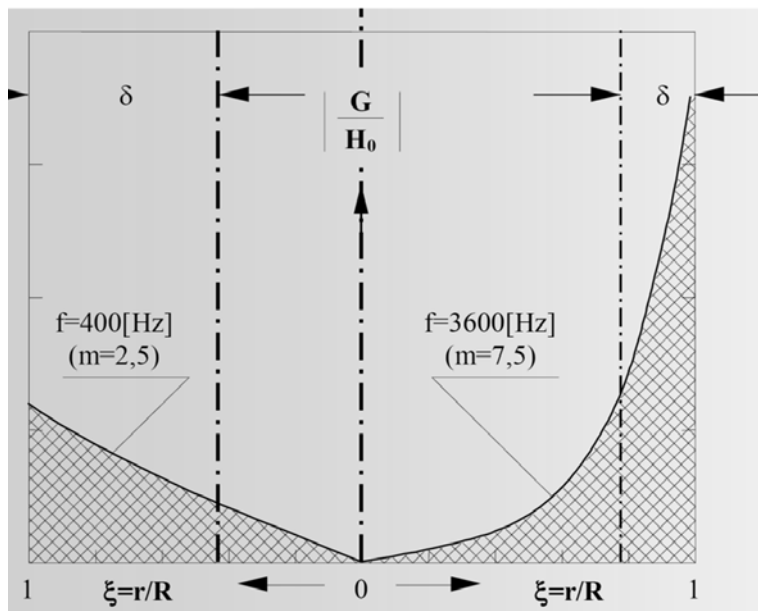


Figure 2.7: current distribution at different frequencies example

- the current distribution is always zero at the axis of the cylinder and it will be closer to the surface when m is higher
- with the same values of R and  $H_0$  increasing m means increasing the magnitude of G
- as it is possible to see in the next example, for "low" frequencies ( $m < 1$ ) the trend of current distribution inside the work piece looks close to be linear and for "high" frequencies ( $m > 12$ ) it looks closer to an exponential function

The power distribution along the radius comes easily from the current one and it can be evaluated like:

$$w = \rho G^2$$

$$w_0 = \rho G_0^2$$

from eq.2.11 and eq.2.12 results:

$$\frac{w}{w_0} = \frac{ber'^2(m\xi) + bei'^2(m\xi)}{ber'^2(m) + bei'^2(m)} \quad (2.15)$$

$$w_0 = \rho \frac{H_0^2}{R^2} m^2 (P^2 + Q^2)$$

That means that the specific power is always not uniform and it decreases quickly moving through the axis as it is shown in the next picture (fig.2.8).

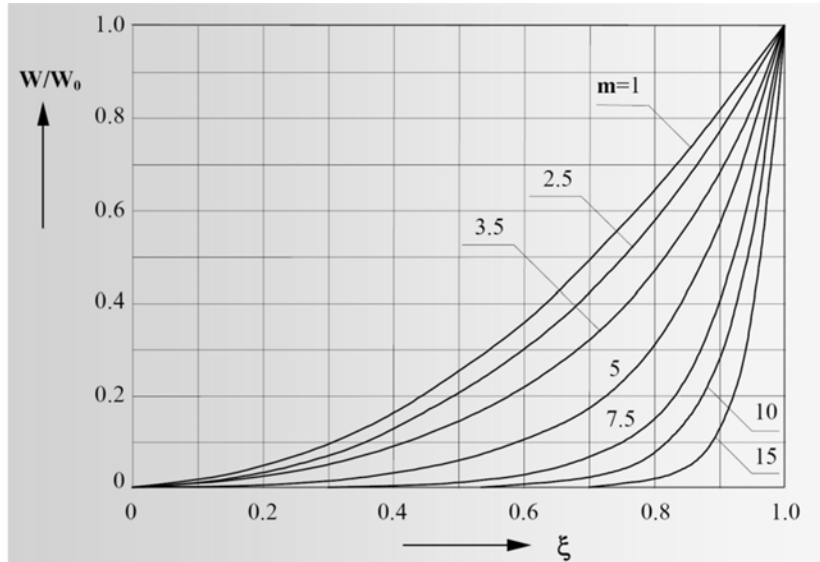


Figure 2.8: relative volume power distribution along the radius

So with induction technology the heating will be always inhomogeneous and if the frequency is very high it can be considered completely shallow.

## Electrical efficiency

The efficiency of the inductor can be evaluated as the ratio between the induced power inside the work piece and the active power drained by the coil.

$$\eta_e = \frac{r'_c}{r_i + r'_c} \quad (2.16)$$

where:

$$r'_c = \frac{N^2 \rho 2\pi R}{l\delta} = \text{load resistance saw by the inductor}$$

$$r_i = \frac{P_i}{I^2} = \frac{N^2 \rho_i 2\pi R_i}{l_i \delta_i} A_i K_i \text{ inductor resistance}$$

$k_i$  = coefficient bigger than one that takes in count of the axial distance from turn to turn

$A_i$  = coefficient used to evaluate the active power in the load

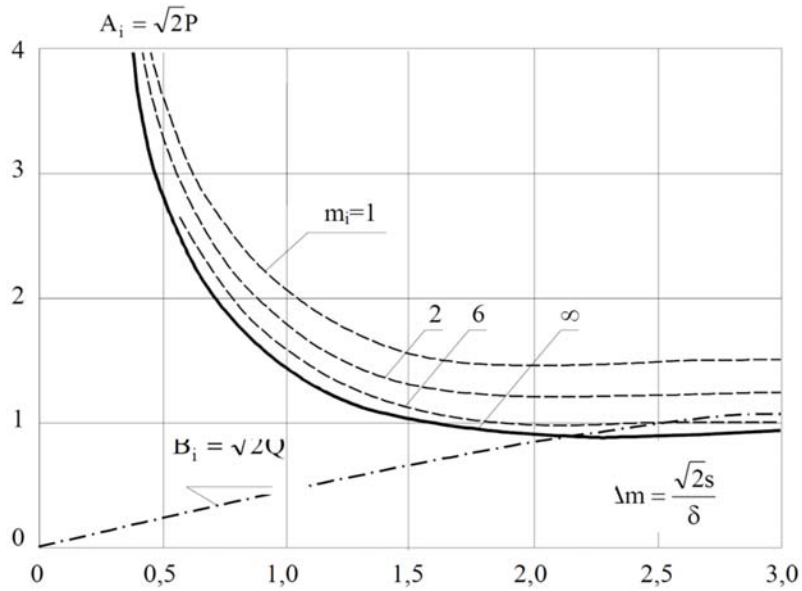


Figure 2.9:  $A_i$  trend as function of  $m$

Putting inside eq.2.16 the value of  $r'_c$  and  $r_i$  the expression of efficiency becomes

$$\eta_e = \frac{1}{1 + \alpha \frac{l}{l_i} \sqrt{\frac{\rho_i}{\rho \mu} \frac{A_i K_i}{\sqrt{2} P}}} \quad (2.17)$$

then it depends from:

- the ratio  $\alpha$  between the diameter of the inductor and the diameter of the work piece and from the ratio between their axial length
- the resistivity of the inductor
- the resistivity and the permeability of the work piece

- the product between  $A_i$  and  $k_i$  that characterize the inductor
- P coefficient which is a function of m (ratio between the radius of the work piece and the penetration depth)

With an optimized design it is possible to reach the best efficiency (for  $l = l_i$ ) which can be written as:

$$\eta_{max} = \frac{1}{1 + \alpha \sqrt{\frac{\rho_i}{\rho \mu}}} \quad (2.18)$$

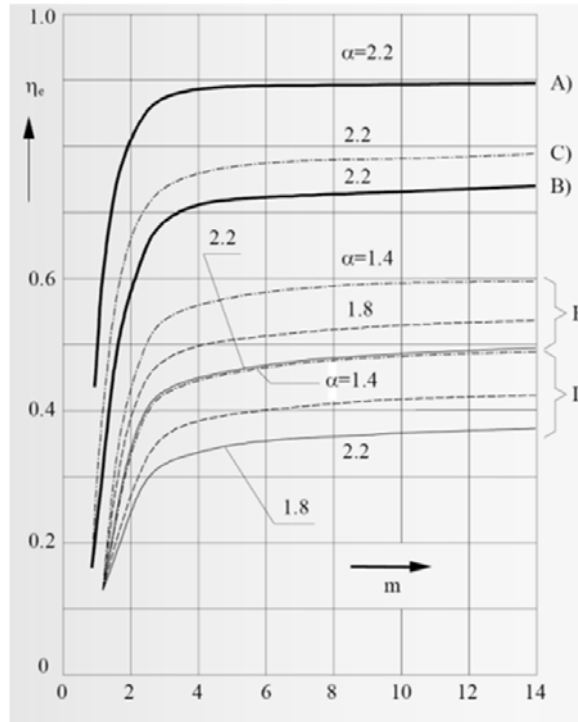


Figure 2.10: electrical efficiency: A - steel heated to 800°C, B - steel heated from 800°C to 1200°C, C - steel from 0°C to 1200°C, D - aluminum heated to 500°C, E - brass heated to 800°C

The picture fig.2.10 shows some examples of the electrical efficiency trend as a function of m and the material.

From these curves is easy to discover that the electrical efficiency is no more frequency dependent when  $m > 2.5$ , but under this value the efficiency is very low. It is important to say that the efficiency falls quickly down increasing  $\alpha$ , that suggests to not use the same inductor for different shaped work piece.

### Thermal transient

Designing an induction heating system, the biggest problem is to estimate the heating time, heating power and how to control the heating power in order to obtain the required thermal distribution inside the work piece. The most common processes are classified in the following two fields:

- differentiate heating : mostly used for hardening, the temperature is different across the section
- uniform heating: mostly used for forging, the temperature across the section should be as equal as possible

Due to what is written in the previous section, with the induction heating technology, it is very easy to get an higher temperature on the surface of the billets so it is very important to analyze the process in order to understand how to control the thermal distribution. The following analysis stays under the following hypothesis:

- long cylinder (length  $\gg$  diameter)
- thermal transmission only along the radius
- material parameter are constant during the heating process.

The Fourier equation in cylindrical coordinates is:

$$\frac{\partial \theta}{\partial t} = k \left( \frac{\partial^2 \theta}{\partial t^2} + \frac{1}{r} \frac{\partial \theta}{\partial r} \right) + \frac{w(r)}{c\gamma} \quad (2.19)$$

where:  $\theta$  = temperature at random radius  $r$  after a time  $t$  from the beginning of heating process

$k = \lambda/c\gamma$  = thermal diffusivity of the work piece (  $\lambda$ -thermal conductivity,  $c$  - specific heat,  $\gamma$  - density)

$w(r)$  = specific power transformed in heat inside the cylinder.

Making the hypothesis of neglecting the surface losses and to begin from  $0^\circ\text{C}$  temperature in every point of the cylinder the eq.2.19 can be solved with the following boundary conditions:

$$\begin{cases} \theta(r) = 0 \text{ for } t = 0 \\ \frac{\partial \theta}{\partial r} = 0 \text{ for } t > 0 \text{ and } r = R \end{cases} \quad (2.20)$$

Introducing the non-dimensional parameters:

$$\xi = \frac{r}{R}, \quad \tau = \frac{kt}{R^2}, \quad \Theta = \frac{2\pi\lambda}{P_u}\theta$$

with:

$$P_u = 2\pi \int_{r=0}^{r=R} r w(r) dr = 2\pi R^2 \int_{\xi=0}^{\xi=1} \xi w(r) d\xi$$

and fixing:

$$\psi = \frac{2\pi R^2}{P_u} w(r) = \frac{w(\xi)}{\int_{\xi=0}^{\xi=1} \xi w(r) d\xi}$$

the Fourier eq. can be rewritten as:

$$\frac{\partial \Theta}{\partial \tau} = \frac{\partial^2 \Theta}{\partial \xi^2} + \frac{1}{\xi} \frac{\partial \Theta}{\partial \xi} + \psi(\xi) \quad (2.21)$$

$$\begin{cases} \Theta(\xi) = 0, \text{ for } \tau = 0 \\ \frac{\partial \Theta}{\partial \xi} = 0, \text{ for } \tau > 0 \text{ and } \xi = 1 \end{cases} \quad (2.22)$$

and remembering eq.2.15

$$\psi(\xi) = \frac{ber'^2 m \xi + bei'^2 m \xi}{ber(m) bei' m + bei(m) bei' m} \quad (2.23)$$

The solution of eq.2.21 is an infinite series obtained using Laplace's transformations. It is very hard to solve it analytically but it can help to obtain a beginning estimation of the process parameters. An uniform heating can be realized only if the parameter  $\tau > 0.25$  that means that the temperature rising speed across the section of the cylinder is the same in every point. That happens when is satisfied the following expression:

$$\pi r^2 c \gamma \frac{\partial \theta}{\partial t} = 2 \pi r \lambda \frac{\partial \theta}{\partial r} + \int_0^r 2 \pi r w(r) dr$$

which balances the power required to increase the temperature with the constant speed  $\frac{\partial \theta}{\partial t}$  and the sum of the power transmitted from the external surface and generated inside the cylinder. Using the non-dimensional parameter it comes:

$$\frac{\partial \Theta}{\partial t} = \frac{4 \pi R^2}{Pu \xi^2} \int_0^\xi \xi w(\xi) d\xi + \frac{2}{\xi} + \frac{\partial \Theta}{\partial \xi} \quad (2.24)$$

The thermal rising speed can be evaluated considering an R radius cylinder with unitary height and the total power Pu turned in heat inside it. Is possible to write:

$$Pu = \pi R^2 c \gamma \frac{\partial \theta}{\partial t}$$

which expressed in non-dimensional parameters is:

$$\frac{\partial \Theta}{\partial \tau} = 2 \quad (2.25)$$

Equalizing the eq.2.24 and 2.25 we have:

$$\frac{\partial \Theta}{\partial \xi} = \xi - \frac{1}{\xi} \frac{\int_0^\xi \xi w(\xi) d\xi}{\int_0^1 \xi w(\xi) d\xi} \quad (2.26)$$

that is not  $\tau$  dependent, so it is possible to determinate  $\Theta$  as a function of  $\xi$  at every time. Solving the integrals and putting inside eq.2.26 the eq.2.21 happens that:

$$\Theta = \frac{1}{2} \xi^2 - \frac{ber^2 m \xi + bei^2 m \xi}{2m(ber mber' m + bei mbei' m)} + C$$

Fixing with  $\Theta_a$  the value of  $\Theta$  for  $\xi = 0$  (axis temperature) it is possible to find the integrating constant C, with the condition:

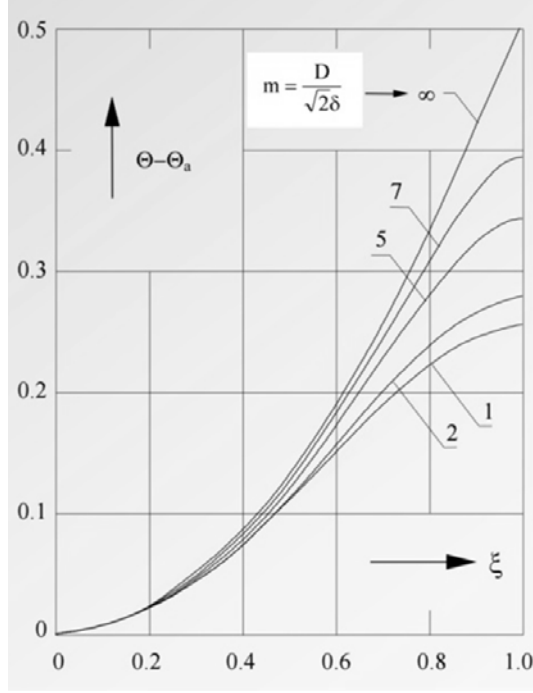


Figure 2.11: radial thermal distribution

$$\Theta = \Theta_a \text{ for } \xi = 0$$

$$\Theta = \Theta_a + \frac{1}{2} \left[ \xi^2 - \frac{ber^2 m \xi + bei^2 m \xi - 1}{m(ber(m)ber' m + bei(m)bei' m)} \right] \quad (2.27)$$

This last equation allows to compute the distribution of the temperature along the radius of the cylinder as a function of axial temperature at a generic time. The picture 2.11 shows how that distribution can be:

For  $m \rightarrow \infty$  it is easy to see that:

$$\Theta - \Theta_a = \frac{1}{2} \xi^2$$

so, considering this particular condition, the process is equal to a surface heating and the distribution follows the parabolic trend. For lower values of  $m$  it is possible to describe the transient with the formula:

$$\Theta_s - \Theta_a = \frac{1}{2} F(m) \quad (2.28)$$

where:

$$F(m) = 1 - \frac{ber^2 m + bei^2 m - 1}{m(ber(m)bei' m + bei(m)ber' m)}$$

then  $F(m)$  can be considered as a correction factor from the surface heating, keeping in count that in the induction heating process the heat is generated inside the cylinder.

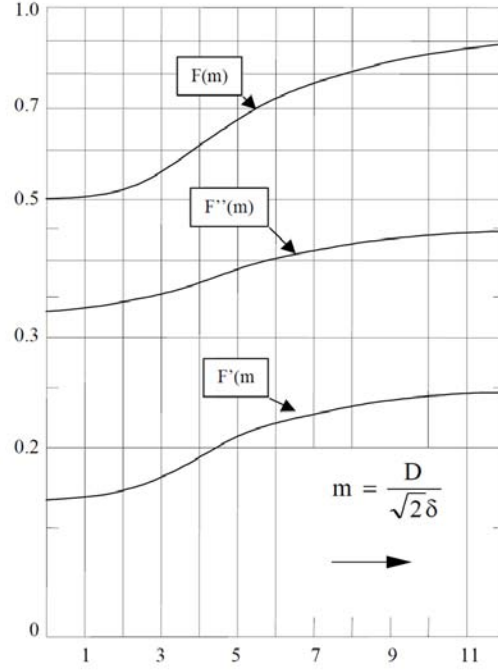


Figure 2.12:  $F(m), F'(m), F''(m)$  trends

The graph fig.2.12 shows the values of  $F(m)$ . To evaluate the heating time is better to consider the average temperature of the cylinder (instead of axis temperature), then:

$$\Theta_m = \frac{2\pi\lambda}{Pu} \theta_m = 2 \int_0^1 \Theta \xi d\xi$$

considering the eq. 2.28 comes:

$$\Theta_m = \Theta_a + F'(m) \quad (2.29)$$

where:

$$F'(m) = \frac{1}{4} - \frac{ber(m)bei'm - bei(m)ber'm - \frac{m}{2}}{m^2(ber(m)ber'm + bei(m)bei'm)}$$

Still considering no surface losses, according to eq.2.25:

$$\Theta_m = 2\tau \quad (2.30)$$

Then mixing eq.2.29 and eq.2.30 we have:

$$\Theta = 2\tau - F'(m) + \frac{1}{2} \left[ \xi^2 - \frac{ber^2 m \xi + bei^2 m \xi - 1}{m(ber(m)ber'm + bei(m)bei'm)} \right] \quad (2.31)$$

and for  $\xi = 1$ :

$$\Theta_s = 2\tau - F'(m) + \frac{1}{2} F(m) \quad (2.32)$$

The equations 2.28 and 2.32 are used to determinate the heating time and the heating power for trough heating process fixing the temperature difference between the core and



the surface. So, calling  $\varepsilon = \frac{(\theta_s - \theta_a)}{\theta_s}$  the temperature difference, it is possible to go on with the formulation writing:

$$\tau = \frac{F(m)}{4\varepsilon} [1 - \varepsilon F''(m)] \quad (2.33)$$

with:

$$F''(m) = 1 - 2 \frac{F'(m)}{F''(m)}$$

At the end we can write the following system:

$$\begin{cases} t = R^2 \frac{F(m)}{4k\varepsilon} [1 - \varepsilon F''(m)] = R^2 \frac{\pi\gamma c}{Pu} \theta_s [1 - \varepsilon F''(m)] \\ P_u = \frac{4\pi\lambda}{F(m)} (\theta_s - \theta_a) = 4\pi\lambda \frac{\varepsilon}{F(m)\theta_s} \end{cases} \quad (2.34)$$

It is important to say that when  $\varepsilon$  is very small (0.05-0.1) the factor  $\varepsilon F''(m)$  can be neglected.

These relations show how important is to choose the right time, the right heating power and frequency in order to obtain a fixed  $\varepsilon$  value and the required thermal profile. As a matter of fact it is possible to conclude that:

- increasing the frequency means to increase  $F(m)$  value then to decrease the specific power  $P_u$  and to increase the heating time
- requiring small  $\varepsilon$  means (at fixed frequency) to decrease the specific power  $P_u$  and to reach the same temperature in a longer time
- fixing the surface temperature and heating time, the specific power is fixed too. The only parameter which can change is the frequency but without an important effect
- fixing the surface temperature and  $\varepsilon$  it is possible to increase the specific power  $P_u$  decreasing the heating time.

It is also now possible to consider the surface radiation losses at the surface of the cylinder. These losses reduce the heating power and increase the heating time, but they reduce also the difference between the surface and axis temperature. In this case then it is possible to use this new system:

$$\begin{cases} t = R^2 \frac{\pi\gamma c}{Pu^*} \theta_s [1 - \varepsilon F''(m)] \\ (\theta_s - \theta_a) = \frac{Pu^*}{4\pi\lambda} F^*(m) \end{cases} \quad (2.35)$$

where  $Pu^*$  is evaluated as the electromagnetic power  $Pe$  minus the surface losses.  $F^*(m)$  can be found in fig-2.13.

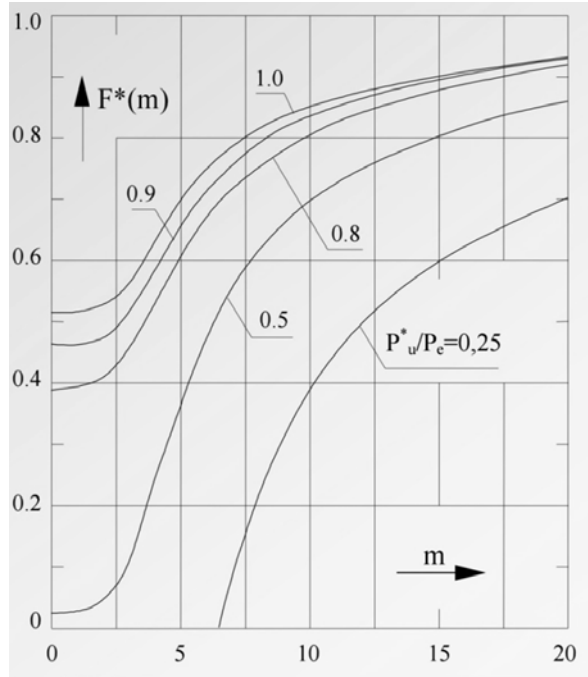


Figure 2.13:  $F^*(m)$  trends as a function of  $m$

### Changing of material properties during the process

The equations from the previous section are written under the hypothesis of constant material parameters during the heating transient. That is a very strong hypothesis that could be considered valid only for short intervals of time. For example, using the magnetic steel, it is very important to pay attention not only at the electrical resistivity, thermal conductivity, specific heat, but also to the permeability that could change with the temperature or with the magnetic field intensity.

$$\mu = \mu(H, \theta)$$

It is possible to say that:

- in the magnetic steels the resistivity changes in a non linear way: it increase five times its values from  $0^\circ\text{C}$  to  $800^\circ\text{C}$  then at higher temperature the rising trend slows down.
- the magnetic permeability depends on the amount of carbon inside the steel too and can be approximately estimated with:

$$\begin{cases} \mu = 1 + \frac{B_s}{H_0} \approx 1 + \frac{14.000 \div 16.000}{H_0} \\ \mu \approx 8.130 H_0^{-0.894} \end{cases}$$

- From the beginning temperature ( $20^\circ\text{C}$ ) to  $500^\circ\text{C}$ - $600^\circ\text{C}$  the permeability is nearly constant, then it decreases quickly at the Curie's point:  $700^\circ\text{C}$ - $800^\circ\text{C}$

Then it is possible to split the heating process in two intervals in which the permeability is nearly constant: the range under the Curie's point and the range over the Curie's

point. The following relations shows an example of typical behavior of a piece made by magnetic steel during an heating process.

$$\begin{aligned} \rho' &= 50 \div 60 \cdot 10^{-8} \text{ [ohm}\cdot\text{m] resistivity under Curie's point} \\ \rho'' &= 100 \div 115 \cdot 10^{-8} \text{ [ohm}\cdot\text{m] resistivity over Curie's point} \\ \mu'' &= 1 \text{ permeability over Curie's point} \end{aligned}$$

$$\frac{\delta''}{\delta'} = \frac{m'}{m''} \approx 3 \div 10 \text{ then } m' \geq (3 \div 10)2.5 = 7.5 \div 25$$

This quickly description is useful to give an idea of the phenomena but is very approximated. In the truth the value of  $m$  changes continuously from an high value (so the eddy currents and the induced power are in a thin layer in the work piece) to lower values so power and currents can enter deeper in the cylinder. It is possible to write the power as:

$$P_0 = H_0^2 \frac{\rho}{\delta} \sqrt{2} P \approx 2.81 \cdot 10^{-3} \sqrt{\rho \mu f P}$$

then if  $\rho$ ,  $\mu$  and  $P$  change with the temperature  $\theta$ , the induced power follows the curves in fig.2.14

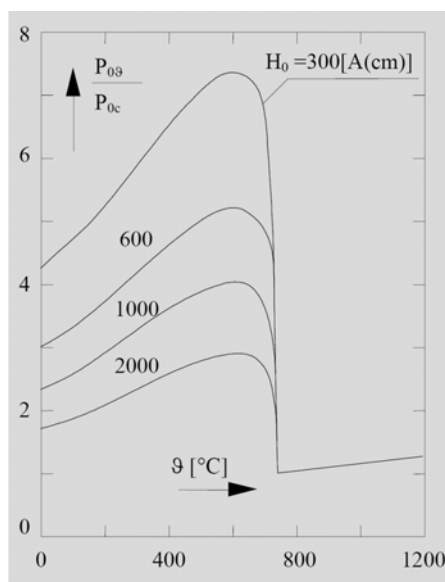


Figure 2.14: trends of the specific power  $P_0$  as a function of temperature.  $P_{0c}, P_{0\theta}$  are the maximum power and the power at  $\theta$  temperature.  $H_0$  is the intensity of the surface magnetic field

It is clearly shown that at the beginning the power rise up due to the rising of the electrical resistivity; then at 500°C-600°C it starts do decrease due to the effect of the magnetic permeability and then it falls down at the Curie's point when the effect of the permeability is much stronger over the rising of the resistivity.

## 2.2 Forging Process

The forging process allows to change the geometric shape of a metal work piece applying compressive forces on it. This is a very important and diffused process in the iron and steel manufacturing industry. Normally metal forging processes are made with an hot work piece because it is better to produce a large amounts of plastic deformation in the part in order to increase the ductility and to have less internal stresses at the end of the operations. Working with hot temperatures allows also to avoid the strain hardening of the material. In any case, if the application requires a strain hardening, it is possible to work with lower temperature. Cold die forging manufacture, which require higher forces, is able to produce better surface finishes and the process is carried on with an higher accuracy than the hot die forming. It is possible to classify the forging processes in three categories:

- open die forging: the work piece is compressed between two die and the metal is not constrained during the process
- impression die forming: the metal flow is controlled using cavities in the die in order to produce the required shape
- flashless forging: in this case all the metal flow is controlled, there is no material that flows outward from the die

A simple way of open die forging is called upsetting in which two flat dies press the work piece changing its shape.

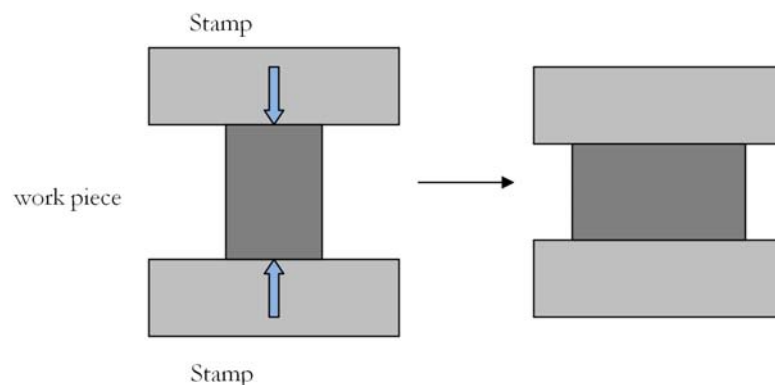


Figure 2.15: example of open die forging

The friction plays an important role during this process, at the work piece-die interface it generates a force that keep the material locked, but in the center of the work piece it can be possible to have some deformations which usually are not wished. This phenomena is called barrel effect. Another thing to consider is that the material near the die decreases its temperature faster than the material in the middle of the work piece. The colder material is more resistant than the hot one, so this also increase the barrel effect. It is possible to control this phenomena using a particular kind of lubrication. Another important open die forging is the cogging process. In this operation two flat or slightly contoured die are employed to compress a work piece, reducing its thickness and increasing

its length. The process goes on by steps in which the dies compress the work piece then they open and move forward and then they close again. The distance travel of the dies is called bite and it is usually between 40-70% of the die length.

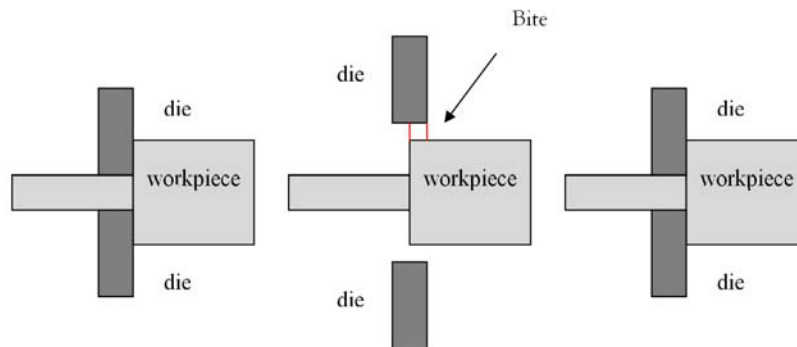


Figure 2.16: cogging forming step example

As written above, the impression die forming is made in order to control the flow of material using particular cavities in the mold. Once compressed, the metal flows to the cavities filling them as long as it is possible to maintain the plastic deformation condition. This kind of process can change the grain structure of the material, then it is better to consider this phenomena during the design of the die. In this operation a variable amount of flash is generated. For this reason usually the initial work piece has a higher volume than the desired piece and the flash is removed in a further process.

Modern technologies allow also to make a process called "precision forming" in which the flash can be produced or not. The result in this case is very close to the final one and needs maybe just few finishing elaborations. The number of working operation is reduced and the waste of material too. The disadvantages are that special machinery are required and the control can be seriously complex. Under this category of processes can be found the flashless forging; there is no waste of material which fills completely the cavities placed in the dies. This operation requires a very precise design and control, if it is not right set it is possible to brake the forging machine with very dangerous consequences.

The metal choice is very important in order to have a good result. The ability of the work piece to experience deformation without cracking or failure is an essential

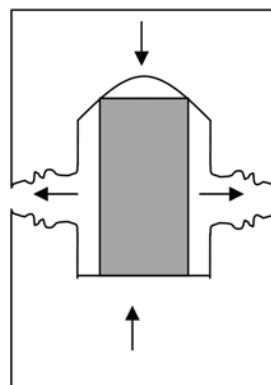


Figure 2.17: example of impression die forming

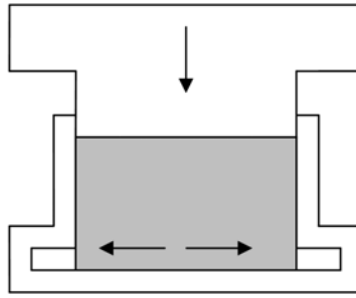


Figure 2.18: example of flashless forging

characteristic. In this kind of industry several test have been done in order to quantify and qualify this ability. The amount of deformations that a metal can sustain without failure is called metal forgeability.

### Induction heating and forging process

The heating of metal billets, rods or sheets for hot forming must be done in order to achieve the best temperature distribution to allow the plastic deformation. The next table shows the typical temperature range for metal forging.

Process type	C-steel	Inox steel	Copper	Aluminum	Titanium
Extrusion	1320°C	1300°C	870°C	480°C	950°C
Lamination	1320°C	1260°C	760-840°C	480-540°C	930°C
Forging	1100-1300°C	1200-1320°C	870°C	450°C	930°C

This method is replacing the traditional gas or coal heating. The advantages of induction heating for metal forging are:

- continuous and automatized process with better final results
- short heating time and controlled temperature
- increasing of production
- minor surface oxidation
- longer dies lifetime
- less space required by the machinery
- possibility to stop the process for short time
- less pollution

and the disadvantages

- higher price of the machinery

- hard to reach uniform temperature distribution for complex shaped work pieces
- the inductor must be changed every time that the shape of the work piece changes

These heating process can be divided in three different kind:

- static heating: the work piece is put inside the coil until it reaches the required temperature, then it is picked out and transported to the working machineries. The inductor is now free to heat another piece. The typical temperature trends that come out from this kind of heating process are shown in fig.2.19:

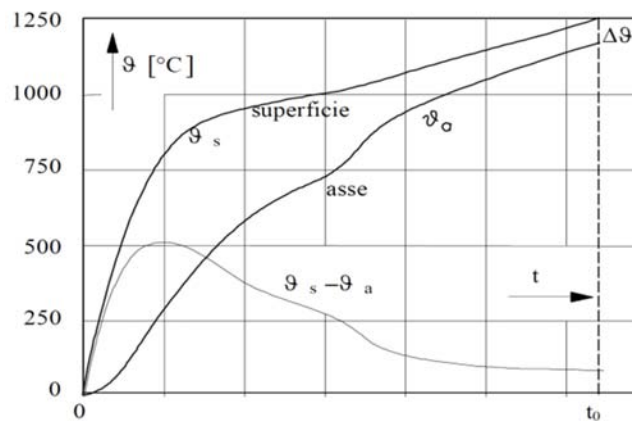


Figure 2.19: face and axis temperature trend during a static heating process

- step heating: three or four inductors are used and the work piece occupies each of them for 1/2 -1/3 of the whole process time. After the first cycle every inductor is working so the process becomes semi-continuous. With this technology the impedance of every inductor is fixed in order to have the best result for every step of the heating time. Typical temperature trends are shown in fig.2.20:

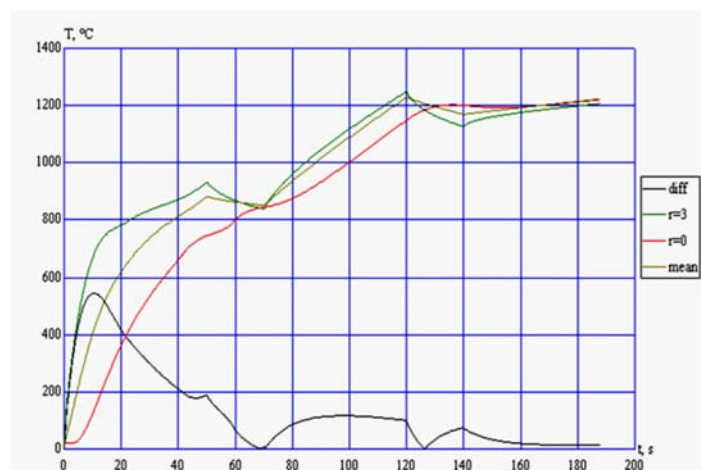


Figure 2.20: surface and axis temperature trend during a step heating process

A plant for through heating is made by one or more inductors and further electrical machineries ,like transformers, converters, switches and capacitors, in order to achieve the required frequencies and currents and by other mechanical machines to load and unload the inductors.A typical scheme to connect the whole system to the grid is:

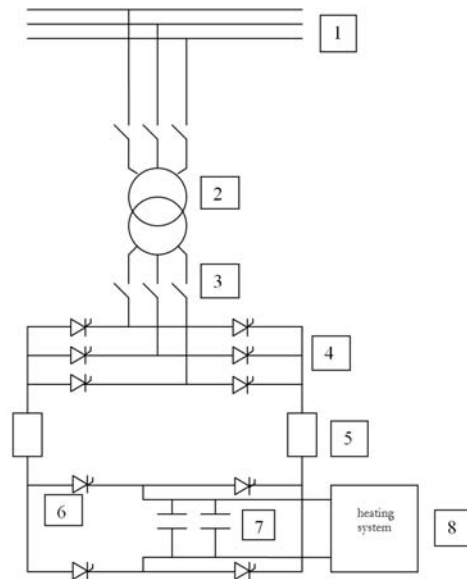


Figure 2.21: electric scheme for hot metal forming: 1 grid supply, 2 transformer, 4 rectifier, 5 leveling inductance, 6 inverter, 7 capacitors for power factor correction, 8 inductor and load

The choice of the frequency is connected to the section diameter of the billets, keeping in mind that to decrease the process time is better to have low values of "m" and remembering that it should be at least bigger than 2 -2.5 to have a good efficiency. Anyway an high value of "m" is not advisable because it will affect the thermal efficiency and it will generates hot spots in the surface of the work piece. So it is possible to summary:

- $m < 2$  low electrical efficiency
- $m = 2.5$  optimal efficiency
- $2 < m < 5$  reasonable efficiency
- $m > 7$  low thermal efficiency

With these information it is possible to find the values for the best efficiency as a function of the diameter, the pictures 2.22 shows them for magnetic steels heated from environment temperature to 1200°C. The middle zone represents the optimal choice and the border zone represents the reasonable choice.

As the choice of the frequency, it is very important also to estimate the process time and the specific power; it is better to focus at the radial temperature distribution that must be as uniform as possible in order to avoid cracks. For magnetic steels, keeping in mind that at the Curie's point the material parameters change drastically, to analyze the process it is possible to split it in two parts, each at the same specific power. Under this



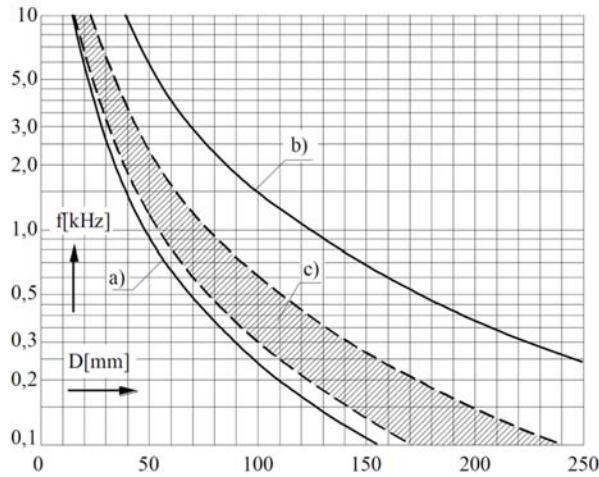


Figure 2.22: range of optimal efficiency for magnetic steel 20°C-1200°C, c = best option, a,b are the border for reasonable choice

hypothesis the heating time can be evaluated considering an ideal heating process made at constant power with the material parameters estimated over the Curie's point. So, for uniform inductors it is possible to say that:

- under the Curie's point the value of  $m$  is very high, normally greater than 25
- the induced power over the Curie's point is totally minor than before the Curie's point
- the first part of the work piece that reaches the Curie's point is the border
- the time can be estimated referring to the 50% of the time estimated with the method explained above.

Regarding the efficiency, it is better to analyze separately the electrical one and thermal one and then combine them. The electrical efficiency for magnetic steels can be defined weighting the values before and under the Curie's point. Generally it is between 0.75 and 0.8. The thermal efficiency keeps in count the radiation and convection losses from the work piece and from the coil. It is possible to reduce them using opportunely a refractory material between the coil and the work piece. Normally the thermal efficiency is around 0.8-0.9. The picture 2.23 shows the trends of the electrical, thermal and global efficiency.

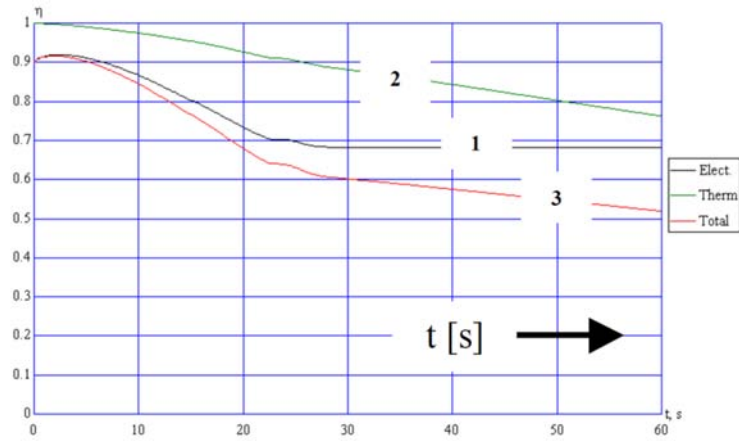


Figure 2.23: 1 electrical, 2 thermal, 3 global efficiency trends

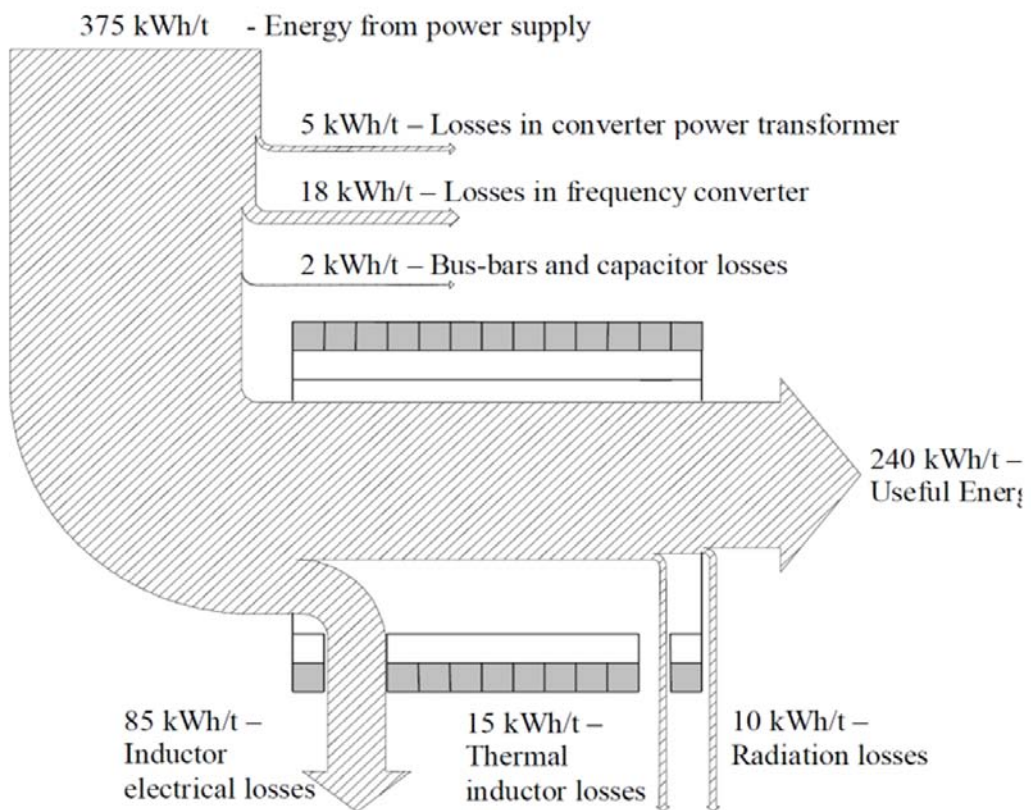


Figure 2.24: 1 electrical, 2 thermal, 3 global efficiency trends

# Chapter 3

## Description of the problem

Induction heating is a very flexible technology which can be realized in many different ways. It is possible to adapt it for many custom processes for example to heat complex shaped objects, to heat in a localized way and to make all operations faster. In this research project, a particular field of this technology has been investigated. There is not much literature about it, so the analysis that has been done is very new and innovative. It is important to say that this topic is still in its initial state and has to be developed further. The problem is about "inhomogeneous heating", so about a specific kind of process which its aim is to heat different zones of a work piece at different final temperatures. This can be very useful for the metal manufactory because, heating only the parts of a billet which need to be formed, allows to save energy for the whole process and to make all the operation in a more precise and controlled way. The investigations have been done building a FEM model which is made by a 42CrMo4 cylinder, several inductors disposed in a particular way, iron flux controllers and cooling system. To reach the results many tests have been tried, improving step by step the accuracy of the thermal profile on the billet and extending the analysis for other possible pieces, like changing the axial length or the diameter.

### 3.1 The goal of the investigation

As it is written in the introduction chapter, the main aim of this investigation is to realize an induction heating system that is able to heat a billet in different zones at different temperatures. To make this idea more understandable it is necessary to define the concept of hot zone and cold zone. The hot zones are the parts of the material that have to be formed by the forging machines. So they must be heated to a suitable temperature in order to turn the material in its forging status. The cold zones are that parts which do not require to be machined, so they do not need to be heated up to the hot forging temperature but just to the cold forging temperature.

To realize this heating process, the idea is to heat the hot zones and the cold zones with different inductors which means different currents supply, different induced power and then different temperature distribution.

The problem which makes this thermal configuration hard to reach is that the temperature must be very homogeneous along the radius and the division between hot and cold zones should be as clear as possible. These last two things do not behave in the

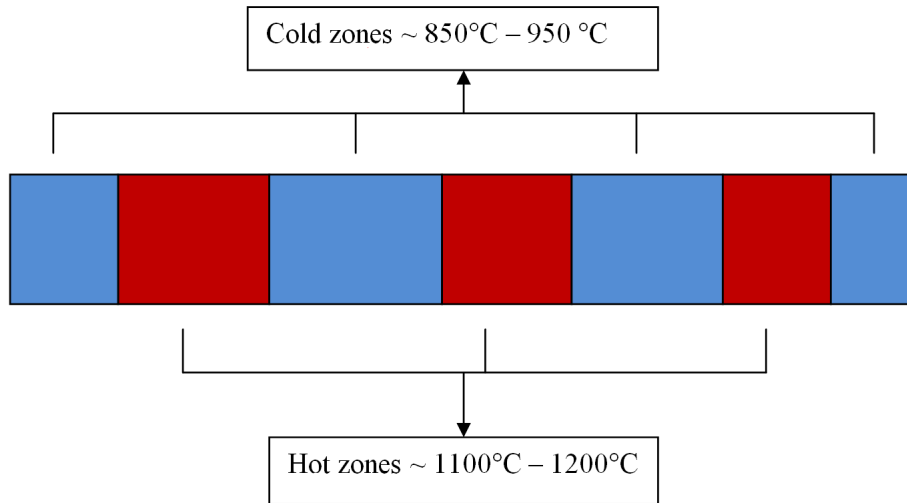


Figure 3.1: example of hot and cold zones division in a work-piece

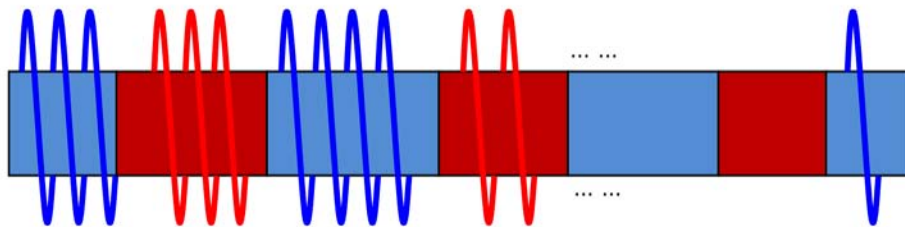


Figure 3.2: different inductors example

same direction because, as explained in chapter II, the heat, generated with induction technology, starts to rise from the surface of the work-piece and, as the penetration depth increases, goes to the core. In the same time the thermal flux diffuses from the hot zone to the cold zone due to the high thermal gradient. In other words, requiring an uniform temperature distribution in the cross section involve to have a longer heating time, but a longer heating time weakens the boundaries between hot and cold zones. So it is essential to choose the right heating power and the right heating time in order to combine these phenomena as better as possible.

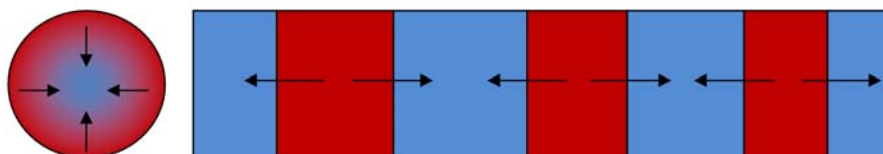


Figure 3.3: thermal fluxes direction

Also the temperature in each zone must be as equalized as possible along the length and along the radius. This can be complicated because the induced power inside the work piece is not uniform during the process and it is possible to have some distortions in the

thermal profile due to the border effect in the induction coil, or, for short coils, a bigger induced power in the center. So, after these consideration, the ideal thermal profile along the axis and along the radius is shown in fig-3.4.

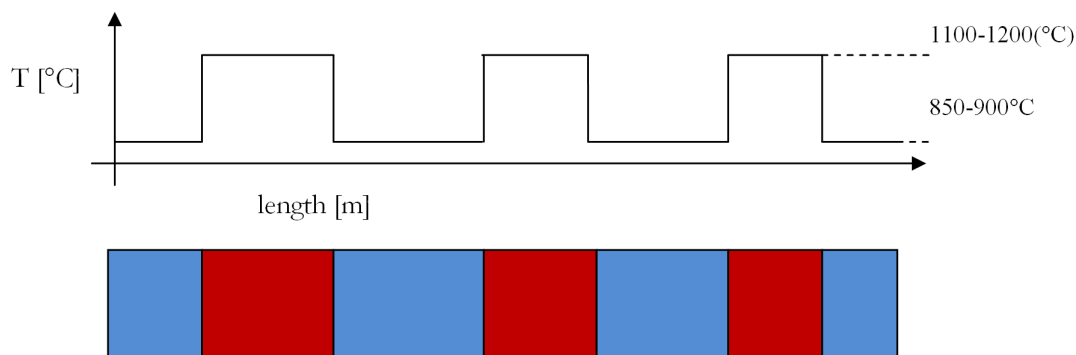


Figure 3.4: ideal thermal profile example

Obviously this profile is not physically possible because at the interfaces between the hot and the cold zone there will be always a "transition zone" in which the temperature decreases or increases connecting the two zones.

## 3.2 The work-piece

As it is written in the introduction of the chapter, the work-piece is a cylinder of 42CrMo4 steel. 42xx steel is a family of SAE steel grades, as specified by the Society of Automotive Engineers (SAE). Alloying elements include chromium and molybdenum, and as a result these materials are often informally referred to as chromoly steel (common variant stylings include chrome-moly, cro-moly, CrMo, CRMO, CR-MOLY, and similar). They have an excellent strength to weight ratio and are considerably stronger and harder than standard 1020 steel, but are not easily welded (need pre and post weld thermal treatment to avoid cold cracking). 42CrMo4 alloy is a high grade steel alloy containing Ferro (Fe) rest, Carbon (C) 0.38-0.45, Chromium (Cr) 0.90-1.20, Molybdenum (Mo) 0.15-0.25, Silicon (Si) 0.17-0.37, Manganese (Mn) 0.50-0.80, Sulphur (S). Many automotive companies and manufacturers use 42CrMo4 alloy to produce automotive parts by Cold and Hot Forging. This material is commonly used to make components that are used for high stress applications and subject to mechanical wear, such as axles, drive rods, crankshafts, pinions, gears, springs, saw blades, and bolts. Other examples of applications for 42CrMo4 steel also include structural tubing, connection rods, stem assemblies, tool holders and locomotive traction.

The figure 3.5 shows 42CrMo4 technical data.



(a) *pinion shaft.*



(b) *crank shaft.*

### 3.2.1 42CrMo4 material properties for FEM analysis

To carry the analysis it is necessary to know how the following parameters change with the variation of the temperature:

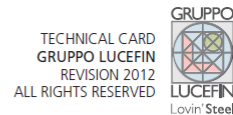
- thermal conductivity -  $\lambda$
- specific heat capacity -  $c_p$
- electrical resistivity -  $\rho$
- relative magnetic permeability -  $\mu_r$

The thermal conductivity  $\lambda$  is the property of materials to conduct heat and its reciprocal is called thermal resistivity. In the SI system the unit for the thermal conductivity is  $W/(m \cdot K)$ . The effect of the temperature on this parameter is different for metals and non metals. For metals this effect is due to the number of free electrons in their chemical composition. According to the Wiedemann-Franz law it is possible to say that the thermal conductivity is proportional to the absolute Kelvin temperature times the electrical conductivity. Then, for metals, the thermal conductivity is quite high compared as others materials and the metals which are the best electrical conductors are also the best thermal conductors. In the graph fig.3.6 the trend of  $\lambda$  for the 42CrMo4 is shown.

The specific heat capacity of a substance is defined as the amount of heat necessary to increase (or decrease) the temperature of a unit mass of 1K (or equivalent  $1^\circ C$ ). In the SI unit system the  $c_p$  is expressed as  $J/KgK$ . From the electron theory of the specific heat it is known that the increase in heat capacity as a function of the temperature is linear at small temperature alterations, but is in accordance exponential functions in other ranges. The anomalous increase of the specific heat capacity which occurs when heating up to the Curie temperature  $T_c$  is necessary for overcoming the exchange forces causing the magnetic properties. In the next figure it is possible to see the trend of the specific heat capacity for 42CrMo4 as a function of the temperature.

As it is possible to see from the fig.3.7, the Curie's temperature for 42CrMo4 is between  $750^\circ C$  and  $800^\circ C$ . The electrical resistivity  $\rho$  is a property that describes how strongly a given material opposes the flow of the current. In the SI unit system it is expressed as  $\Omega m$ . On fig.3.8 it is shown how the resistivity changes with the temperature. As it is

<b>Quality</b>	<b>42CrMo4</b>
According to standards	<b>EN 10269 (AC: 2008)</b>
Number	<b>1.7225</b>



### Chemical composition

C%	Si%	Mn%	P%	S%	Cr%	Mo%	
0,38-0,45	0,40	0,60-0,90	0,025	0,035	0,90-1,20	0,15-0,30	Product deviations are allowed
± 0.02	+ 0.03	± 0.04	+ 0.005	+ 0.005	± 0.05	± 0.03	

### Temperature °C

Hot-forming	Normalizing +N	Quenching +Q	Quenching +Q	Tempering +T	Stress-relieving +SR		
1100-850	870 air	860 oil or polymer	850 water	540-680 air	50° under the temperature of tempering		
Soft annealing +A	Isothermal annealing +I	Spheroidizing annealing +AC	End quench hardenability test	Pre-heating welding	Stress-relieving after welding		
720 air (HB max 241)	820 furnace cooling to 670, then air (HB 180-240)	730-740 furnace cooling (HB max 200)	840 water	300	550 furnace cooling		
				<b>Ac1</b> 745	<b>Ac3</b> 790	<b>Ms</b> 335	<b>Mf</b> 120

### Mechanical properties

Hot-rolled +QT EN 10269 (AC: 2008)

size mm		Kv and traction test at room temperature in longitudinal								
from	to	R	Rp 0.2	A%	C%	Kv +20 °C	Kv -40 °C	Kv -100 °C	HB	
	60	860-1060	730	14	50	50	40	27	258-322	

+QT = quenched and tempered

Min. proof strength 0.2 % at high temperatures				Rp 0.2 N/mm <sup>2</sup> - EN 10269: 2001								
d. max	60 mm	720	702	677	640	602	562	518	475	420	375	
	°C	50	100	150	200	250	300	350	400	450	500	550

### Plastic deformations and creep rupture resistance

°C	$\sigma_1$ (1%) N/mm <sup>2</sup>		$\sigma_R$ N/mm <sup>2</sup>	
	10.000 h	100.000 h	10.000 h	100.000 h
450	190	137	320	240
500	88	49	137	96
550	29	15	29	15

$\sigma_1$  = permanent creep strain strength 1%

$\sigma_R$  = creep rupture strength

<b>Thermal Expansion</b>	$10^{-6} \cdot K^{-1}$	▶	12.1	12.7	13.2	13.6	14.0	14.4		
<b>Mod. of Elasticity long.</b>	GPa		210	205	195	185	175	155		
<b>Mod. of Elasticity tang.</b>	GPa		80	78	75	70	67	59		
<b>Specific Heat Capacity</b>	J/(Kg.K)		460							
<b>Thermal Conductivity</b>	W/(m.K)		33.5		34.0		34.2			
<b>Density</b>	Kg/dm <sup>3</sup>		7.85							
<b>Specific Electric Resist.</b>	Ohm.mm <sup>2</sup> /m		0.19							
<b>Electrical Conductivity</b>	Siemens.m/mm <sup>2</sup>		5.26							
°C			20	100	200	250	300	400	500	600

The symbol ▶ indicates temperature between 20 °C and 100 °C, 20 °C and 200 °C ...

Kv and traction test at room temperature in longitudinal on hot-rolled +QT material. **Lucefin** experience

diameter mm	grain size	R	Rp 0.2	Rp/R	A%	C%	Kv +20 °C	Kv -20 °C
		N/mm <sup>2</sup>	N/mm <sup>2</sup>		min.	min.	J min.	J min.
40	6	995	845	0,85	15,2	58	90-90-92	60-58-58
60	5-6	947	767	0,81	16,0	60	84-78-80	50-50-56

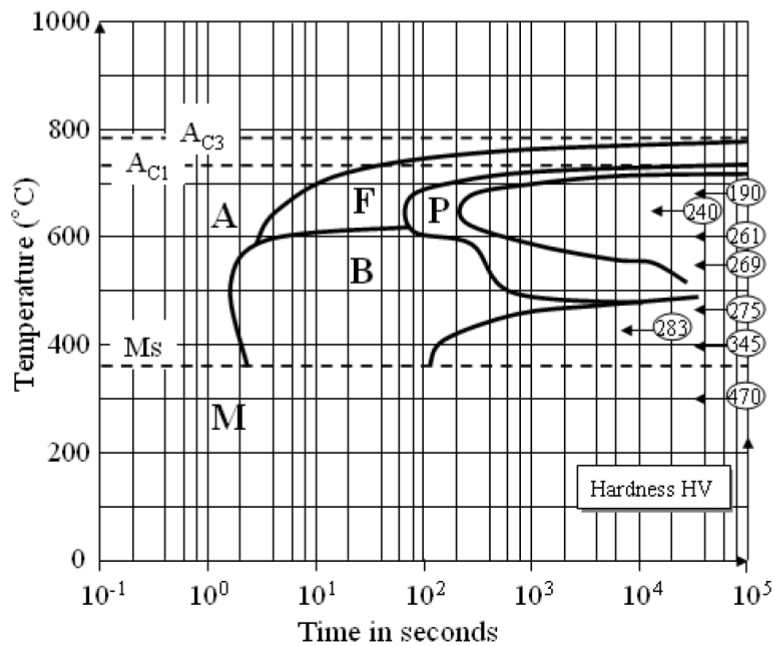
### 42CrMo4 1.7225

#### Data under fatigue +20 °C

+N	328	Cyclic yield strength, $\sigma_y'$
+QT	716	N/mm <sup>2</sup> low cycle number
+N	0.12	Cyclic strength exponent, $n'$
+QT	0.10	low cycle number
+N	673	Cyclic strength coefficient, $K'$
+QT	1367	N/mm <sup>2</sup> low cycle number
+N	1000	Fatigue strength coefficient, $\sigma_f'$
+QT	1454	N/mm <sup>2</sup> low cycle number
+N	-0.11	Fatigue strength exponent, $b$
+QT	-0.08	low cycle number
+N	-1.00	Fatigue ductility exponent, $c$
+QT	-0.72	low cycle number
+N = normalization +QT = quenching and tempering		

EUROPE	ITALY	CHINA	GERMANY	FRANCE	U.K.	RUSSIA	USA
EN	UNI	GB	DIN	AFNOR	B.S.	GOST	AISI/SAE
42CrMo4	42CrMo4	ML42CrMo	42CrMo4	42CD4	708M40	42HM	4140

T.T.T. curve



THE DATA CONTAINED HEREIN ARE INTENDED AS REFERENCE ONLY AND ARE SUBJECT TO CONSTANT CHANGE. LUCEFIN S.P.A. DISCLAIMS ANY AND ALL LIABILITY FOR ANY CONSEQUENCES THAT MAY RESULT FROM THEIR USE.

Figure 3.5: 42CrMo4 datasheet



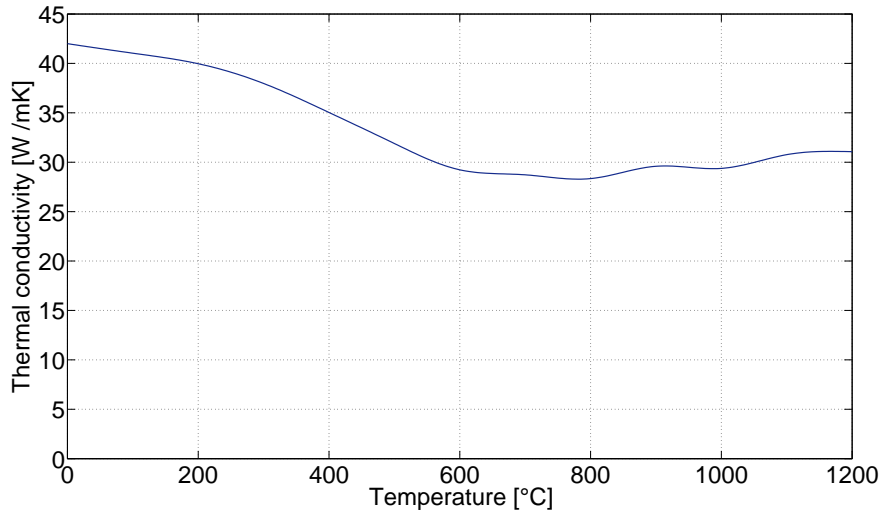


Figure 3.6: 42CrMo4 thermal conductivity variation with the temperature

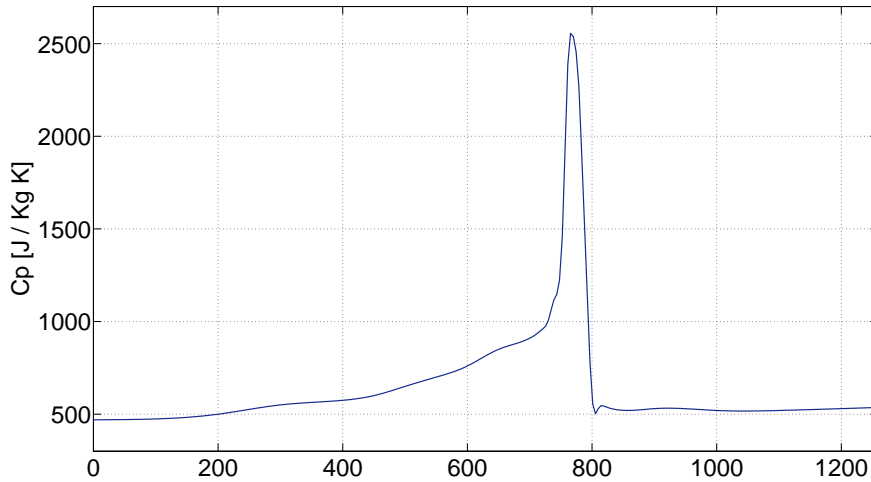


Figure 3.7: specific heat capacity variation with the temperature

written in chapter 2, this parameter rise up in a non linear way: between 0°C and 800°C it increases nearly five times its values and then from 800°C to 1200°C just one.

In physics, in particular in electromagnetism, the magnetic permeability of a material is a physical quantity that expresses the material's ability to become magnetized in the presence of a magnetic field. The magnetic permeability is measured in henry per meter (H /m). Almost all homogeneous media have a magnetic permeability that can be considered constant, however, for some substances (such as iron, cobalt, nickel) it has a behavior that manifests a certain hysteresis, for example the permeability shows a dependence on previous magnetization and demagnetization suffered by such materials. The substances for which such behavior occurs are said ferromagnetic. Regarding the magnetic relative permeability of our work-piece, it has been evaluated from a chart in which it is reported a family of B-H curves at different temperatures for the 42CrMo4.

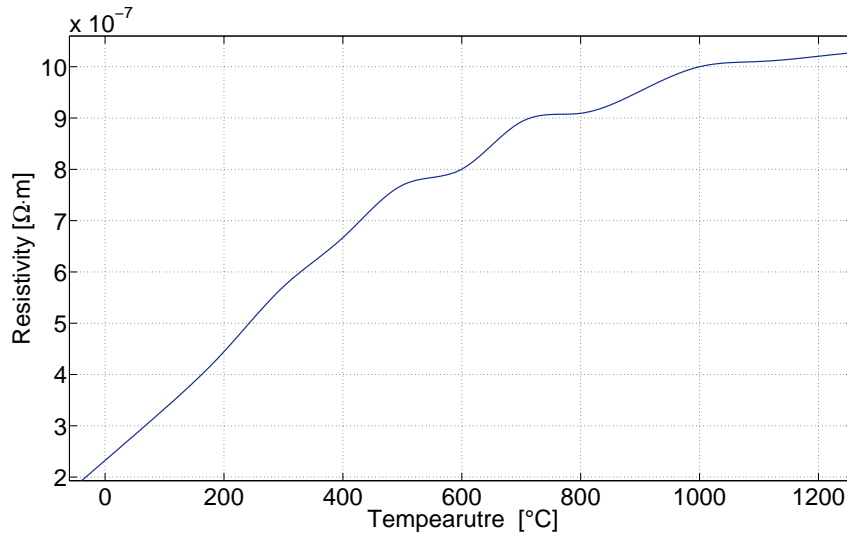


Figure 3.8: 42CrMo4 thermal conductivity variation with the temperature

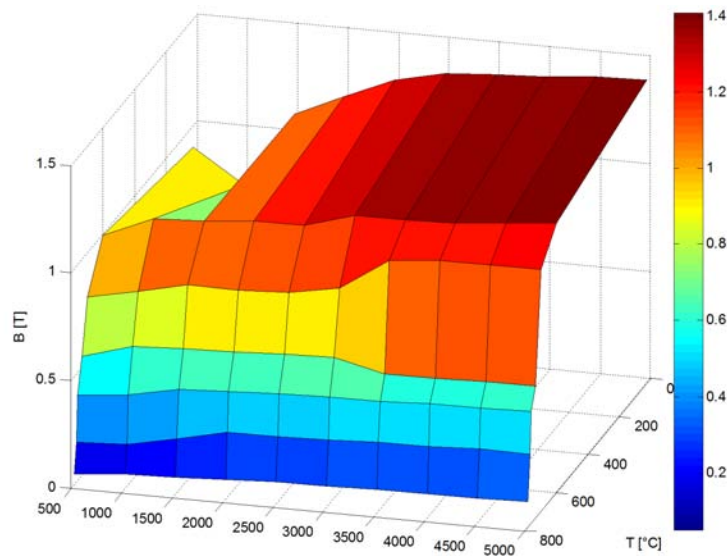


Figure 3.9: 42CrMo4 B-H-T surface

Knowing the relation

$$B = \mu H$$

it is possible to build the  $\mu_r$ - $H$ - $T$  surface starting from the formula:

$$\mu_r = \frac{B}{H \cdot \mu_0}$$

obtaining the fig.3.10:

To implement this parameter in the fem model it is better to neglect the H dependence. This simplification is reasonable because in this application the magnetic field is always bigger than 5000A/m and focusing on the surface of fig.3.10 it is easy to notice that

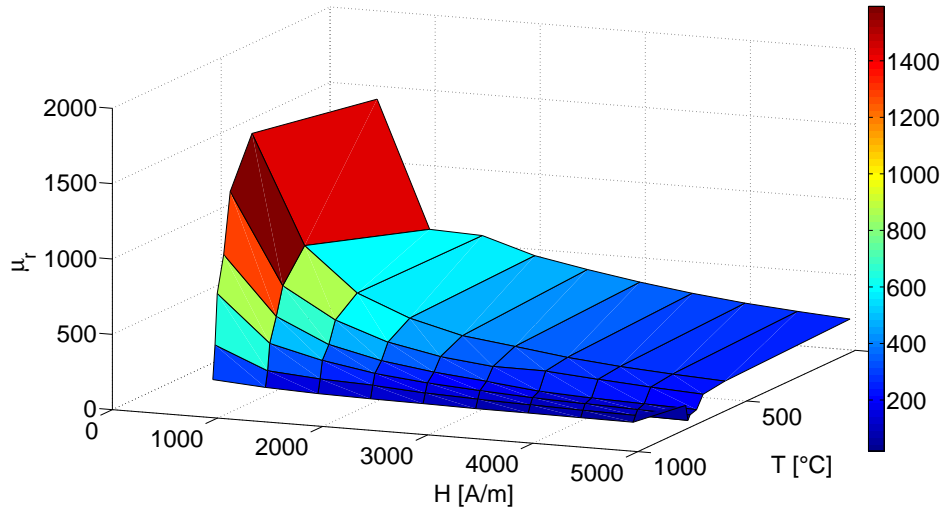


Figure 3.10: 42CrMo4  $\mu_r$ -H-T surface

the biggest effect of H is between 0 and 1000 A/m. So, in the range between 1000A/m and 5000A/m ten values of B have been sampled for each level of temperature, then ten values of  $\mu_r$  have been computed, and at the end the lowest values has been chosen. The result of this computation is the next figure, in which the trend of the relative magnetic permeability is shown as a function of the temperature (and only the temperature). For further and more accurate analysis it can be useful to implement the effect of the magnetic field over the magnetic permeability and then to compare the results to see how big error can be with this method.

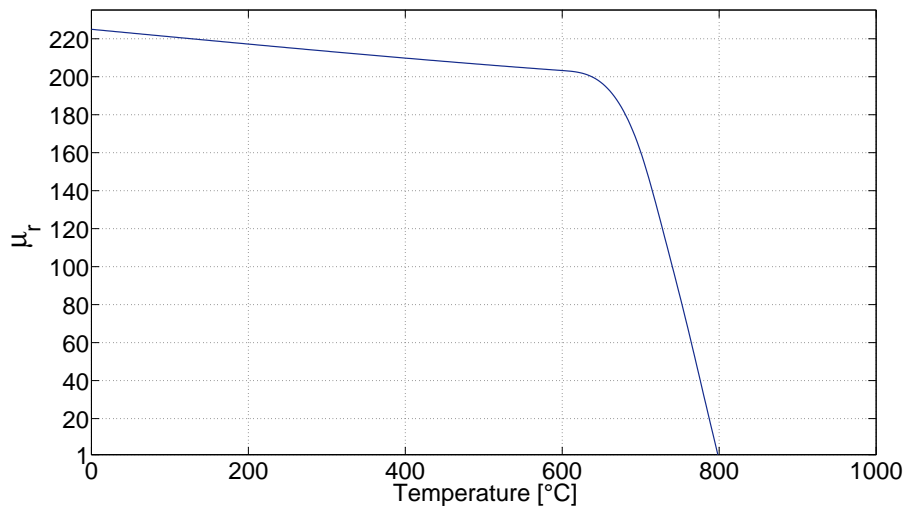


Figure 3.11: 42CrMo4 magnetic relative permeability variation with the temperature

Both fig.3.7 and fig.3.11 converge in showing that the Curie's point is between 750°C and 800°C.

## 3.3 Finite elements method and ANSYS software

### 3.3.1 Fem Method (hints)

To solve the equation that stays behind the phenomena, a finite elements code can be used. This kind of software operate by following a precise step order:

- data input and geometry definition
- mesh generation
- materials parameters upload
- boundary condition and input quantities upload
- solution

During the first step several domains are defined (depending on the model geometry) and discretized in little elements (finite elements) which can be: segments for 1D models, triangles or quadrilaterals for 2D model, tetrahedrons or prisms for 3D model. The reticulation of the domain has to satisfy some basic conditions:

- the union of all the elements has to cover the whole domain
- the elements cannot be overlapped
- the elements must be in contact vertex by vertex (1D), edge by edge (2D), face to face (3D)
- the elements can be different

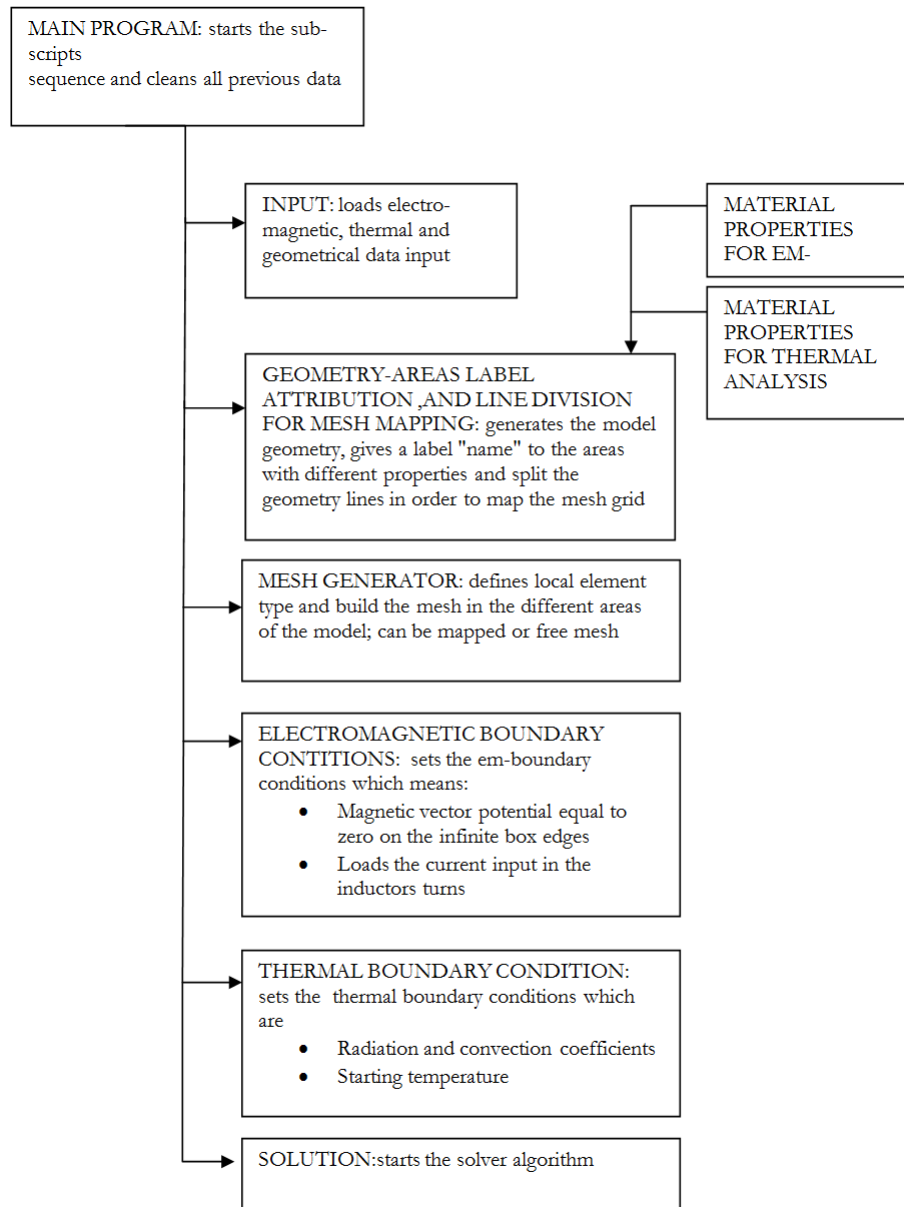
Following these conditions a net ( or mesh) is generated and the unknown variables are set on the nodes. The method is based on defining the trend of the solution from a node to another. For the numerical solution of differential equation it is possible to use two methods: one is called "variational method" which is based on physical consideration (mostly used), the other is purely mathematical (less used). The variational method does not solve the equations directly but focus on the minimization of the correspondent energy function. For example let's suppose to have an equation like  $ax+b=0$ , is possible to solve it finding the minimum of the function  $f(x) = 1/2ax^2 + bx + c$ . The minimum of  $f(x)$  is  $df/dx = ax + b = 0$ . In other words this method works following the physic axiom which says that the status where the energy function reaches the minimum point is an equilibrium status that every physical system which includes a form of potential energy try to reach.

### 3.3.2 Ansys Mechanical Apdl

The software used for the fem analysis is ANSYS MECHANICAL APDL. ANSYS Mechanical software is a comprehensive FEM analysis tool for structural analysis, including linear, non linear and dynamic studies. The engineering simulation product provides a complete set of elements behavior, material models and equation solvers for a wide range

of mechanical design problems. In addition, ANSYS Mechanical allows thermal analysis and coupled-physics capacities involving acoustic, piezoelectric, thermal-structural and thermo-electric analysis.

For the analysis done in this project, the software has been used by running a main script which includes several sub-functions in order to follow all the steps required by the finite element method. Making a flux diagram, the sequence of the scripts and related tasks is:



For the magnetic and thermal solution, harmonic and transient analyses has been used. Harmonic magnetic analysis calculates the effects of alternating current (AC) or voltage excitation in electromagnetic devices and moving conductors. These effects include:

- eddy currents

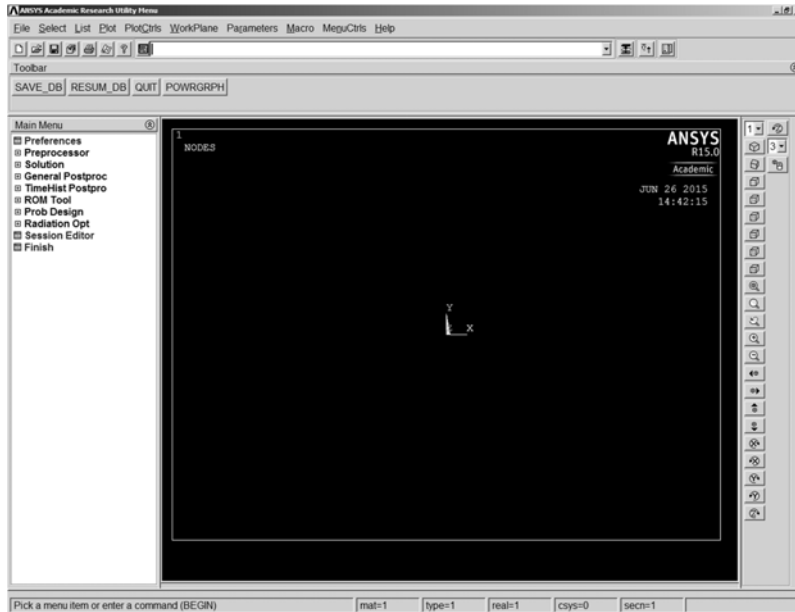


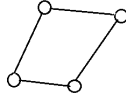
Figure 3.12: ANSYS Mechanical interface.

- skin effects (eddy currents in current conductors carrying an impressed current)
- power loss due to eddy currents
- forces and torque
- impedance and inductance

Typical applications for harmonic analysis are transformers, induction machines, eddy-current braking systems, and most other electromagnetic devices that work on AC. Permanent magnets are not permitted in a harmonic analysis. Material hysteresis effects are neglected. For low saturation cases a linear time-harmonic analysis can be run with assumed constant permeability properties. For moderate to high saturation conditions a nonlinear time-harmonic or time-transient solution should be considered. In moderate to high saturation cases, an analyst is often most interested in obtaining global electromagnetic force, torque and power losses in a magnetic device under sinusoidal steady state excitation, but less concerned with the actual flux density waveform. Under such circumstances, an approximate nonlinear time-harmonic analysis procedure may be pursued. This procedure can predict the time-averaged torque and power losses with good accuracy, and yet at much reduced computational cost compared to a transient time-stepping procedure. The basic principle of the nonlinear time-harmonic analysis is to replace the DC B-H curve input by the user with a fictitious or effective B-H curve based on an energy equivalence method. With the effective B-H curve, a nonlinear transient problem can be effectively reduced to a nonlinear time-harmonic one. In this nonlinear analysis, all field quantities are all sinusoidal at a given frequency, similar to the linear harmonic analysis, except that a nonlinear solution is computed. It should be emphasized that in a nonlinear transient analysis, given a sinusoidal power source, the magnetic flux density  $B$  has a non-sinusoidal waveform. While in the nonlinear harmonic analysis,  $B$  is assumed

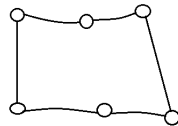
sinusoidal. Therefore, it is not the true waveform, but rather represents an approximation to the fundamental time harmonic of the true flux density waveform. The time-averaged global force, torque and loss, which are determined by the approximated fundamental harmonics of fields, are then subsequent approximations to the true values. The elements that has been used for this type of analysis are defined as:

- PLANE 13: 2D element, quadrilateral or triangular shaped, 4 nodes Degree of free-



dom : magnetic vector potential AZ, displacements, temperature, time-integrated electric potential

- PLANE 53: 2D element, quadrilateral shaped, 8 nodes, triangular , 6 nodes



Degree of freedom : Up to four at each node : magnetic vector potential (AZ), time integrated electric potential, current, electromotive force drop

ANSYS/mechanical supports transient thermal analysis. This kind of analysis determinates the temperature and other thermal quantities which are time dependent, at the nodes. The transient thermal analysis has nearly the same procedure of a steady-state analysis; the most important difference is that in transient analysis the loads are functions of time. In order to declare the time dependent loads, the time-load curve must be divided in time steps. So, considering the transient analysis as a sum of little steady states analyses, it is possible to say that this method allows to determinate:

- temperature
- thermal gradients
- heat flow rates
- heat fluxes

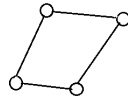
For such load, the following quantities can be set:

- convection
- radiation
- heat fluxes
- heat generation

- constant temperature

A steady state thermal analysis can be non linear with temperature dependent material properties. So it is important to make a kind of database which includes the material properties variation as a function of temperature. The elements that have been used for this type of analysis are defined as:

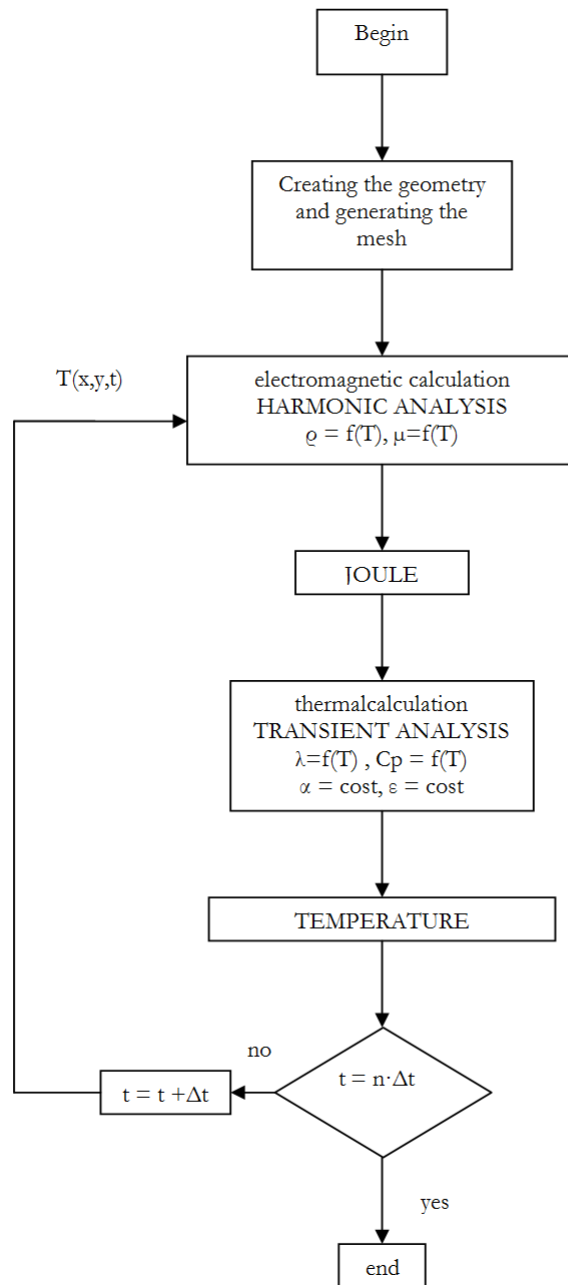
- PLANE 55 Dimension 2D, quadrilateral, four nodes



Degree of freedom: temperature at each node

To solve the electro-thermal problem, the solution algorithm must be a loop that switch from the electromagnetic problem to the thermal transient problem each step. After the geometry and mesh generation it starts the harmonic calculation reading the electrical material parameters (function of time) and loading the input loads (currents) from the boundary conditions script. After the electromagnetic harmonic analysis it takes the solutions in order to find the eddy currents distribution and their heat generation as joule losses. Setting thermal boundary conditions, reading the thermal material properties and putting the heat generation evaluated with the electromagnetic simulation, it starts the transient thermal analysis finding the results according to the degree of freedom allowed by the chosen elements. This loop-step repeats until the fixed heating time is over. It is possible to decide the number of steps for a fixed time keeping in mind that a bigger number of steps means a more accurate result but means also a bigger computational cost.







# Chapter 4

## First analysis

In this chapter the evolution of the model, starting from the first set up is presented. It begins with a very simple geometry and then it turns more accurate and detailed step by step. The first results are not very successful but they are very important in order to build a path to follow during the development of the analysis. The method used to find the required thermal profile is to put as input reasonable values for the currents and the process time and then, after seeing the results ( thermal distribution, heat generation sources, thermal fluxes and gradients, magnetic fields and magnetic flux density) modify them in order to fix possible distortions and improving the quality of the profile shape.

### 4.1 Initial parameters

Due to the lack of literature about this topic, at the beginning there were no possibility to find a starting point analytically. In particular the unknown parameters were:

- work-piece diameter
- work piece length
- hot zone length
- cold zone length
- number of turns
- input currents
- air gap length
- frequency
- heating time

So after many tests, step by step, they have been fixed in order to find the required results.

### 4.1.1 Geometry of the work-piece

To start the investigation it is necessary to know/choose the geometry and the shape of the work-piece. The idea was to take a simple cylindrically shaped work-piece available in the workshop of the institution to set the theoretical fundament of further experimental investigation . Experimental results will be carried by following the work.

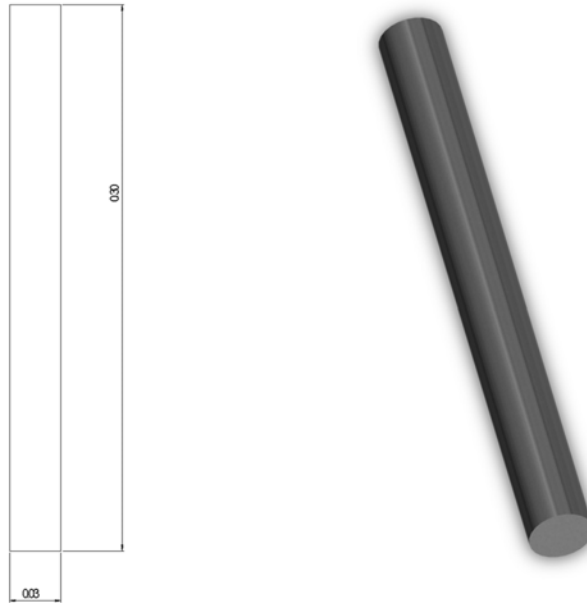


Figure 4.1: work-piece geometry and 3D rendering

As is possible to see from the fig.4.1 the work-piece is really simple shaped and its geometrical quantities can be summarized as:

- diameter : 0.03 m
- axial length: 0.3 m

Almost all the simulations have been done on this geometry but at the end of the work it is possible to find some tests with different diameters and length. These have been made in order to investigate if the proposed method can be applied to different work-piece sizes too. After the determination of the work-piece geometry it is possible to think about some reasonable values for the other parameters.

### 4.1.2 Hot and Cold Zone Dimension

To begin the analysis it has been decided to take the same values for the hot/cold zones length. In particular, remembering that the work-piece length is 30cm, it has been divided in five zones (6 cm each), three of them have been chosen as cold zones and two as hot zones. Proceeding with the tests, the length of these zone will be not the same because it will be found that this choice is not the best one. In any case, at the beginning, is not possible to know which are the perfect parameters so it was a reasonable choice.

### 4.1.3 Frequency

Knowing the work-piece diameter it is possible to find the frequency following the criteria of best efficiency. From chapter II it has been explained that the best cost-effective efficiency comes when the parameter  $m$  is equal to 2.5. Taking in count that the values of the material parameters change during the heating process (especially the penetration depth which is inside of  $m$ ) a range of optimal frequencies is defined by the empirical formula:

$$\frac{3}{D^2} < f < \frac{6}{D^2} \quad (4.1)$$

Plotting this inequality:

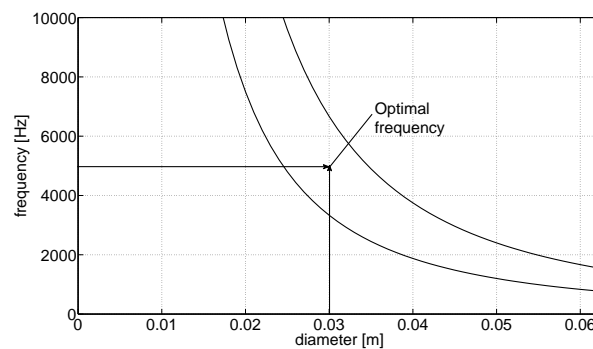


Figure 4.2: optimal frequencies range

Considering that the diameter of our work-piece is 0.03 m it is easy to find that the frequency to have the best efficiency is 5 kHz. Once the frequency is fixed and knowing the behavior of the resistivity and magnetic permeability it is possible to estimate the trend of the penetration depth during the process. This is useful to do because it gives an idea of what happen during the process and, more important, it allows to map the mesh in an accurate way putting a reasonable number of elements in the penetration depth zone.

### 4.1.4 Inductor - Work-piece Air Gap

The inductor should be coupled as close as possible to the work-piece. The next table shows the recommended values for this parameter.

Frequency [KHz]	Coupling distance [mm]
1-3	3-6
10-25	2-3.8
50-450	1.5-2.25

So, following the indications, a value of 5mm has been chosen. The ratio  $\alpha$  is equal to 1.33.

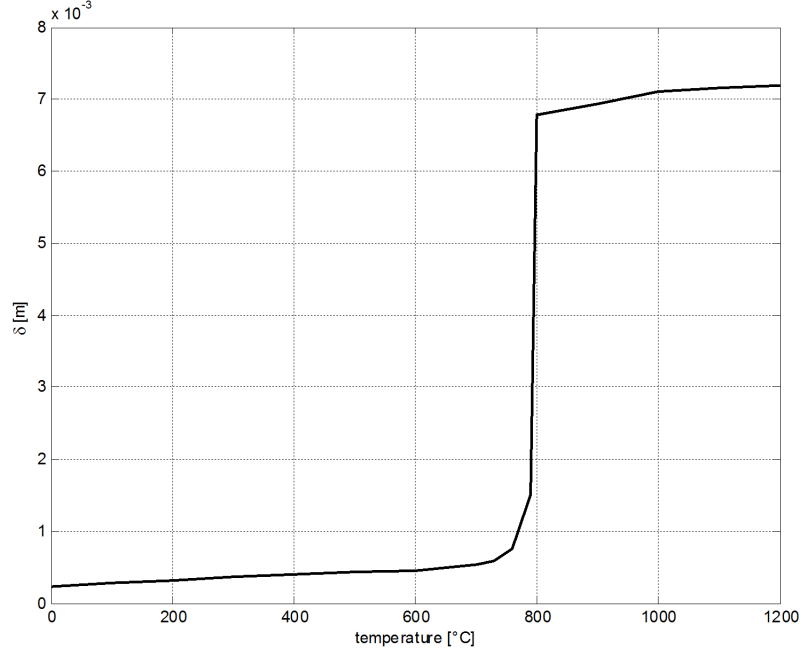


Figure 4.3: penetration depth as a function of temperature

#### 4.1.5 Inductors

At the beginning of the study it has been decided to take a simple geometry for the inductors. The section of the coil is squared with 1cmx1cm edges. The coils are equipped with a channel for the cooling system. The thickness of copper to carry the current has been evaluated considering the relation:

$$d_{opt} = \delta_{inductor} \cdot \frac{\pi}{2}$$

where  $d_{opt}$  is the thickness and  $\delta_{inductor}$  is the penetration depth. In this way it is possible to find the best choice for the copper section. There are no benefits in taking a bigger section because of the proximity and skin effect. As a matter of fact the current used to be pushed on the surface of the conductor so it is useless to increase the copper section because it would not be interested by any current. Considering that the coil should not be hot (less than 100°C) at the end of the process, to evaluate  $\delta_{inducotr}$  a constant value of the resistivity can be used.

$$\begin{aligned}
 d_{opt} &= \delta_{inductor} \cdot \frac{\pi}{2} \\
 &= \frac{\pi}{2} \cdot 503 \cdot \sqrt{\frac{\rho_{cu}}{f}} \\
 &= 503 \sqrt{\frac{1.60 \cdot 10^{-8}}{5000}} \cdot 1.5708 \\
 &= 1.44 \cdot 10^{-3} \longrightarrow 1.5mm
 \end{aligned}$$

As it is possible to see from the fig.4.4 the coil has four equally spaced turns. The air space between the turns is 5mm. In this way the total length of the inductors is six

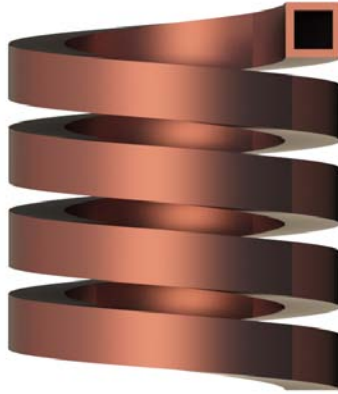


Figure 4.4: penetration depth as a function of temperature

centimeters and this means that it has been designed to be long as the first estimation of the hot zone.

Quantities	Values [mm]	Units
Length	0.06	m
Number of turns	4	/
Diameter (internal)	0.04	m
Copper section per turn	51	mm <sup>2</sup>
Cooling channel section	49	mm <sup>2</sup>
Turns spacing	5	mm

## 4.2 First fem model analysis

Several tests have been done to find the right temperature for the hot zones and cold zones, but in this work it will be reported only the most significant results.

### 4.2.1 Preprocessing

In the preprocessing session the input data, geometry, mesh and boundary conditions are defined.

Quantities	Values [mm]	Units
Current	950	A
Heating Time	80	s
Frequency	5000	Hz

The geometry consists of the work-piece and two inductors symmetrically placed with respect to the horizontal plane. The problem configuration is 2D axis symmetric so all the analyses have been done referring to the rotation axis placed along  $y = 0$  coordinate.

Referring to fig.5.6 the work-piece has been divided in three sections in order to map the mesh: one section for the penetration depth under Curie's point, one section for the

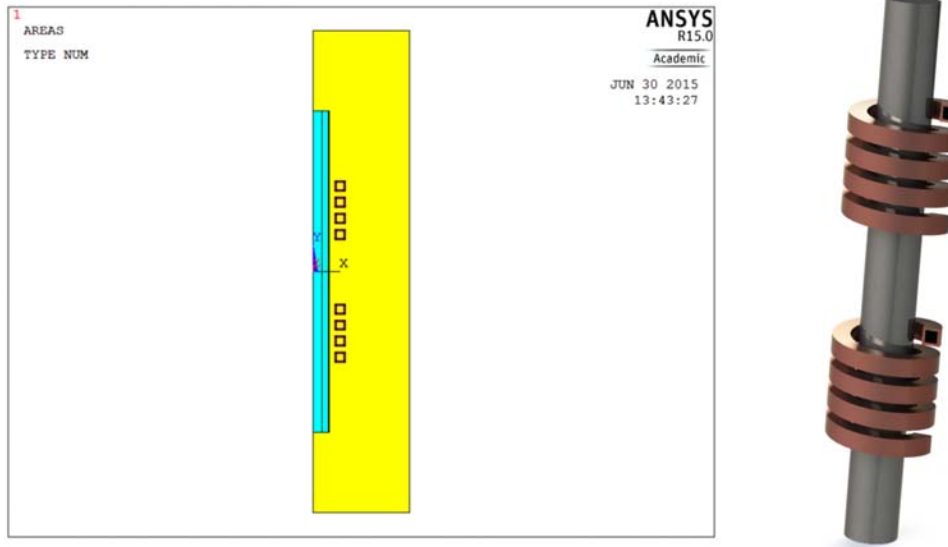


Figure 4.5: ANSYS model geometry and model 3D rendering

penetration depth over Curie's point and the last section for the remaining part of the work-piece.

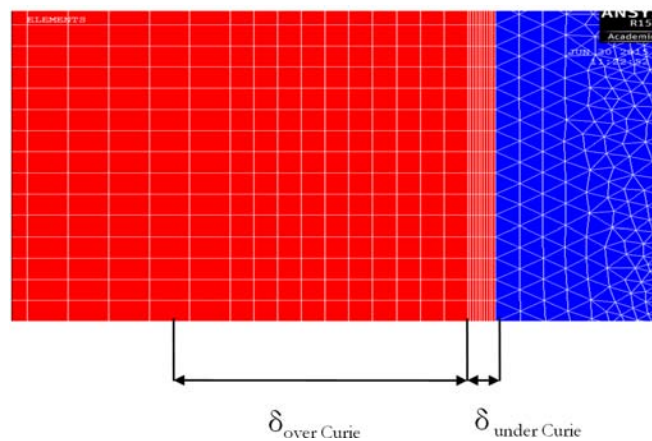


Figure 4.6: work piece mesh mapping

In order to have a good accuracy with the results, ten elements for each sections have been mapped. The boundary conditions are: the magnetic vector potential  $A_z$  has been set equal to zero on the edges of the infinite box, the convection coefficient  $\alpha$  has been set equal to  $3 \text{ W/m}^2\text{K}$  on the surface of the work-piece, the radiation coefficient has been set equal to 0.1 on the surface of the work-piece and the initial temperature of the system is  $20^\circ\text{C}$ .

## 4.2.2 Postprocessing

After obtaining the solution, the temperature distribution and the thermal profile on the work-piece length have been investigated.



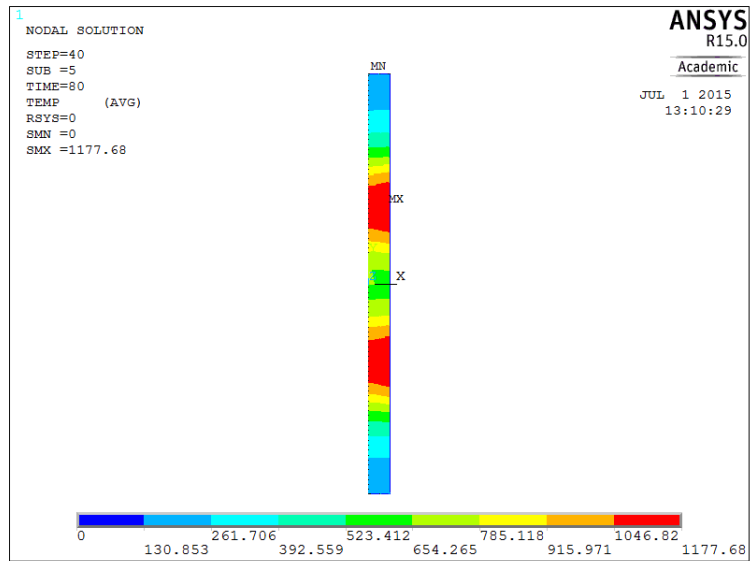
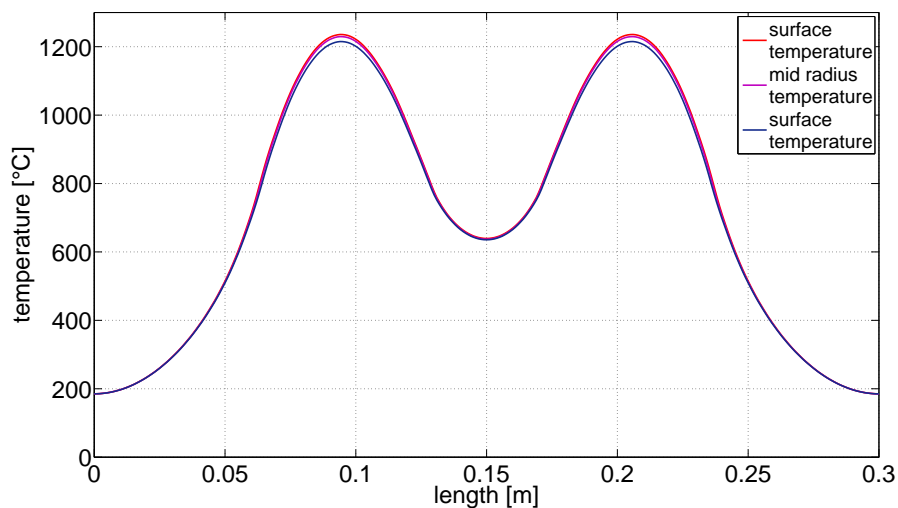


Figure 4.7: Temperature distribution on the work-piece

As it is possible to see, with this system configuration, the hot zone temperature is reached. Anyway the cold zone are under heated, the thermal conductivity of the work-piece is not high enough to allow a passive heating. This means that other inductors have to be added to the model in order to control the cold zones temperature. Investigating the thermal profile it is possible to find out other problems that must be improved.



The shape of the thermal profile is very far from the required one. The problem is that using short inductors (diameter and length comparable) there is a bigger flux density in the middle of the coil which generates those two peaks. Observing the second graph, it is possible to notice that the temperature is homogeneous along the radius; the highest distortion is nearly 24°C which is an acceptable value. The higher difference is collocated at the external borders of the inductors. Focusing on the work-piece temperature you

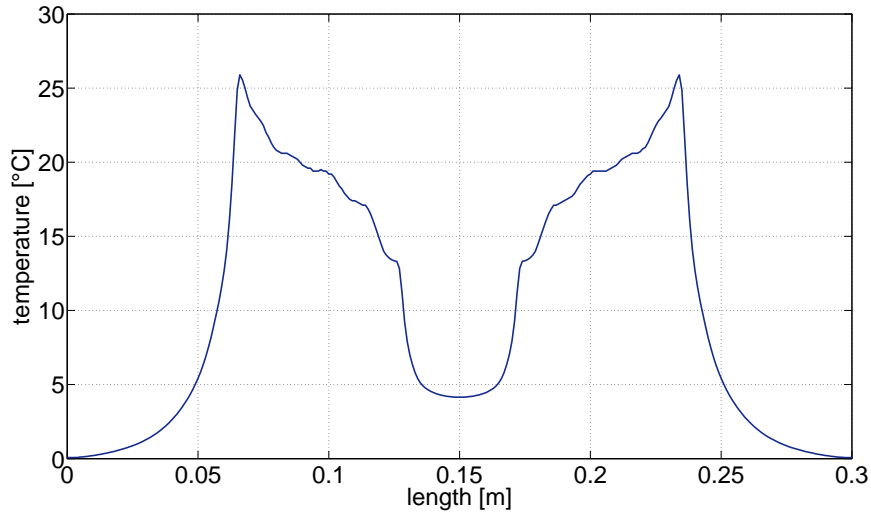
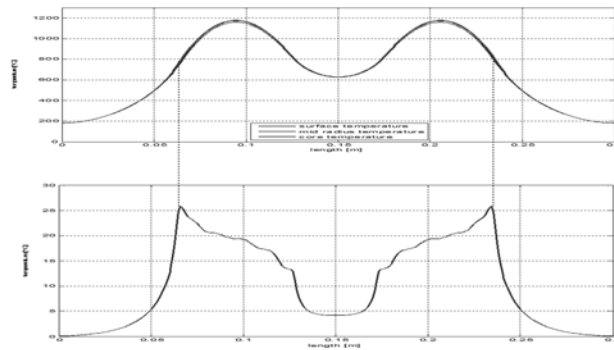


Figure 4.8: first: profile on the work-piece, second: temperature difference between the surface and the core

can notice that in these point the Curie's point is not reached. So the eddy-currents are concentrated on the surface of the cylinder and that generates this thermal difference along the radius.



Another thing that is better to report is that the thermal profile, and the thermal distribution, are symmetrical with respect to the horizontal axis of the work-piece. It is possible to make the model lighter computationally speaking, but it is better to keep on working with the whole model in order to use this symmetry property to verify the correctness of results.

## 4.3 Second model

### 4.3.1 Preprocessing

In the second model an inductor has been added in the middle cold zone in order to get some information about the cold zone controlling. The inductor has the same characteristics of the orders except the number of turns which is two. Regarding the mesh mapping and the boundary conditions the previous considerations are still valid. It is not expected to reach the wanted thermal profile with this configuration but in order to build the final model it is very important to understand how more inductors behaving coupled with the same work-piece and supplied with different currents. This problem cannot be challenged analytically because probably (not for sure) it is not possible to solve the equations (or even write them) because almost all the hypotheses from the ideal model are violated.

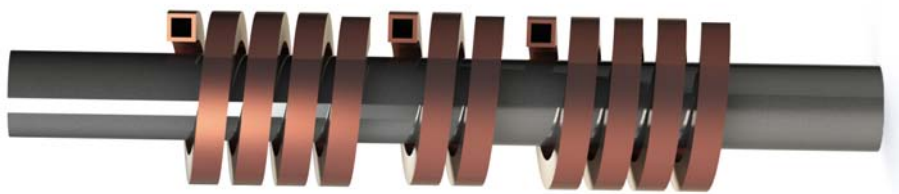


Figure 4.9: second model 3D rendering

In this case, in the middle inductor, a smaller current should be injected in order to generate less heat power inside the work-piece. To make the analysis more understandable let's call "A" the four turned inductors and "B" the middle one. The cold zones at the border are not directly heated by any inductor so it is expected that their temperature will not change so much from the previous investigation. They will be investigated in the next tests. The input data are:

Quantities	Values [mm]	Units
Current A	950	A
Current B	600	A
Heating Time	80	s
Frequency	5000	Hz

### 4.3.2 Postprocessing

This time, as expected, the temperature in the middle zone is higher than before. The colder point is around 885°C which is a good result. Many tests have been done modifying the input data values in order to achieve the desired results step by step. So, the thermal distribution is shown in fig.4.10. It is very easy to notice that the temperature of the hot zones is a little bit higher than the previous calculation. The simulation parameters are the same, so the middle inductor has an effect (even if not so important) to the hot zone. The temperature along the radius is not so homogeneous as before even if still acceptable ( $\Delta T < 50^\circ\text{C}$ ). If desired it is possible to reduce it increasing the heating time

and decreasing the current input (induced power), but it would not change the profile shape so it is useless to report. From the results of these analyses it is possible to conclude that it can be possible to heat the work-piece in different zones at different temperatures, but with traditional short inductors it is not possible to generate a squared profile.

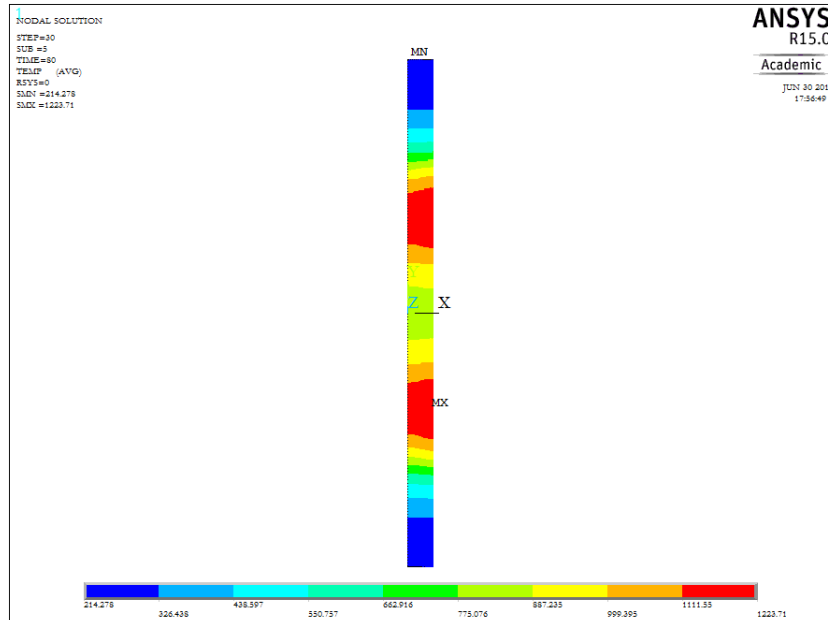
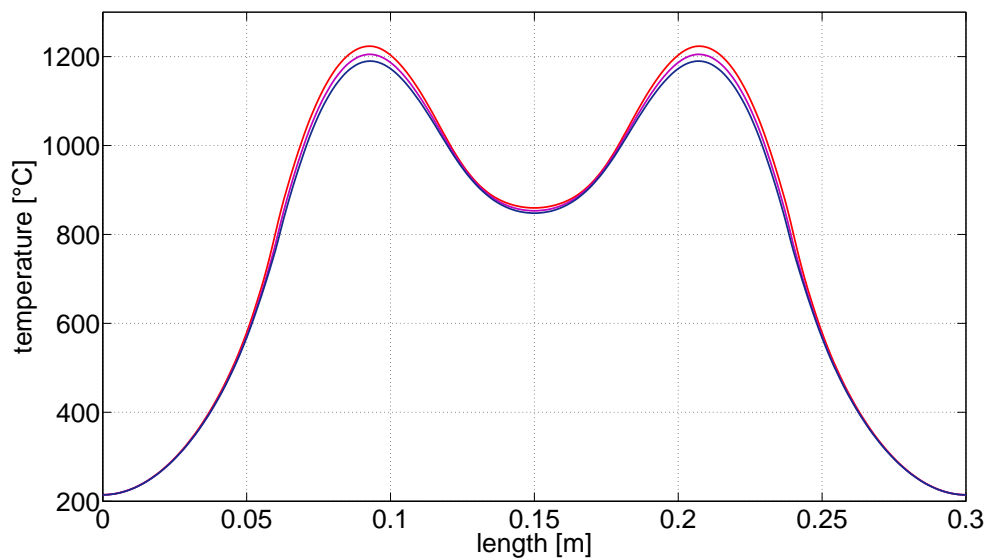


Figure 4.10: second model temperature distribution



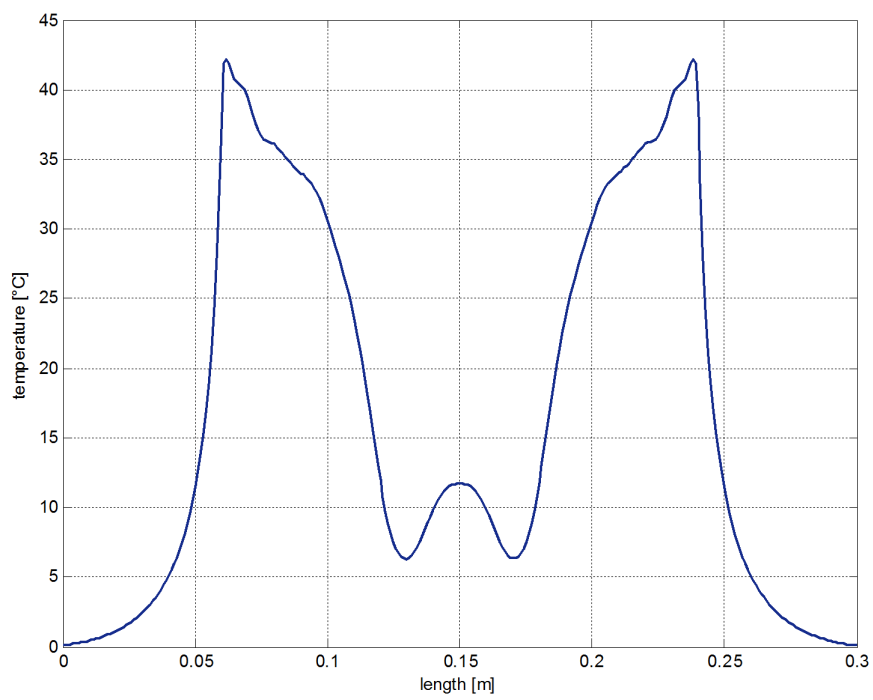


Figure 4.11: temperature profile and difference between surface and core



# Chapter 5

## Third model analysis

### 5.1 Magnetic flux controllers and active em-field shielding

The main distortion that effect the founded thermal profile consists in the shape which results to be very curvy and not enough squared. It is possible to suppose that the reasons which are on the base of these problems are:

- Putting "n" inductors, with the same characteristic, in a cylindrical work-piece, makes them working together since part of the flux lines generated by the "i" inductor are linked with the other n-1 inductors. This phenomenon interferes with the necessity to create a clear distinction between the hot and the cold zones. The flux-lines run in the work-piece, from a zone to another, connecting all the inductors together making it difficult to control each zone.
- The traditional short inductors ( equal spaced turns, same current in each turn) are affected by a non uniform magnetic field distribution. Compared to an infinite inductor, which has a totally uniform magnetic field inside, the short real inductor presents a bigger value of the magnetic field in the middle and presents also some distortions at the external borders called border effects.

#### 5.1.1 Magnetic Flux Controllers

It is known that when a current is injected in a coil, a magnetic field is generated and its flux flows along a closed path around the coil. The air, which is not a magnetic material, constitute a non suitable track for the magnetic flux lines. Magnetic materials, for example iron, provide an easier way for magnetic flux to flow. For this reason, the magnetic flux controllers are particular shaped pieces made by magnetic materials and they are placed in specific zones to fit the magnetic field value and distribution. Magnetic flux controllers can be used as concentrators, diverters, shields. To use the flux controllers as concentrator the most common way is to take the C-shaped configuration. In this way the magnetic material is disposed around the turns of the coil such as a metal frame.

This kind of flux concentrators allow to generate an higher induced power in a specific zone and its distribution under the "face" of the coil has a surface closer to be rectangular

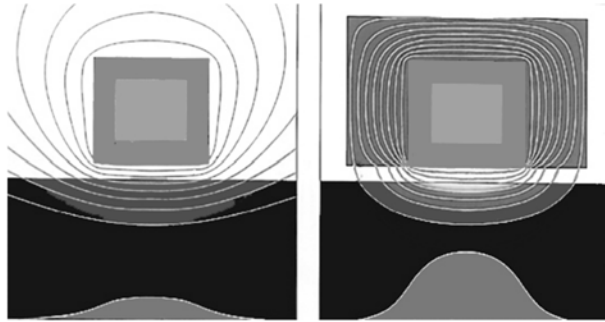


Figure 5.1: example of magnetic flux concentrator [FLUXTROLinc]

which is exactly our goal. For this application "Fluxtrol A" which is a product from FLUXTROL company has been chosen.

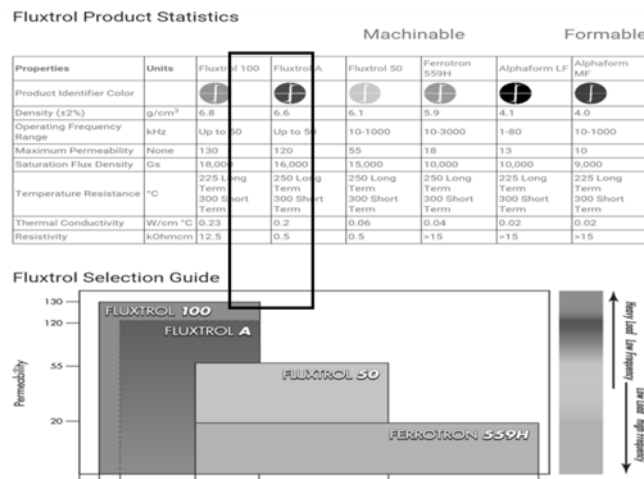


Figure 5.2: Fluxtrol products

In order to implement the action of the flux concentrators in the FEM model, their material parameters are required. On the web site of the company there are some useful sections that contains all the needed information.

As it is possible to see from the fig.5.3, this kind of material has an high value of magnetic permeability and also a very high value of electrical resistivity. Combining them it gives a very good performance since it is able to "catch" most of the magnetic flux (high magnetic permeability) and the joule losses are relatively small due to the high resistivity. So they will not be heated by the induction coil and their losses are less the one before their application.

### 5.1.2 Active em-shielding

To make an homogeneous power distribution along the length in each zone, the magnetic field and the eddy currents must be as uniform as possible. In order to balance the profile of the magnetic field inside the coil, it is possible to use one (or more) turn to increase or decrease its value along the length. This can be theoretically done feeding the turns of





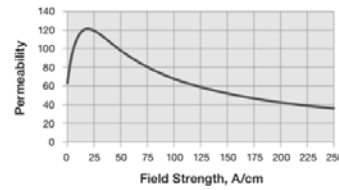
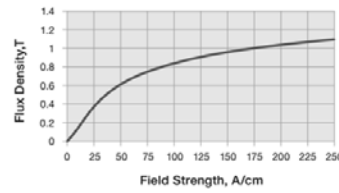
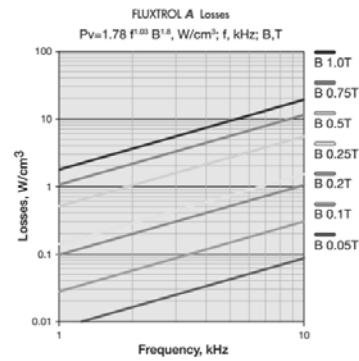
# FLUXTROL A



**Low to Medium Frequency Soft Magnetic Composite** [Frequency Range: up to 50 kHz]

FLUXTROL A is a proven material made of electrically insulated iron particles and organic binder. It is designed for a wide range of frequencies up to 50 kHz. This material has significant anisotropy with best magnetic and thermal properties in direction perpendicular to the pressing direction. It has high thermal conductivity which allows it to handle high thermal loads. The properties below are given for the favorable direction.

Properties	Units	FLUXTROL A
Density ± 2%	g/cm <sup>3</sup>	6.6
Initial Permeability	None	63
Maximum Permeability	None	120
Saturation Flux Density	T	1.6
Operating Frequency Range	kHz	up to 50
Major Frequency Range	kHz	3–30
Temperature Resistance	Centigrade	250 Long Term 300 Short Term
Thermal Conductivity	W/cm °C	0.2
Resistivity	kOhmcm	0.5



Each grade of Fluxtrol material has its own distinctive properties that are the most beneficial to certain application conditions, process type, coil design, frequency, etc. Contact Fluxtrol or your local distributor for more information about which material is optimal for you.

- FLUXTROL 100
- FLUXTROL 50
- FERROTRON 559H
- ALPHAFORM LF
- ALPHAFORM MF

Figure 5.3: FluxtrolA datasheet

the coil with different currents. The result is like to split the coil in different pieces which work in a restricted zone. So by controlling the values of the currents it is possible to monitor at anytime the magnetic field distribution and the induced power. To make this phenomenon more understandable, a little, but useful, example is shown. Let's take an inductor with three turns and let's feed it in a three different ways. The first one involve a current of 100A 5KHz which is equal in every turn. As expected the magnetic field and the flux density are stronger in the middle and the flux lines are close to be parallel only in the central zone.

The second one is still fed with a current of 100A 5Khz but only in the first and the last turn. The central turn is just a shortcut copper ring which behave like a shield. The shield effect comes from the Faraday-Lenz law since a conductive turn is crossed by an alternating magnetic field. The consequence is that a current is induced on that turn and its direction is such as to oppose the magnetic field which generated the current itself. So the main magnetic field is effected by a localized minimum due to the second magnetic field generated by the induced current in the middle turn. In this way the first and the last turn are less connected than before since some of the flux lines, due to the shield,

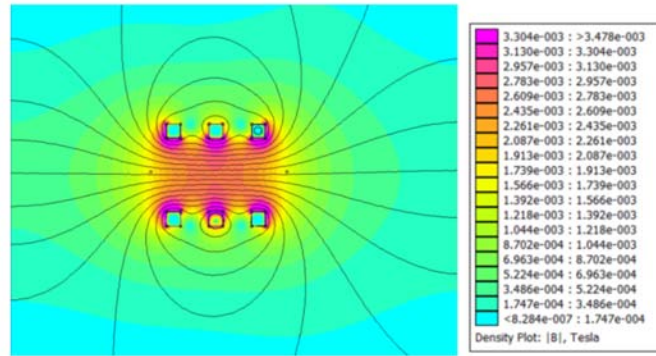


Figure 5.4: magnetic field distribution for a short coil with equal currents

deviate their path reclosing near the middle of the coil. Integrating the current density over the central turn it comes a current magnitude about  $-70A$ .

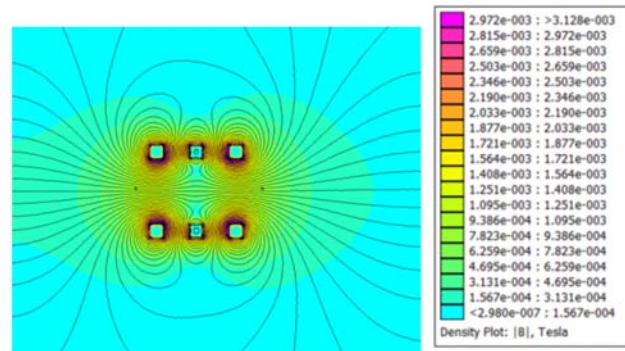


Figure 5.5: example of passive shielding

The third case is an example of active shielding. The inductor is fed with a current of  $100A$   $5kHz$  in the first and last turns. The middle turn is not anymore "naturally" induced by an opposite current but a stronger opposite current is injected in it. In this case the shielding effect is even stronger because the central turn generates a magnetic field whose distribution opposite to the other one. As it is possible to see, in the center of the coil, the magnetic field is now really low.

Using this method it is possible to modify the eddy currents distribution inside the hypothetical work-piece. Modifying the current distribution is equal to change the positions of the thermal sources and consequentially to change the trend of the temperature profile. The values of the magnetic field in each example are shown in the graph 5.7.

So it is easy to notice that using equal currents the magnetic field is stronger in the middle (higher curve) and then decreasing the current in the middle turn it is possible to reduce the magnetic field inside the coil. The second curve comes from  $50A$  input in the middle coil and then, going on, the third one is obtained with a central current of  $-50A$ . The fourth one represents the passive em-shielding and the last one is made by a current of  $-100A$  in the middle turn.

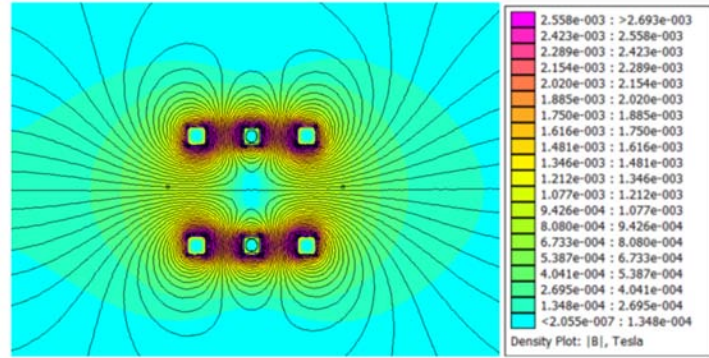


Figure 5.6: example of active shielding

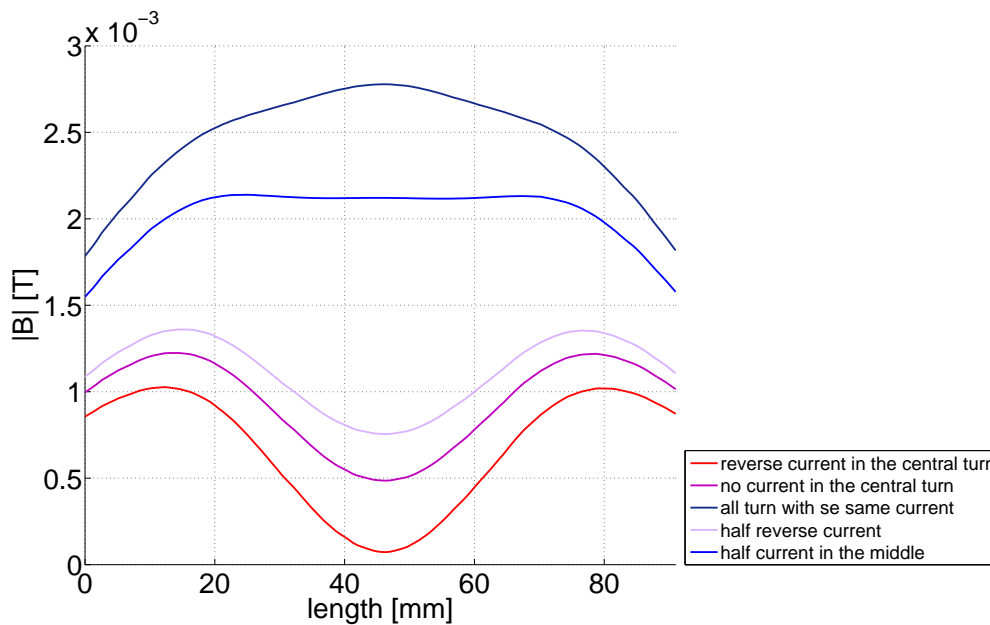


Figure 5.7: induction field profiles

## 5.2 Third model

### 5.2.1 Second model updates

In this section is explained how the previous techniques (flux controllers and active em-shielding) are applied to the induction heating system. In other words the second model has been updated with the insertion of the following elements:

- the middle inductor has three turn instead of two
- the hot zone inductors have five turns instead of four
- another two inductor have been added on the border of the work-piece
- each inductor have a flux controller frame

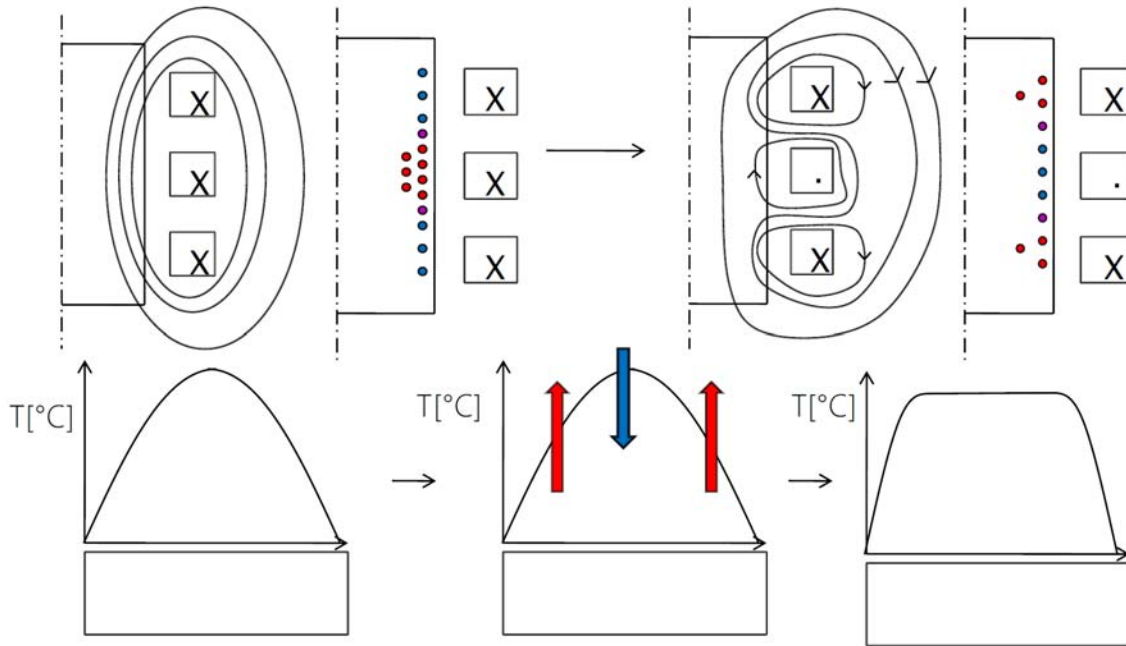


Figure 5.8: shielding effect

- the turns of the inductor are fed with different currents during the process

One turn has been added to the inductors. This has been done because it is much better to have an odd number of turns for each inductor. With an odd number of turns it is possible to use the central turn as electro-magnetic field active shield in order to split the coil in two parts to modify the thermal profile. With an equal number of turns it would be not possible to divide the coils in symmetric regions. The inductors on the border of the work-piece have been added in order to rise up the temperature also in that zones which are cold zones.

## 5.2.2 Preprocessing

### Geometry

In this model the geometry is different from the previous one due to the updates.

As it is possible to see from fig.5.9 the work-piece is now heated by five inductors. The blue frames around the inductors are the flux controllers. On the border they cover the work-piece bases in order to catch the flux of the magnetic field which exit from that zone of the work-piece and so to reduce the border effect.

The inductors in the middle and in the border are smaller than before; since the turns have been increased and in the same time the space decreased. Before the explanation of the input data for the analysis is mentioned it is better to show how the process has been carried.

### Two interval process

In order to use the idea of em-active shielding, the process has been divided in two steps. The first step of heating has something different from the traditional heating process.

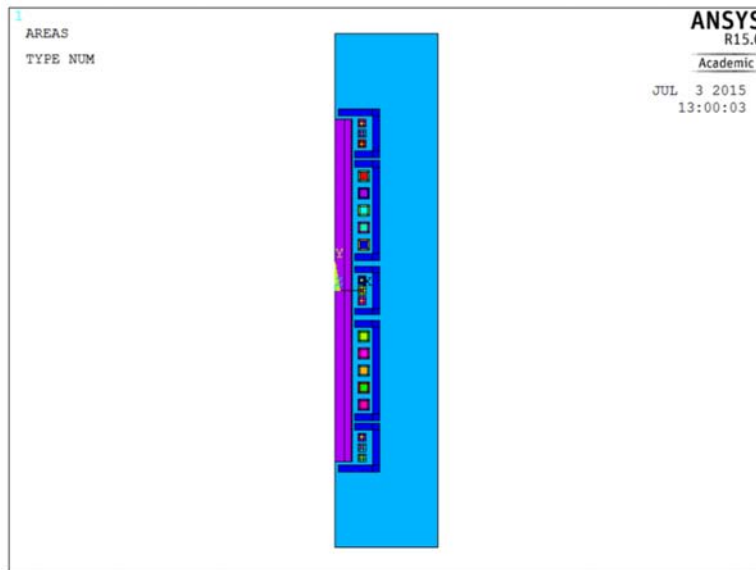


Figure 5.9: third model geometry

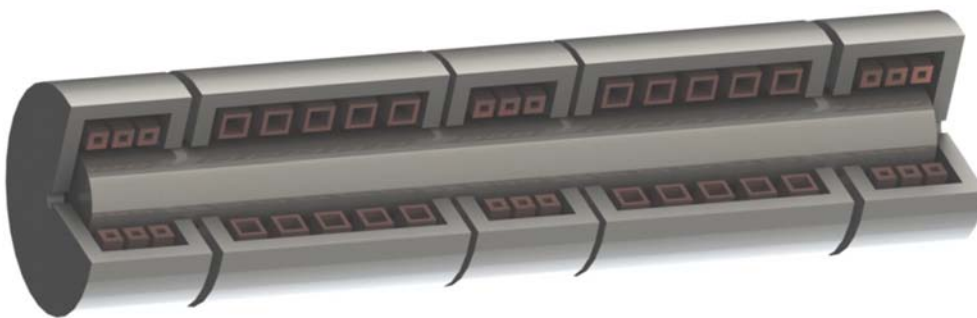


Figure 5.10: third model 3D rendering

The current is not the same in the turns of the inductor. Starting from the big inductors (they are equal) the current in them is all positive. The only "strange thing" is that the first and the last turns have an higher current in order to force the magnetic field to stay inside the work-piece at the border of the coil. The middle and the border inductors are supplied with a positive current in the first and in the last turn but with a negative one in the middle. The explanation for this choice is written more forward. At the end of the first interval, the currents supply changes its configuration. Starting from the bigger coil, in the middle turn a negative current is now injected. This because we want to push down the peaky trend which comes from the second model. So, after reaching the required temperature in the first interval, the active em-shielding starts to effect , in the hot zones, and the heat sources changes their position in order to heat the border of the zone and to cool the center. In this way the profile over the zone is very flat and balanced. The coil is now literally split in two parts which work in a separate way. The insulation degree between the upper and the lower part of the coil depends by the amount of negative current injected in the central turn. So it is possible to realize a control system which regulates the shielding effect continuously in order to achieve an

high level of process precision. The other coils do not change their configuration. All continue like the first part of the process. The reason why the inductors on the cold zones starts directly with the negative current in the middle turn is that they do not have to reach high temperature. In other words, considering that in the same time the work-piece has to be heated at different temperatures, the hot zones are heated faster and then balanced but the cold zones rise their temperature in a balanced way from the beginning.

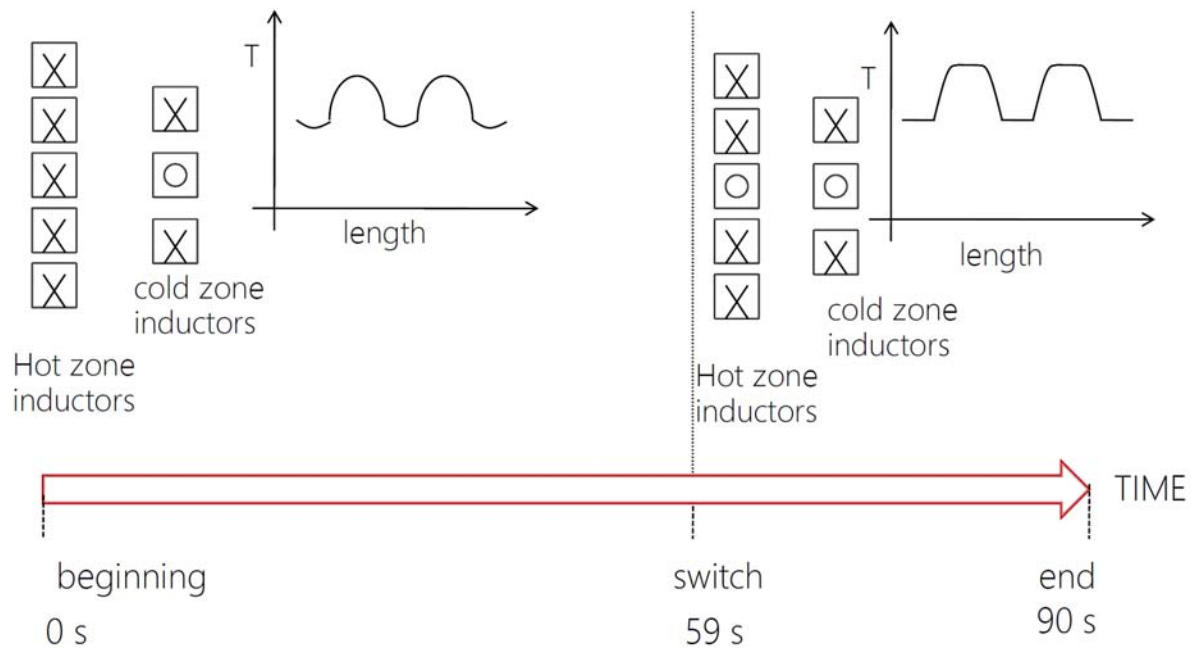
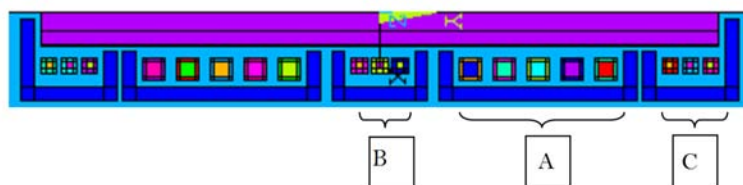


Figure 5.11: process scheme

### Input data

As a little premise it is important to underline that there is still a rule to decide how to make the process. There are many possibilities to combine the parameters in order to find out the required result. In this work the task is to check if the result is possible to reach, to choose the best parameter for practical realization will be studied in the future. Many tests have been done, and only the most significant result is reported.



Interval 1:0-59sec	Interval 2: 59-90 sec	Turn
820 A	820 A	C1
-500 A	-500 A	C2
820 A	820 A	C3
1050 A	1050 A	A1
800 A	800 A	A2
800 A	-800 A	A3
800 A	800 A	A4
1050 A	1050 A	A5
820 A	820 A	B1
-350 A	-350 A	B2
820 A	820 A	B3

The currents of the lower side are completely symmetric ( that is the reason why they are not reported). The heating time is written in the table, it is split into two intervals, 0 to 59 s for the first one and 59 to 90 s for the last one. The frequency is still 5Khz.

### 5.2.3 Postprocessing

It is very important to check what happens from the electro-magnetic side of the problem. To understand how the quantities change during the process two key point in the time flow have been investigated: the end of the first interval and the end of the second interval. First of all the magnetic field distribution inside the work-piece and the related eddy currents generated are shown.

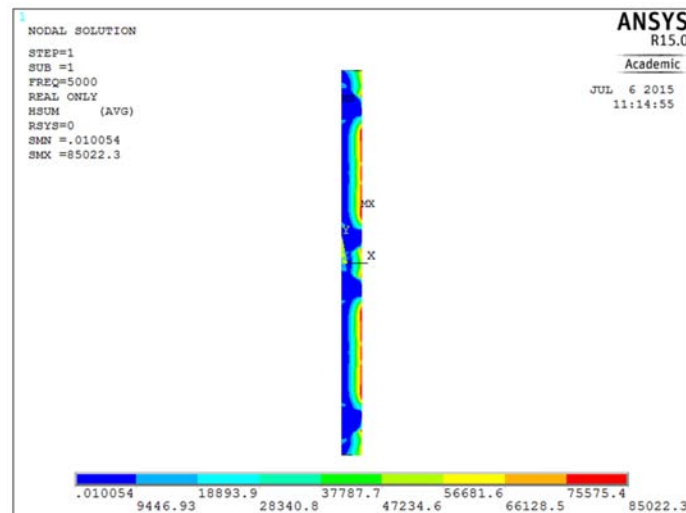


Figure 5.12: magnetic field distribution in the first step

The effect of the shielding is very clear. So in the first interval the eddy currents are distributed along the coils of the hot zones and concentrated in the middle of the zone. In the second one they follow the separation of the magnetic field splitting in the middle zone of the coil. The consequence of this behavior is that also the heat sources and the induced power follow them modifying the temperature profile. In other words the center

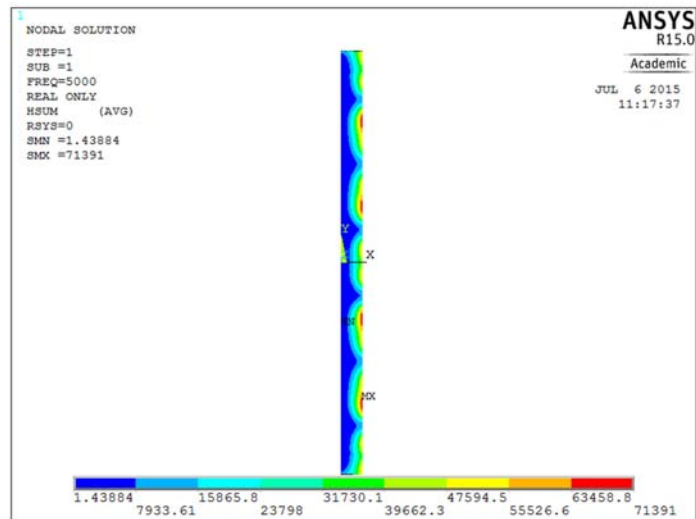


Figure 5.13: magnetic field distribution in the second step

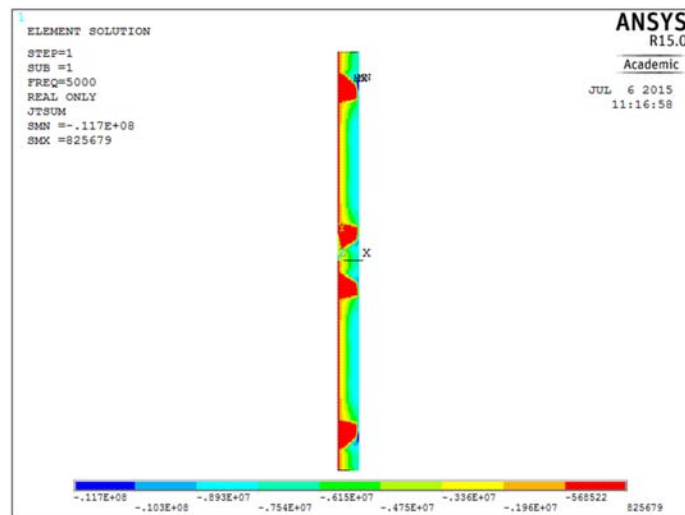


Figure 5.14: eddy current distribution in the first step

of the coil is not (or very less) directly heated during the second interval but the border are heated. The consequence is the achievement of the homogeneous temperature along the zone.



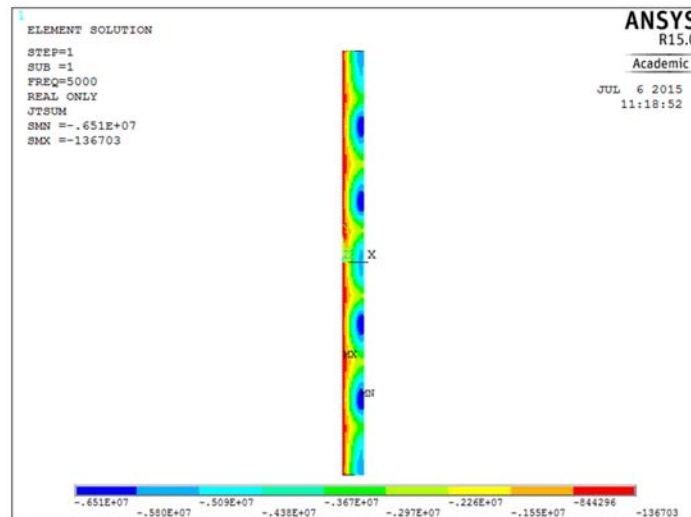


Figure 5.15: eddy current distribution in the second step

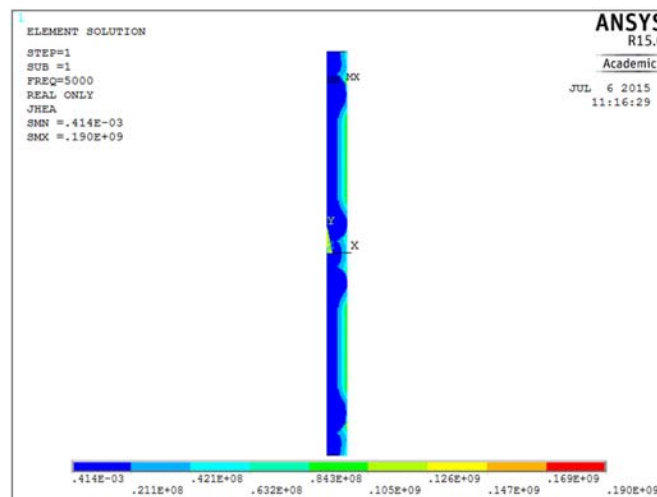


Figure 5.16: power distribution in the first step

It is now interesting to check how the temperature is distributed along the work-piece. This is the most important result of this investigation.

From the fig.5.18 it is easy to notice that the hot and cold zones are very well defined. The border zone are a little bit hotter than the middle zone but the difference is about 20°C and it is not a problem for our investigation and for the forging process. The temperature along the radius is almost constant like the temperature in each zone. This can be seen in the graph of the thermal profile.

In this case the maximum temperature difference from the surface to the radius is about 20°C which is much better than the second model. This difference is lower because in the second interval there is the equalization of the hot zone temperature and, at the same time, the temperature equalizes from the surface to the core. This process has been done to reach an hot zone between 1100°C to 1200°C but changing the input parameters it is possible to increase or decrease this range. Due to the complex interaction of the parameters it is not easy to find analytical rules to describe this design in general. Looking

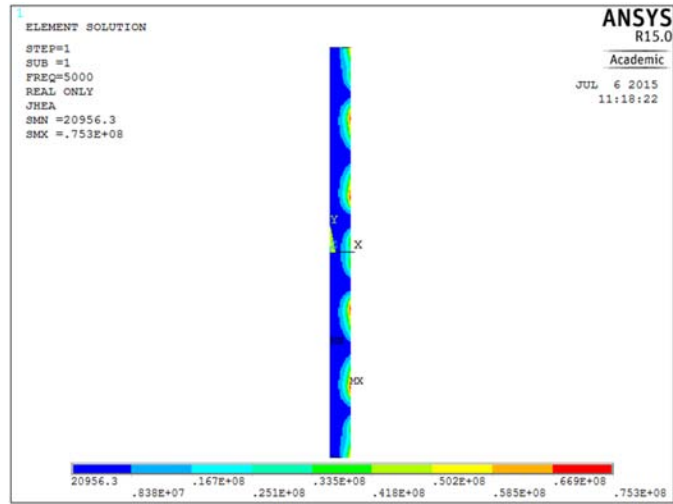


Figure 5.17: power distribution in the second step

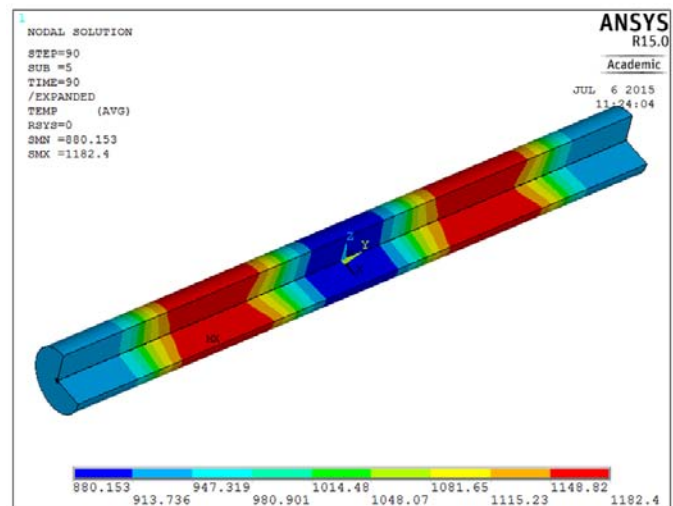
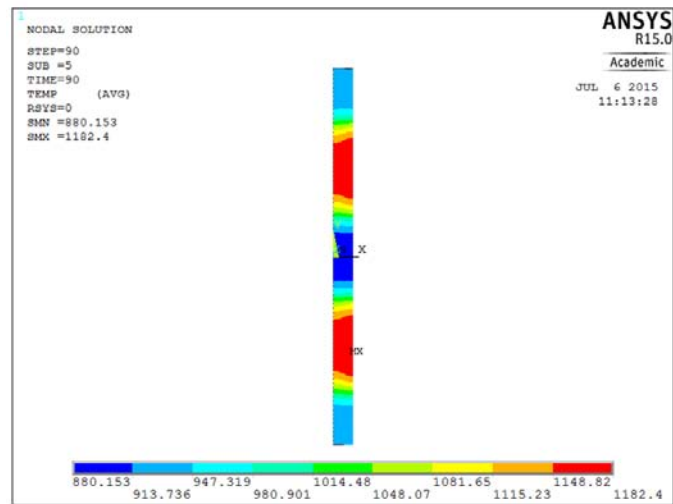


Figure 5.18: third model - temperature distribution along the work-piece

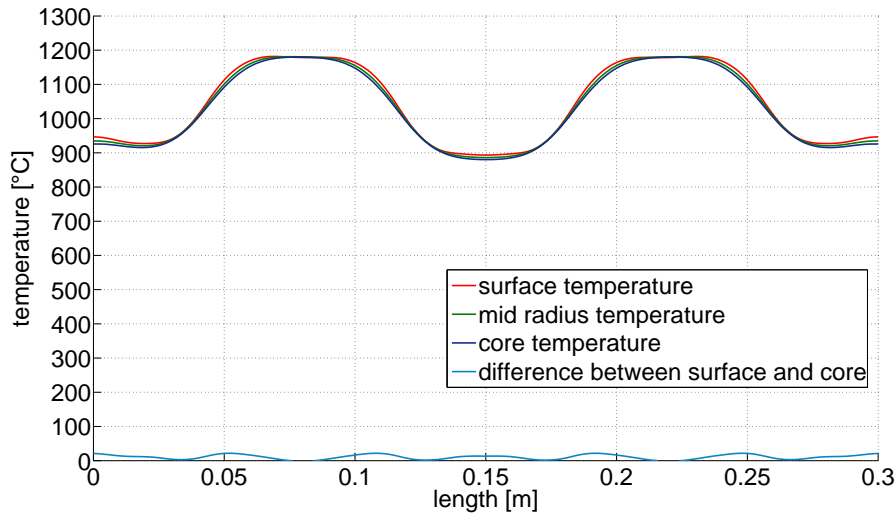


Figure 5.19: third model - thermal profile

at the temperature along the time in the hot-zone (fig.5.20 and 5.21), it is possible to see that the surface temperature rise up very fast due to the high power density in the first stage of the penetration depth. The mid radius and the core temperature goes quietly. It is important to notice that at 59 second (interval changing) the surface reaches 1200°C , then, in the second interval it is possible to confirm the presence of the equalization along the radius. From 59 to 60 seconds the three lines converges overlapping together.

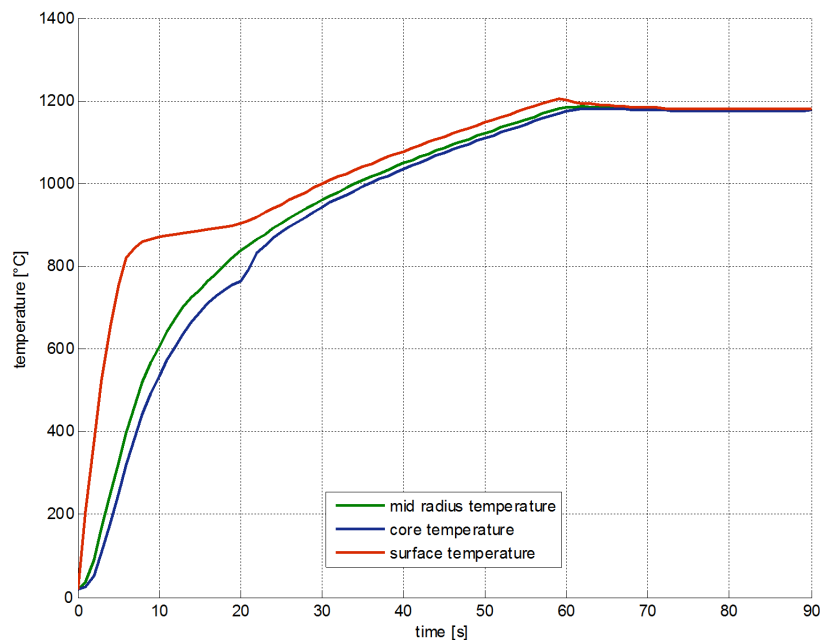


Figure 5.20: temperature over time in an hot-zone

Comparing the hot and the cold zones, it is possible to underline that, as expected, in the cold zone the temperature rises slower than the hot zone because there is the effect of the magnetic field shielding from the beginning of the process. In the cold zone the

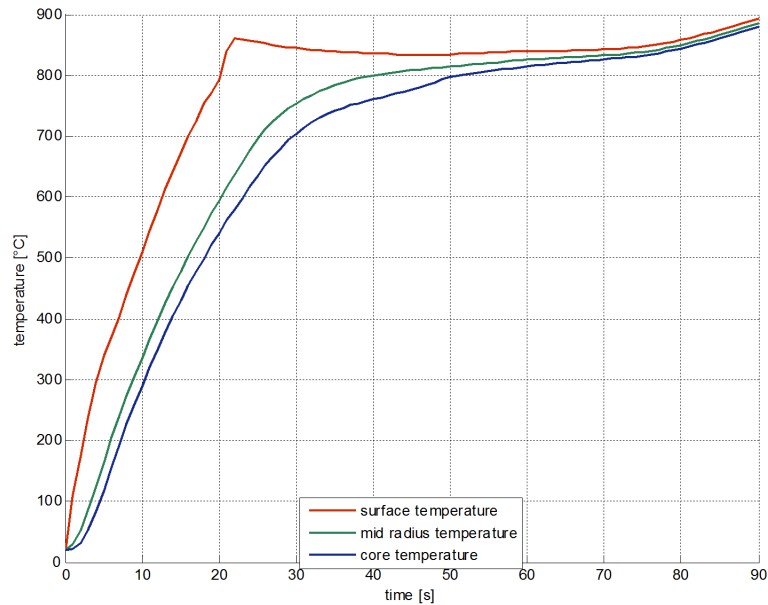
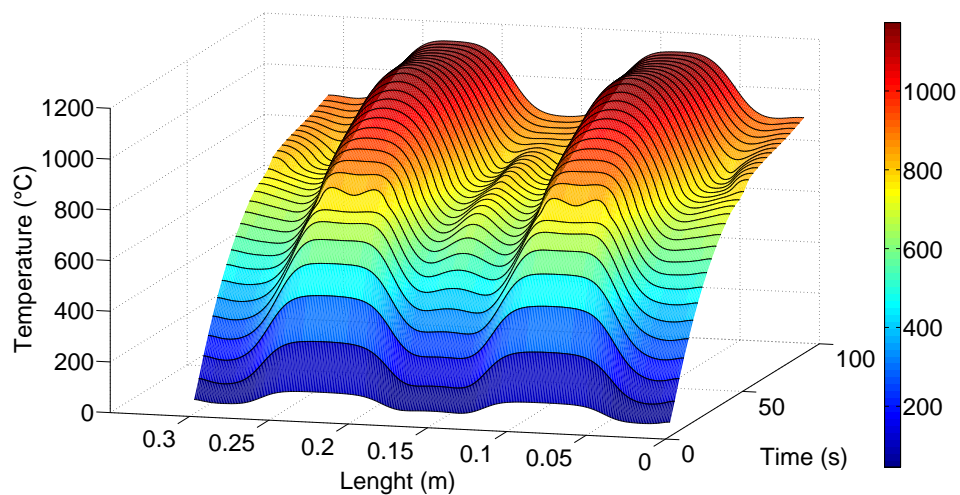


Figure 5.21: temperature over time in a cold-zone

Curie's point is crossed after 25-30 seconds then the trend is almost flat until the final temperature. Important to add that during this time there is an equalization between the core and the surface temperature. In fig.5.19 it is possible to see that the biggest temperature difference is still in the "transition zone" because of the border effects. It is also interesting to see how this thermal profile evolves during the process. In the pictures 5.22 there is a surface which shows how the temperature changes along the length and along the radius of the work-piece during the time.



The hot forging process can take maximum 30-35 seconds, after the hot zones go under 1100°C which is the minimum temperature for the hot forming process. During the cooling time it is interesting to notice that the cold zones increase their temperature while the hot one are decreasing. After 150 seconds from the end of the heating process

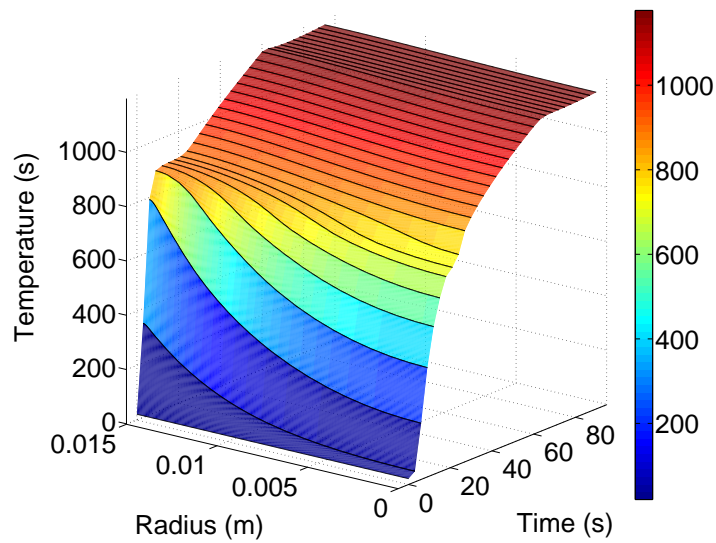


Figure 5.22: thermal profile evolution up: along the length, down along the radius (hot zone)

the work-piece is still over  $850^{\circ}\text{C}$  so it is still possible to make some operations of cold forging if required.

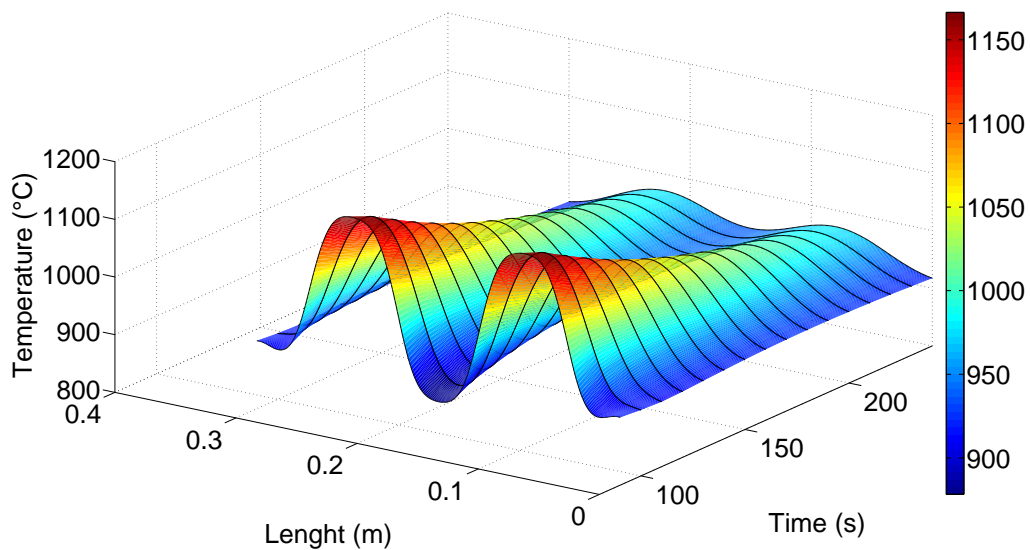


Figure 5.23: cooling profile

The efficiency during the process has been analyzed. The trend is shown in the picture 5.24.

Following the curve it is possible to notice that:

- at the beginning the efficiency rises because the resistivity of the work-piece rises too.

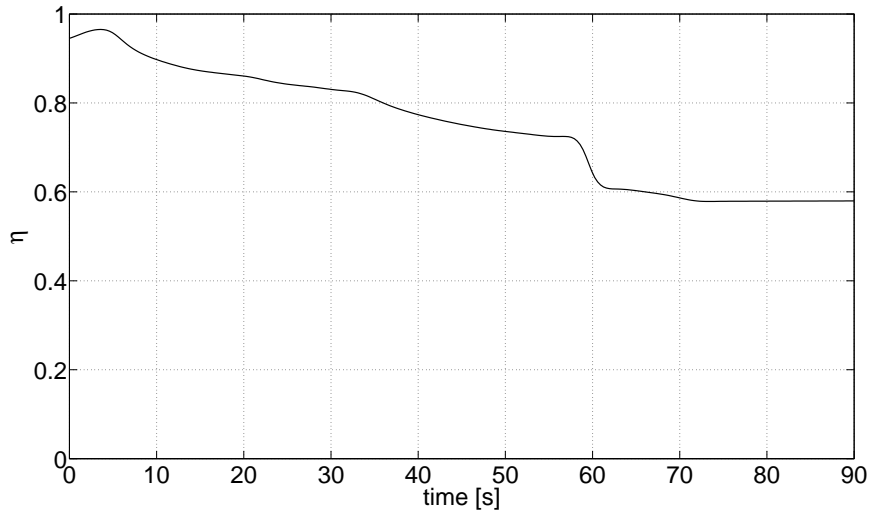


Figure 5.24: efficiency

- after the first peak (around 5 sec) the efficiency decreases because the work-piece is losing its material properties
- between 59 and 60 seconds there is a step: this is because some turns change their function; the energy produced by these turns is not totally transmitted to the work-piece but most of it is used to separate the magnetic field.
- the average efficiency of the process is 74%

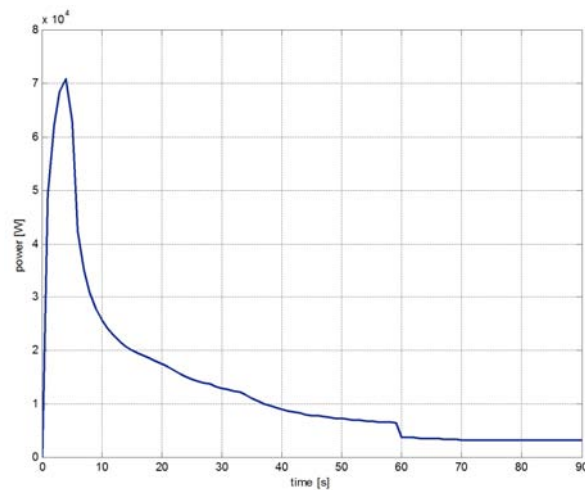


Figure 5.25: power induced in the work-piece

Looking at the power trend it is easy to notice that the maximum power comes after 4 seconds and it is about 70kW. After that point the surface of the hot-zones starts to cross the Curie's point and this is the reason why the induced power falls down. Here it is possible to identify the same step found in the efficiency trend. Between 59 and 60 seconds the power makes a little step down because some turns now are working to split the magnetic field in the hot-zones and not to heat the work piece.

## 5.2.4 Inductor thermal analysis and cooling system

In order to make an approximate estimation about the physical realization of the model the temperature of the inductor has been investigated. This problem is very complex because there are many factors to keep in count. In an induction heating system it is common to use the channel inside the inductors in order to make a cooling water flow. The water is pumped inside the system in order to export the heat generated by the currents in the copper of the coil. The speed of the water inside the pipe is not homogeneous: due to the friction forces, the water which flows near the edges of the tube is slower than the one in the middle.

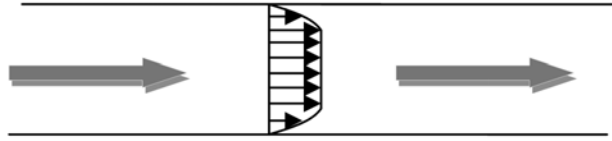


Figure 5.26: speed profile inside a tube

Then, considering that usually the coil (the tube in this case) is interested by an high current density, its temperature rise up very fast. The water near the edges is closed to be stationary so it is possible that some vapor bubble appear. This can be a problem because the vapor is a good thermal insulator and this phenomenon makes the heat exchanging more difficult. Anyway for this investigation is neglected because its effect is not extremely strong and it can be investigated with more accuracy in the future. To find an approximate value of the amount of heat exchanged is very important to determinate the convection coefficient. Finding this parameter is not simple and we need it to make the FEM analysis. First of all it is necessary to understand how the water flows in the tube and to do this is better to start with an analytical approach. The algorithm to find the convection coefficient requires to find the famous non-dimensional ratios which come from the fluid mechanics:

- Reynhold's number:

$$Re = \frac{\textit{inertia forces}}{\textit{viscous forces}} = \frac{\frac{\gamma \cdot w_m^2}{D}}{\frac{\mu_d \cdot w_m}{D^2}} = \frac{\gamma \cdot w_m D}{\mu_d} = \frac{m_w \cdot D}{\mu_d \cdot S}$$

where  $w_m$  is the average speed of the water in the tube,  $D$  is the diameter of the tube,  $S$  is the area of the tube,  $\gamma$  is the density of the fluid,  $\mu_d$  is the viscosity of the fluid,  $m_w$  is the mass flow of the fluid. For high values of Reinhold's number the inertial forces are stronger than the viscous forces which can not avoid quickly and random fluctuations in the fluid. In this case the water flow is turbulent. In the other hand, for small values, the viscous forces are stronger and so the water flow is carried in line.

- Prandlt's number:

$$Pr = \frac{\textit{viscous diffusion rate}}{\textit{thermal diffusion rate}} = \frac{\mu_d C_p}{\lambda}$$

where  $c_p$  is the heat capacity and  $\lambda$  is the thermal conductivity. Usually this number is between 1 and 10 for the water.

- Nusselt number:

$$N_u = \frac{\alpha \cdot D}{\lambda}$$

where  $\alpha$  is the convection coefficient.

To find the convection coefficients the Nusselt number is required. It is possible to find it also as a combination between Reinhold and Prandlt's numbers. But to follow this path it is necessary to know if the water flow is turbulent or laminar. The first step to find the convection coefficient is to study the properties of water; in particular we need the heat capacity, the density, the viscosity, the thermal conductivity as a function of temperature. The inductors has not to be heated too much so a range about 20-200°C is reasonable for these properties.

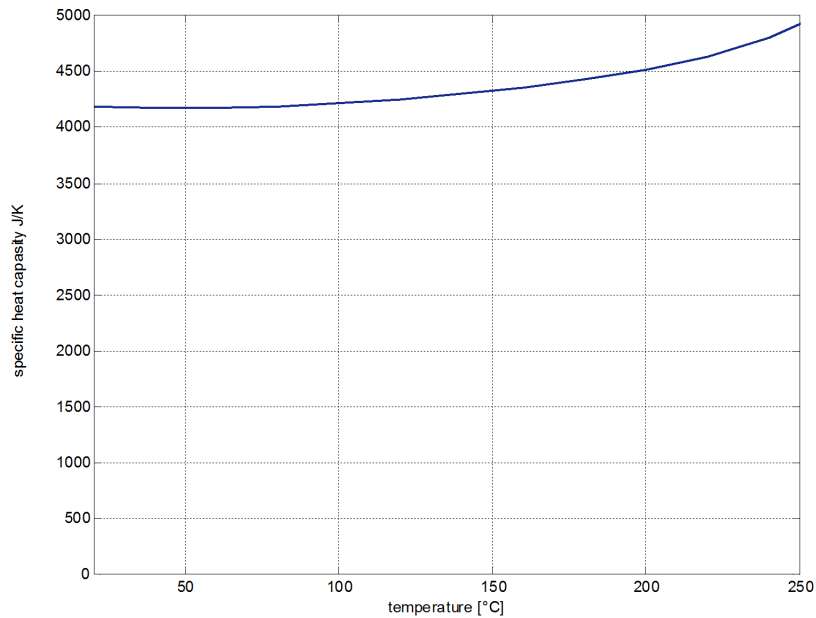


Figure 5.27: water  $C_p$

Having all the required parameter it is possible to start with the computation of the convection coefficient. The parameters for the design of the cooling system are:

- input temperature of water : 20°C
- output temperature of water : 60°C
- inductor heat power : 800W

For the hot zone inductor:



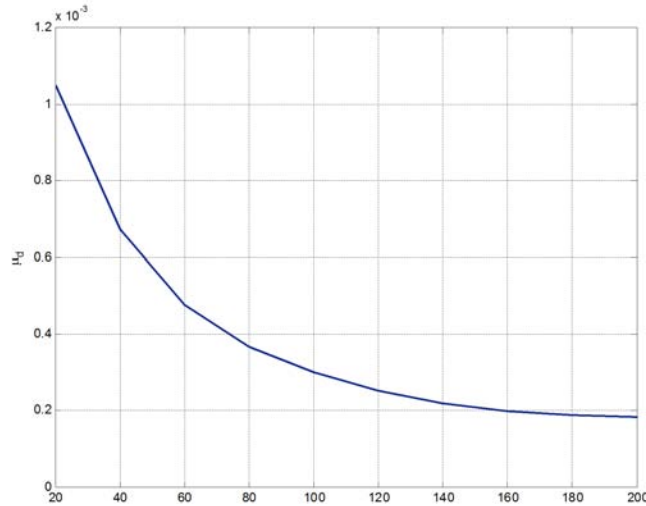


Figure 5.28: water viscosity

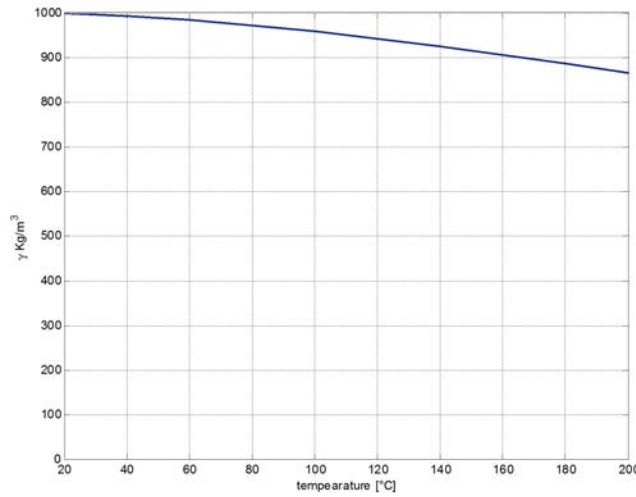


Figure 5.29: water density

$$s = l \cdot l = 0.007^2 = 0.000049m^2$$

$$length = 2\pi rn = 0.785m \text{ (inductor length)}$$

$$W = \frac{power}{length} = 1019W$$

$$q = \text{water flow} = \frac{W \cdot 1000 \cdot 60}{\gamma \cdot \Delta T \cdot C_p} = 0.287 \frac{l}{min}$$

$$w_m = \text{water speed} = \frac{q}{60 \cdot 1000 \cdot S} = 0.09761 \text{ m/s}$$

$$m_w = \text{mass flow} = w_m \cdot S \cdot \gamma = 4.77 \cdot 10^{-3} \text{ m}^3/s$$

$$Re = \frac{m_w \cdot D}{\mu_d \cdot S} = 827$$

Focusing on the Moody's diagram it is easy to see that the water flow is laminar:

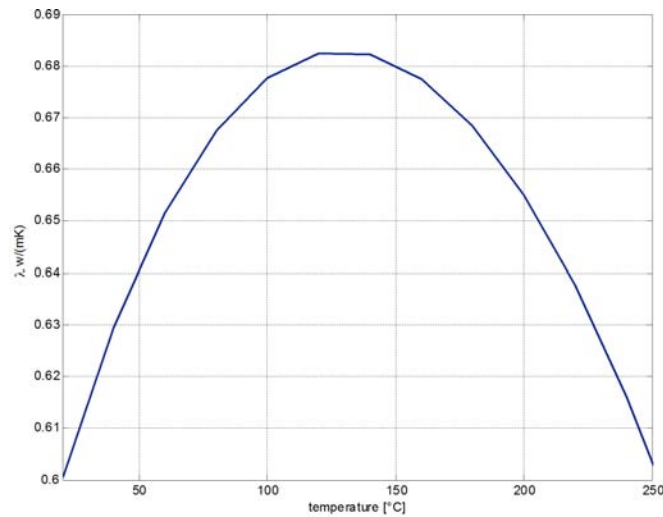


Figure 5.30: water thermal conductivity

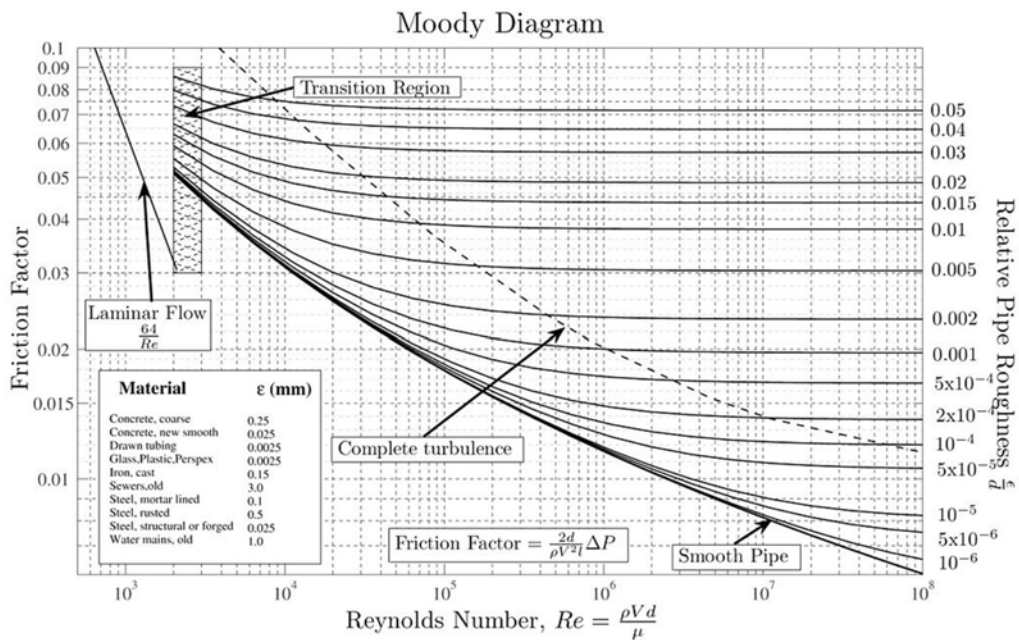


Figure 5.31: Moody's diagram

Now it is possible to find the Nusselt number with the formula for laminar flow which is:

$$N_u = 3.66 + \frac{0.06 Re Pr D}{l} \frac{1}{1 + 0.04 \left( \frac{Re Pr D}{l} \right)^{\frac{2}{3}}}$$

This Nusselt's number is not correct. It is good to remember that the tube under analysis is not straight: it is helicoidally.

In this kind of channel (curved channel) a secondary flow arises because the velocity of the fluid, in the primary flow, is different between the central and the border edges. Then,

the fluid elements near the channel center have larger inertia than fluid near the channel walls, and would tend to flow outward around a curve, creating a pressure gradient in the radial direction of the channel. The channel is closed, then, because of this pressure gradient, part of the fluid near the wall recalculates inward creating two vortices. This phenomenon is described by the Dean number.

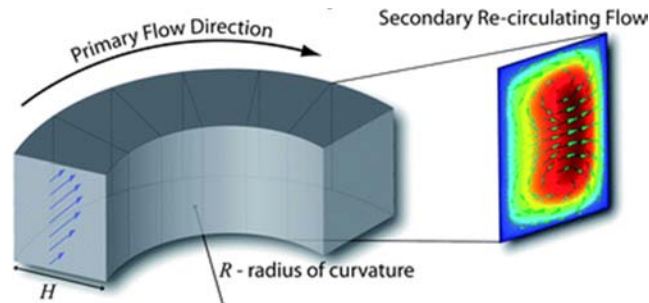


Figure 5.32: Dean's vortex example

The water flow is then not completely laminar, the Nusselt's number must be corrected in order to keep in count of Dean's vortices.

$$D_e = 4 \cdot \sqrt{\frac{D}{R_c}} \cdot Re = 1750$$

Where  $De$  is the Dean number and  $R_c$  is the curvature radius of the pipe. Now is possible to correct the Nusselt's number with the relation:

$$N'_u = N_u \cdot (0.1979) \cdot D_e^{0.5} = 48.76$$

As it possible to see the new Nusselt's number is around ten times bigger than before. So the convection coefficient are:

$$\alpha_{hot\ zone} = \lambda \cdot \frac{Nu'}{D} = 4179 \frac{W}{m^2 K}$$

$$\alpha_{cold\ zone} = \lambda \cdot \frac{Nu''}{D'} = 8158 \frac{W}{m^2 K}$$

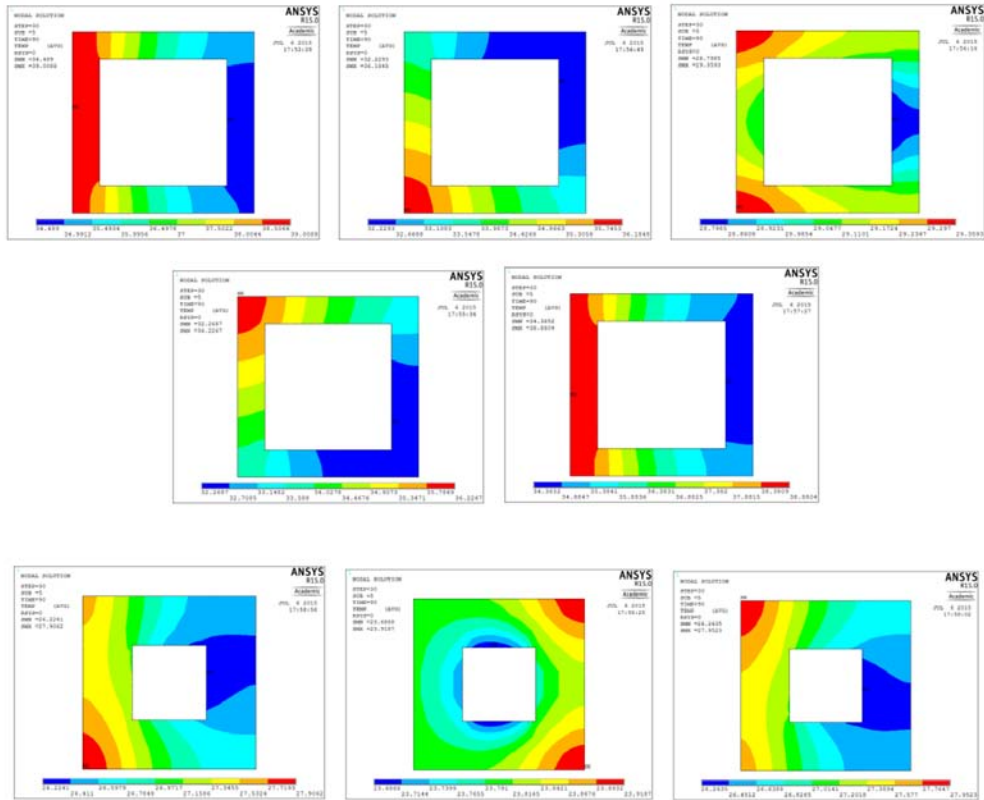


Figure 5.33: temperature distribution in the hot (up) and cold (down) zone inductor

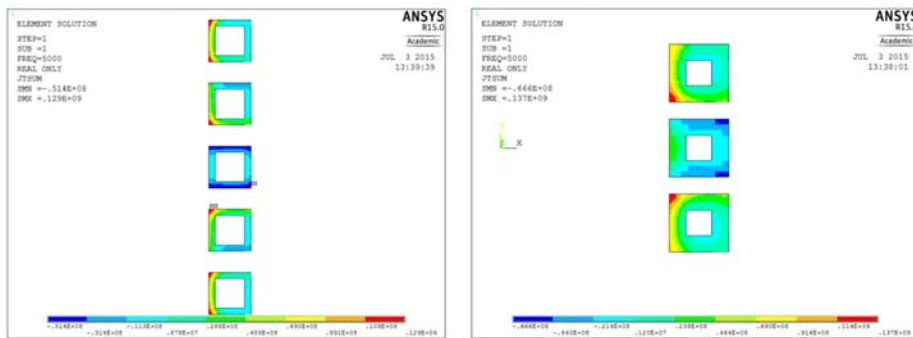


Figure 5.34: current distribution

Then setting these coefficients in the FEM simulation the results are shown in fig.5.33. It is interesting to notice that the temperature distribution follows the current distribution. It is very clear that the hotter zone are the same zones where the current density is higher. This investigation has been done just for this particular experiment. Normally, for practical reasons, a turbulent flow is artificially created by increasing the water velocity. This is done to be sure that the convection coefficient will be enough high.

# Chapter 6

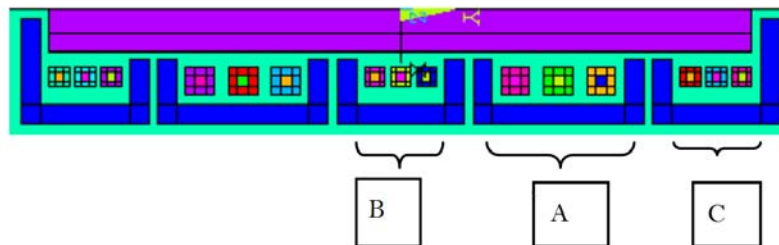
## Further analysis

The results which have been found are valid only for the work-piece under analysis. It can be interesting to extend the investigation to check the feasibility of the process even with different configurations. In particular we have made three extension of this analysis. The first one is to understand what changes increasing and decreasing the work-piece length and adding turns to the inductor and the second one is to see what happens if the diameter changes. The third is a comparison between the energy and the efficiency used in a traditional process and in a processes which involves the method explained in chapter V.

### 6.1 Different length tests

#### 6.1.1 Three Turns Inductor 25cm Work Piece

In this case the work-piece is shorter and the inductors are smaller. All the inductors are made by three turns. Except the input currents, the consideration for the preprocessing are the same as before. The input currents are:



Interval 1:0-59sec	Interval 2: 59-90 sec	Turn
820 A	820 A	C1
-500 A	-500 A	C2
820 A	820 A	C3
1250 A	1250 A	A1
1000 A	-1000 A	A2
1250 A	1250 A	A3
700 A	700 A	B1
-300 A	-300 A	B2
700 A	700 A	B3

The temperature profile which comes from this configuration is:

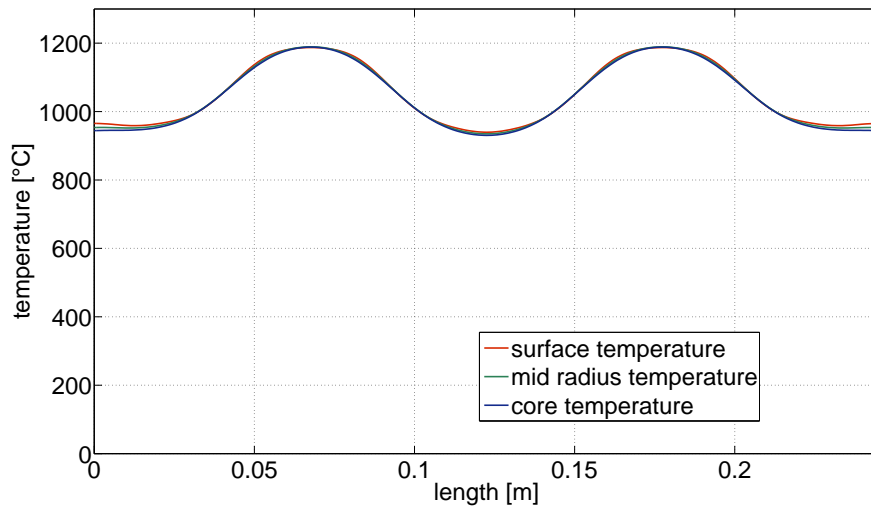


Figure 6.1: three turns, 25cm work-piece temperature profile

This profile is not squared as the one which has been found in the third model in the previous chapter. The reason is that the inductors for the hot zones are shorter and it is harder to control the magnetic field and the power distribution inside the work-piece. Looking at the currents input table, the currents to heat the hot zone have been increased due to the reduction of the numbers of turns. An higher negative current is required to make the active electro-magnetic shielding. It is interesting to investigate the action of the shielding turn feeding it with different values of current. The current in the central turn plays a key role regarding the shape of the temperature profile. As it has been shown in the last chapter, regulating the amount of the current in this turn it is possible to rise up or push down the temperature in the middle of the zone. Then investigating what happens changing this value, it is interesting to see that the decreasing of the temperature is not proportional with the decreasing of the current.

It can be useless to increase the value of the current too much. In any case a good choice is to use more than three turns because even with the flux controllers and the active shielding is not possible make a flat profile, it will be always a little bit curvy.

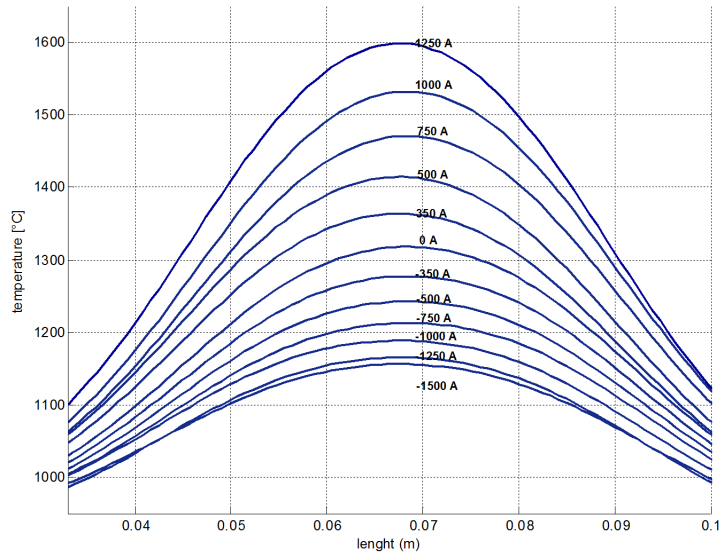
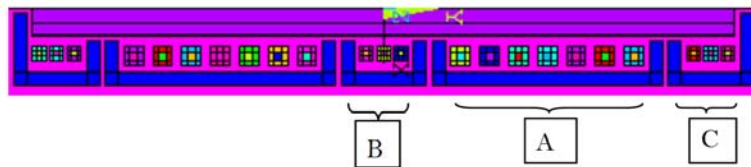


Figure 6.2: zone temperature profile for different currents in the A2 turn

### 6.1.2 Seven Turns Inductor 37cm Work Piece

Using seven turns is completely different than three. In this case the inductor is longer which means that the magnetic field produced inside of it is more uniform. So the current in the middle turn does not have to alter too much the path of the magnetic flux lines, but only to correct or weak it. Even for this model, the preprocessor part is always the same as before. The only thing that change are the number of the turns which are seven, the amount of current in the turns and the length of the work-piece. Then the current inputs and the geometry are:



Interval 1:0-59sec	Interval 2: 59-90 sec	Turn
820 A	820 A	C1
-500 A	-500 A	C2
820 A	820 A	C3
970 A	970 A	A1
720 A	720 A	A2
720 A	720 A	A3
720 A	320 A	A4
720 A	720 A	A5
720 A	720 A	A6
970 A	970 A	A7
820 A	820 A	B1
-300 A	-300 A	B2
820 A	820 A	B3

In this case it is easier to obtain a flat profile temperature in the hot zones. First of all the currents are lower than before because the number of turns is higher. Second, but very important, is that the current is not anymore negative. This means that inside the inductor the magnetic field it is enough uniform that it is not required to use the action of an inverted field to fit the profile. Then weakening the field with a lower current in the middle of the coil is possible to reduce the eddy currents density in front of the "face" of that turn and, consequentially, the power density and the heat generation. This shows the importance of having an active control in the middle turn in order to fit the process to the required results.

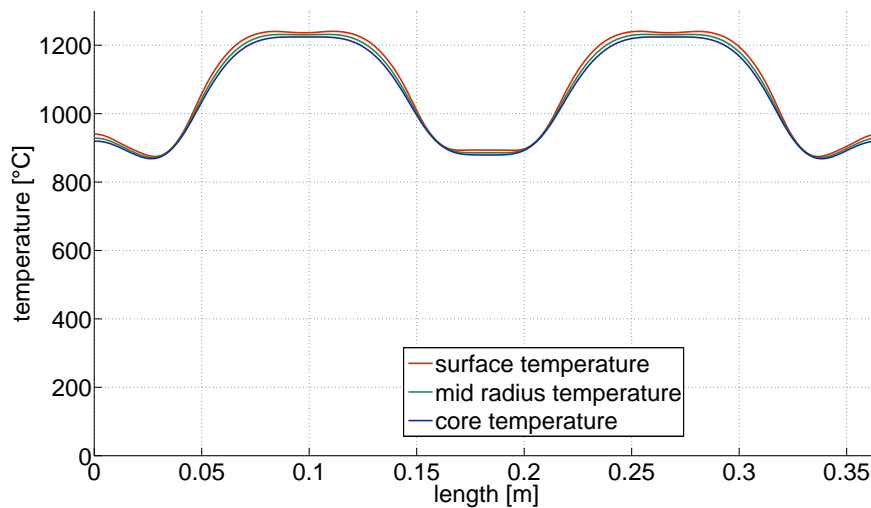


Figure 6.3: 37cm workpiece, 7 turns thermal profile

The borders are not very well controlled but it is not a problem because they are in any case in the cold forging temperature and it can be good in order to do not make the model more complicated.

Fig.6.4 shows that with seven turns there are a lot of possibilities which are acceptable (the range under 320A) and this is because increasing the number of turns the action of



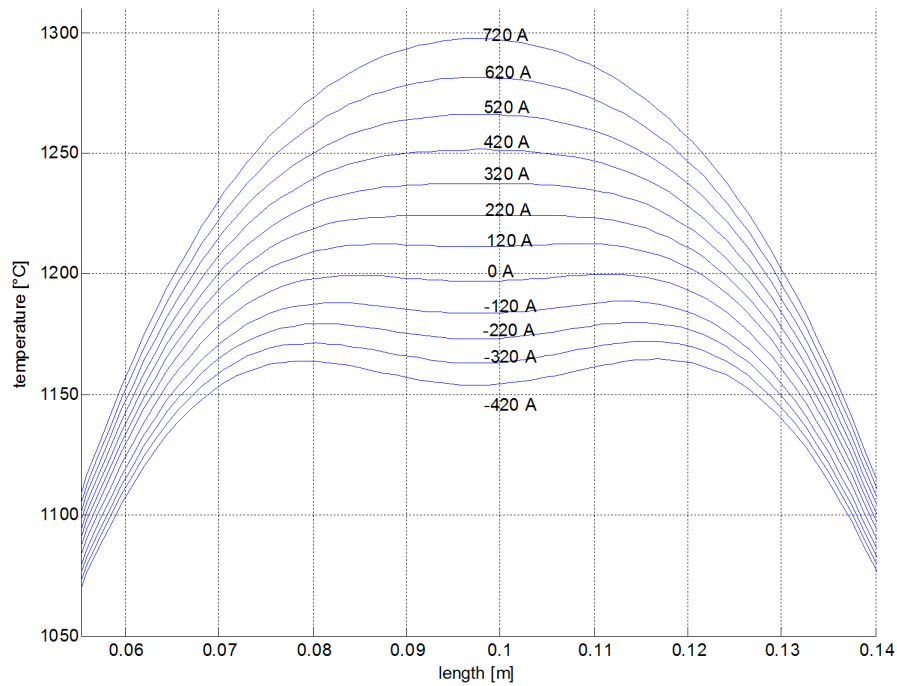


Figure 6.4: hot zone temperature profile for different currents in the A4 turn

the middle turn is more sensible. All the analyses have been done with a fixed heating time, but it would be interesting in future to investigate also changing the time in order, maybe, to make a process more optimized.

## 6.2 Different diameter tests

The next test involve the change of the diameter of the work-piece but with the length which is fixed as the original one: 30cm. This is a preliminary analysis since there are many possible combinations to improve the processes. Extending the study to different shapes is fundamental to adapt it for the industry reality. It is very important to underline that changing the diameter has an effect on the frequency choice. In order to have the best efficiency (which is the criteria we choose) "m" must be around 2.5 and "m" depends by the radius and by the penetration depth. Increasing the radius means also increasing the value of m, so , to lock it around 2.5, the penetration depth must be increased too. Another point is that increasing the diameter also the time should be increased in order to have an uniform temperature along the radius. As a matter of fact, it is harder to keep the hot zones and the cold zones separated. Another thing to keep in mind is that the volume depends by the square of the radius, so increasing the radius means increasing the volume in a quadratic way. The energy required by the process is then higher, so this is another factor with increase the time of the process. Due to these last considerations also the currents should be higher in order to induce a bigger amount of power inside the work-piece and to contain the heating time which is against to the zones boundaries. To carry the investigation three diameter have been taken (except the original one 0.03m). The criteria is to increase it by one centimeter for every test.

### 6.2.1 Diameter: 4cm

In this case the preprocessor considerations are a little bit different because there is the variation of the:

- frequency
- diameter
- currents
- time

So even for this model there are many parameter to chose. Beginning from the frequency, referring to fig.2.22, is easy to choose 2.5Khz. The diameter is fixed to 4cm. Regarding the currents and the time, the same type of method has been used. So there are two different intervals in which the currents are different, in particular in the second one the magnetic field shielding is active. The geometry and the current classification is the same of the one used in the third model: 5 turns inductors for the hot zones and 3 turns inductors for the cold zones. The only difference in the fem draw is only the diameter which is 1 cm bigger.

Interval 1:0-80 sec	Interval 2: 80-120 sec	Turn
1020 A	1020 A	C1
-500 A	-500 A	C2
1020 A	1020 A	C3
1300 A	1300 A	A1
1050 A	1050 A	A2
1050 A	-1050 A	A3
1050 A	1050 A	A4
1300 A	1300 A	A5
1020 A	1020 A	B1
-350 A	-350 A	B2
1020 A	1020 A	B3

As the table shows, the currents required are higher as expected. Also the time is longer, we need more time to heat the cylinder in the first interval and more time in the second one to control the profile.

As expected it is harder to make a sharp distinction between the hot and the cold zones. In any case is still possible to generate a profile similar to the ideal one.

The temperature distribution is less uniform than before (with the previous diameter). In any case, this non-uniformity is not very high. Looking at fig.6.6, and paying attention to the color legend, the maximum temperature differences between the core and the surface is not high, around 30°C .

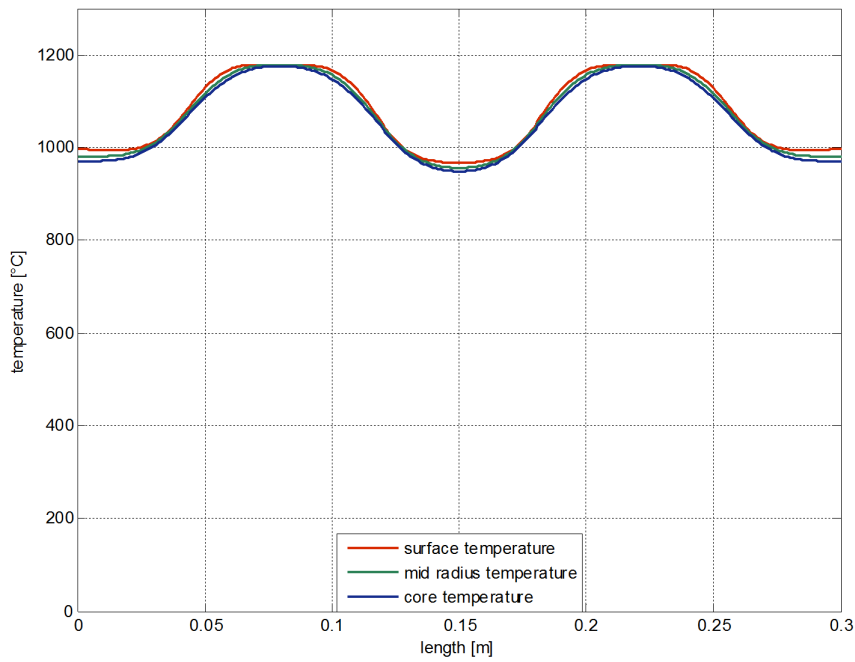


Figure 6.5: 4 cm diameter temperature profile

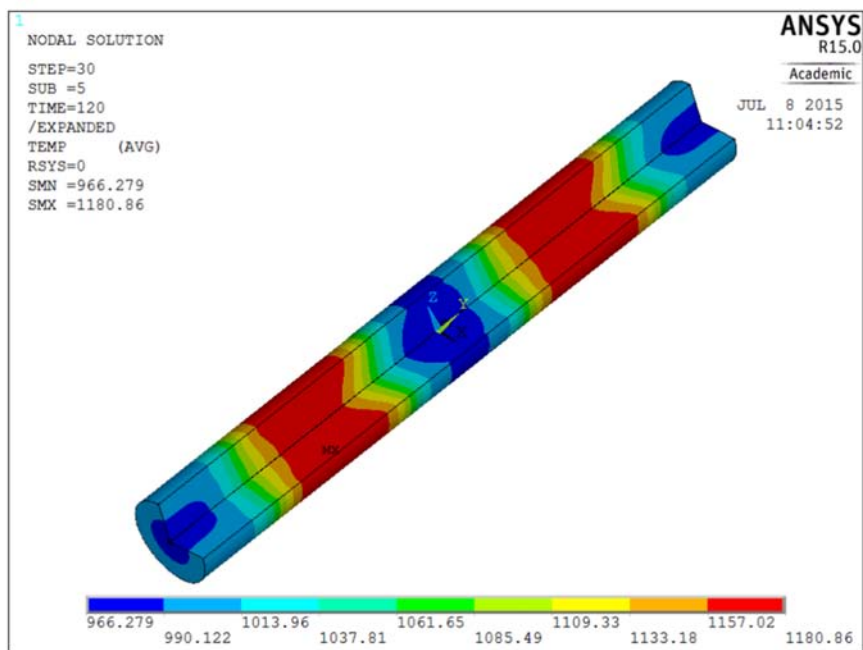


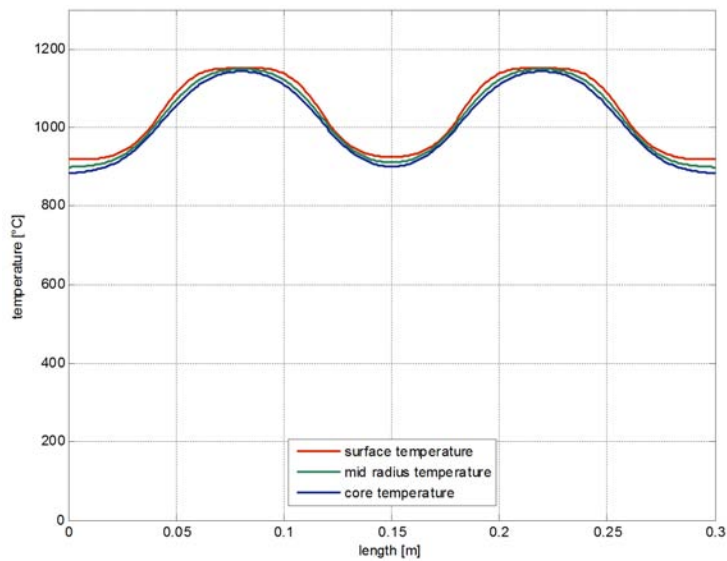
Figure 6.6: 4 cm diameter temperature profile

## 6.2.2 Diameter: 5cm

Following the same consideration of the previous test, the frequency is now set to 2 kHz. The input currents are:

Interval 1:0-85 sec	Interval 2: 85-130 sec	Turn
1020 A	1020 A	C1
-500 A	-500 A	C2
1020 A	1020 A	C3
1450 A	1450 A	A1
1150 A	1150 A	A2
1150 A	-1150 A	A3
1150 A	1150 A	A4
1450 A	1450 A	A5
1020 A	1020 A	B1
-350 A	-350 A	B2
1020 A	1020 A	B3

As expected the currents are higher and the heating process is longer. It is not easy to keep a flat profile in the hot zone without losing the uniformity along the radius. This happens because during the second interval ( the control interval) the heat flux moves from the hot zone to the cold zone. This effect is stronger increasing the diameter because the second interval is longer. In any case the difference of the temperature between the core and the surface is not extremely high; it is under 50°C so it is tolerable.



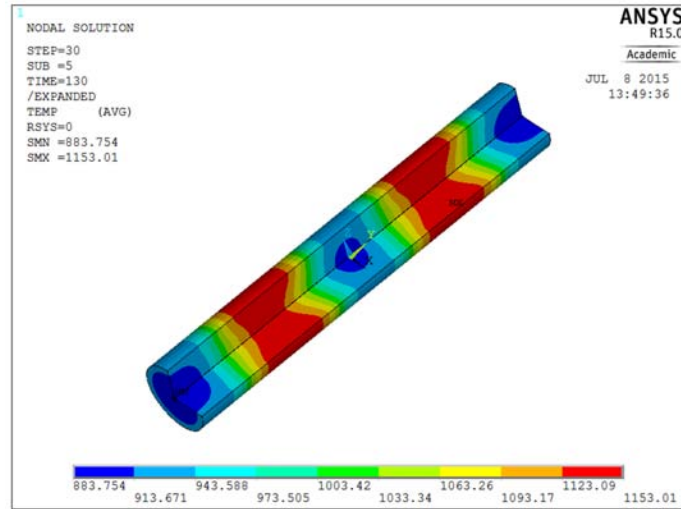


Figure 6.7: 5 cm diameter thermal profile and temperature distribution

### 6.2.3 Diameter: 6cm

In this case the frequency is 1.2 KHz and the input currents are:

Interval 1:0-110 sec	Interval 2: 110-160 sec	Turn
1100 A	1100 A	C1
-500 A	-500 A	C2
1100 A	1100 A	C3
1700 A	1700 A	A1
1350 A	1350 A	A2
1350 A	-1350 A	A3
1350 A	1350 A	A4
1700 A	1700 A	A5
1020 A	1020 A	B1
-350 A	-350 A	B2
1020 A	1020 A	B3

The effect of the bigger diameter is one more time stronger, the total process is 56% longer than the one with the original diameter. The controlling time (second interval ) is 50 seconds which is almost the double of the original process. The distribution along the radius is still less uniform, and the transient zones are bigger. It is important to remember that in this case the inductors for the hot zones are close to have the same length and diameter. In this configuration the temperature profile on the surface is still flat but going deep to the core it is possible to see that it starts to become more curvy. To solve this problem more researches in this field are needed. In any case the quality of the profile depends by the type of the process and, to fix some rules, would be interesting to analyze this problem with the cooperation of mechanicals and materials engineers.

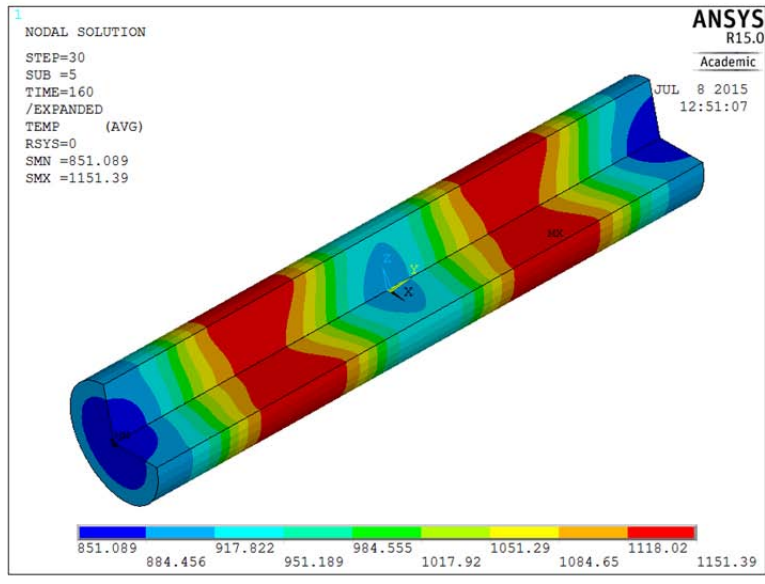
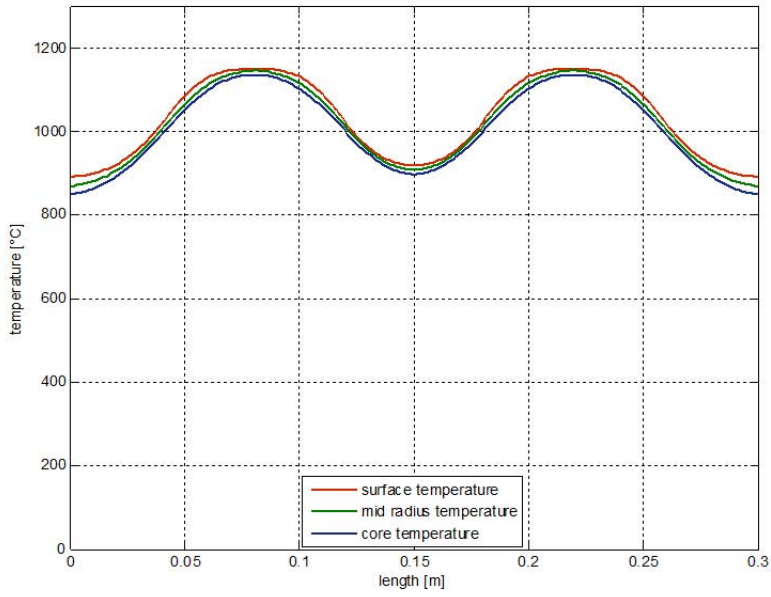


Figure 6.8: 6 cm diameter thermal profile and temperature distribution

### 6.3 Comparison between traditional process and inhomogeneous process

To understand the applicability and the advantages that this method has, a comparison between the traditional heating system and the heating method explained in this work is very interesting. In order to make the test as fair as possible, it has been decided to take the same heating time, the same work-piece and the same final target temperature. The main difference is that instead of having two cold zones and two hot zones, with the traditional method there will be only one big hot zone. To make the report more understandable the model called "third model" presented in chapter V would be called

"model A" and the traditional model, "model B".

### 6.3.1 Geometry

First of all a big difference between the model A and the model B is in the geometry. As is shown in chapter V the geometry of the model A is very complicated, it requires five inductors and flux controllers; the model B has only one inductor and flux controllers.

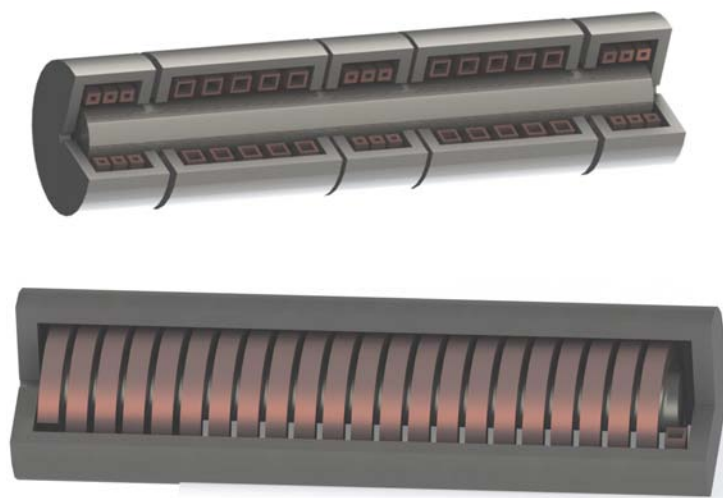


Figure 6.9: model A and model B 3D rendering

The details of the geometry of the model A have been already explained. Regarding the traditional model, the inductor presents twenty-two turns. The section of the turns is the same of the one used for the hot-zone inductor in the model A so, 1cm x 1cm, squared shaped, 1.5 mm for the copper thickness. The internal diameter of the inductor is again the same: 4 cm. Also the space between the turns is the same: 0.5 cm.

### 6.3.2 Input quantities

For the model A the two intervals method is used: the input quantities are the same which are set for the analysis in chapter four. Anyway they have been reported here again.

Interval 1:0-59sec	Interval 2: 59-90 sec	Turn
820 A	820 A	C1
-500 A	-500 A	C2
820 A	820 A	C3
1050 A	1050 A	A1
800 A	800 A	A2
800 A	-800 A	A3
800 A	800 A	A4
1050 A	1050 A	A5
820 A	820 A	B1
-350 A	-350 A	B2
820 A	820 A	B3

For the model B the inputs are very simple:

- equal current in the same turns : 660 A
- frequency : 5 kHz
- heating time : 90 seconds

### 6.3.3 Process comparison

The thermal profiles of the model A and the model B are obviously totally different. The profile of model A is already known, there are two hot zones and two cold zones, respectively at the temperature of 1180°C and 880°C. In the model B the temperature is almost uniform along the length, nearly 1200°C. The temperature along the radius is more uniform in the model A, in the model B the surface is almost constantly 25°C hotter than the core. This can be solved adding an equalization time at the end of the process B.

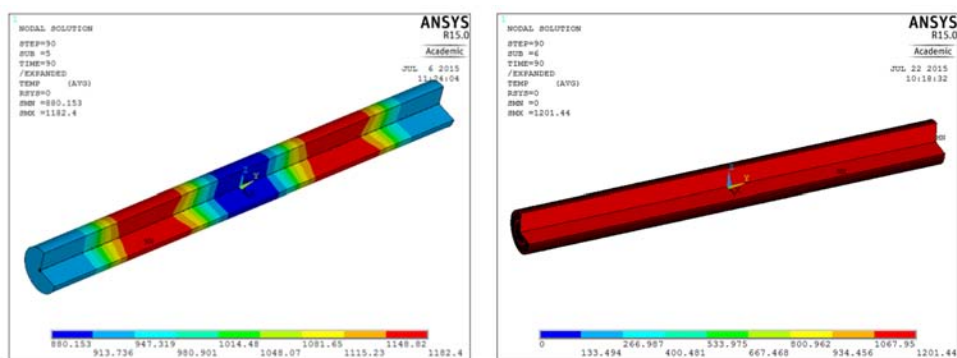


Figure 6.10: temperature distribution model A and B



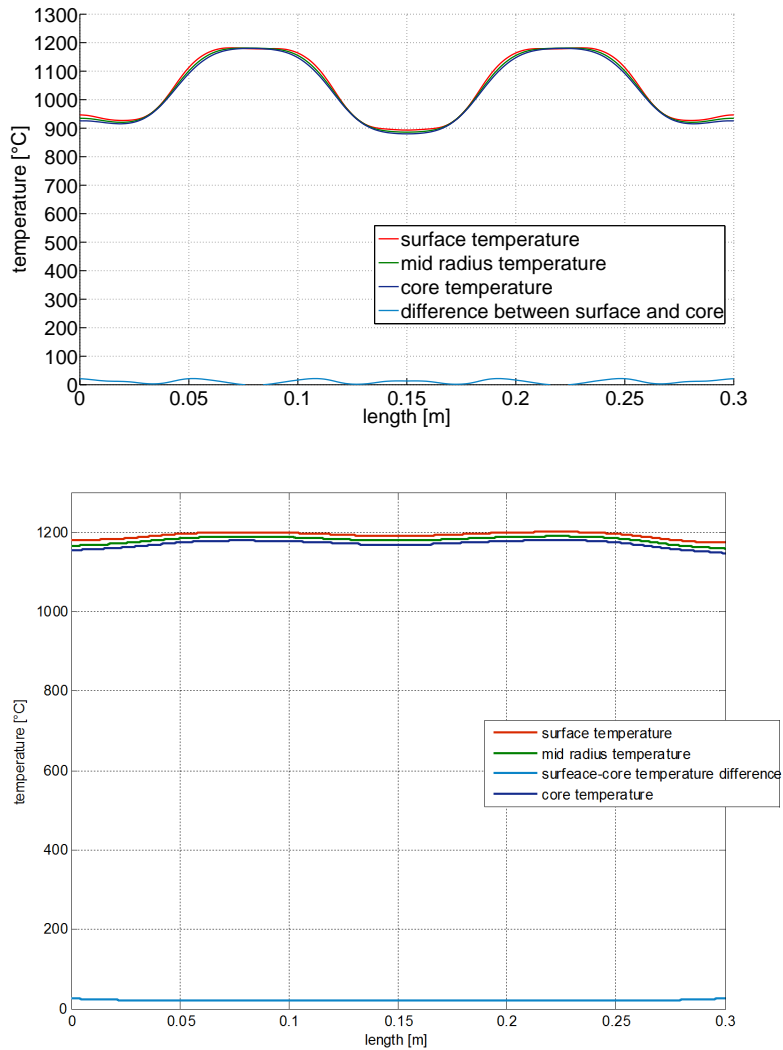


Figure 6.11: temperature profile, model A and model B

### 6.3.4 Power, energy, efficiency

This is the most interesting topic to compare. As it is possible to imagine, the machinery to realize the model A are more expensive and complicated than the one for model B. The model A requires:

- custom power converter which should be able to: guarantee different multi output currents, invert the current: for AC currents is necessary to monitor the phase angle continuously
- custom inductors: they must be designed in order to be supplied with different current in different turns

The model B requires only an inductor, flux controllers, and a simple generator. So is important to verify if the process obtained by the model A is competitive or not. This is only a rough analysis since the model A is not optimized and it can be improved with

further studies. Looking at the power absorbed by the whole system ( iron and copper losses included) it is possible to notice some differences. Starting from the model B, the system dries a bigger amount of power at the beginning, this can be justified explaining that in the model B the power is induced uniformly in the whole work-piece while in the model A, in the cold zones, is induced less power. This means also that the model B reaches the Curie's temperature faster so the power absorbed falls down and, at 15 seconds, it becomes less than the one from the model A. So from 15 to 59 seconds the model A absorbs more power. Between 59 and 60 seconds the model A has the interval changing which is marked by the step in the power trend.

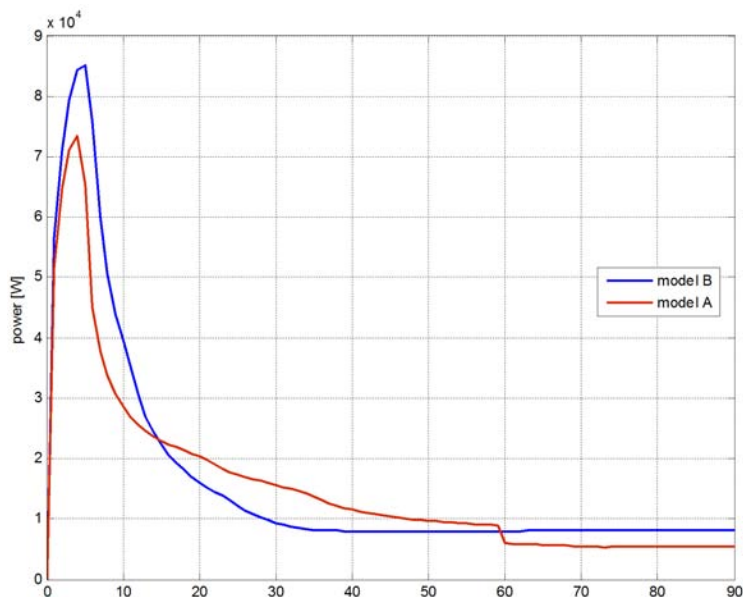


Figure 6.12: power comparison

The efficiency follows the same trend. There is a continuous reversing of the curves since the work-piece reaches the Curie's temperature in different points at different times. In any case is clear that in the model A the efficiency is lower. The reasons are that in the inductors flows higher currents which means higher joule losses in the copper and that in the second interval part of the power is used to split the magnetic field and not to heat directly the work-piece. This is the formula that has been used to evaluate the efficiency:

$$\eta = \frac{P_w}{P_w + P_l}$$

where  $P_w$  is the power induced in the work-piece and  $P_l$  is the power lost in the inductor and in the iron.

The average efficiencies are:

- nearly 74% for the model A
- nearly 81% for the model B

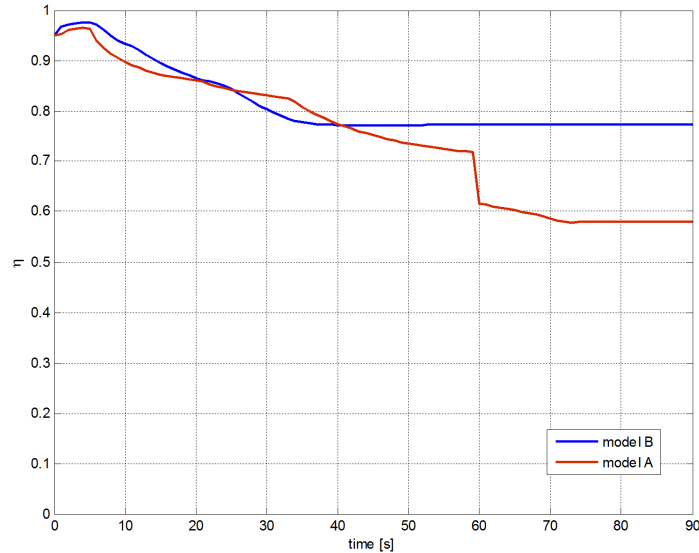


Figure 6.13: efficiency comparison

It is clear that the model B has a better efficiency because an higher amount of the drained power is induced in the work-piece. The energy consumed by both of the processes has been computed as the integral of the drained power over the time.

$$E = \int_0^{t_{finish}} P_e(t) dt$$

This integral corresponds to the area under the curve of the power. As long as we do not have an analytical expression of the function of the power over the time, a numerical method must be used. Using the trapezoidal rule for numerical integration is then possible to have the value of the amount of energy used by the process.

- Energy used by the model A: 1.369 MJ
- Energy used by the model B: 1.453 MJ
- $\Delta E = 83.4$  KJ

This is a very interesting outcome since the process from the model A uses less energy than the one from the model B. The energy saved is about 5.57% which is a great success since saving 5.57% of energy for every heating process means saving a lot in a long time period. An economic analysis would be very interesting to verify the investment prospective; as it has been write above, the model A has a lower efficiency and an higher machinery cost but less energy is consumed. Probably is possible to rise the efficiency of the model A with an optimization study so it can be even more competitive.



# Conclusions

The idea of the inhomogeneous induction heating for forging parts is very innovative and it has not so deeply investigated in the past. In this work it has been analyzed the theoretical possibility to realize this kind of heating process. To achieve the required temperature profile on the steel billet it has been developed a numerical model which includes a new idea of heating process. Supplying the turns of the inductors with different values of the currents allows to control the distribution of the heating power inside the work-piece and then to control the final temperature profile along the length and along the radius. In this way it is possible to heat up to the hot forging temperature only the parts which need to be formed in order to save energy during the heating process. From the results of the analyses it is shown that this kind of process is theoretically possible. It is fast ( around 90 seconds) and the final temperature is very homogeneous along the length (in the different zones) and along the radius. The average process efficiency is about 74% which is a good value but, implementing an optimization study, probably it can be raised up. Employing this method allows to save around 5.6% of energy in each heating application if compared with a traditional through heating. This is a very interesting result considering that in a common company, many pieces are heated every hour continuously and saving 5.6% of energy for each piece means a lot. Then keep on researching in this field can be very important in order to bring a new induction heating technology in the industry. In future it will be important to develop these points:

- check the physical realization of the model
- experimental tests
- optimization of the model
- extend the analysis to different materials
- extend the analysis to non cylindrical work-pieces
- analyze the steel composition after the heating process and check the forging reliability.



# Bibliography

- [1] S. Lupi , *Appunti di elettrotermia (2005-2006)*
- [2] A. Nikanorov, E. Baake, H. Brauer, Ch. Weil, *Approaches for numerical simultion of high frequency tube welding process (September 16-19, 2014)*
- [3] Mustafa Bayrak, Fahrettin Ozturuk, Mehmet Demirezen, and Zafer Evis, *Analysis of Tempering Treatment on Material Properties of DIN 41Cr4 and DIN 42CrMo4 Steels (Journal of Material Engineering and Performance, 600- Volume (16) 5 October 2007)*
- [4] R. Shankar Subramanian, *Heat transfer to of from a fluid flowing through a tube (2015)*
- [5] MSpittel T. Spittel, *Landolt-Börnstein - Group VIII Advanced Materials and Technologies 4.4 Specific heat capacity of steel (Springer 2009)*
- [6] M. Fiorindo, N.Sempreboni, M.Tollardo, *Computational Electrical Engineering (Padova 15/08/2014)*
- [7] F.Bressan, S.Lupi, B.Nake, A. Nikanorov, M.Forzan, *Analisi e simulazioni numeriche dei processi di riscaldamento ad induzione con alte densità di corrente (ETP-Hannover, LEP-Padova 2011)*
- [8] Di Richard, E. Haimbauhg *Practical Induction Heat Treating"( ASM International, Materials Park Ohio, December 2001)*
- [9] [thelibraryofmanufactory.com/forging.html](http://thelibraryofmanufactory.com/forging.html)- (7/22/2015)
- [10] [thelibraryofmanufactory.com/metal\\_roling.html](http://thelibraryofmanufactory.com/metal_roling.html)- (7/22/2015)
- [11] Chapter4: Harmonic Response Analysis  
[http://mostreal.sk/html/guide\\_55/g-str/GSTR4.htm](http://mostreal.sk/html/guide_55/g-str/GSTR4.htm), (June2015)
- [12] Chapter 5 Transient Dynamic Analysis  
[http://mostreal.sk/html/guide\\_55/g-str/GSTR5.htm](http://mostreal.sk/html/guide_55/g-str/GSTR5.htm), (June2015)
- [13] D.Di Carlo , *Inertial microfluidics*  
<http://pubs.rsc.org/en/content/articlehtml/2009/lc/b912547g>- (22/09/2009)
- [14] E. Haye, *Industrial Solutions for Inductive Heating of Steels (Lulea University of Technology Department of Engineering Sciences and Mathematics, 2013)*